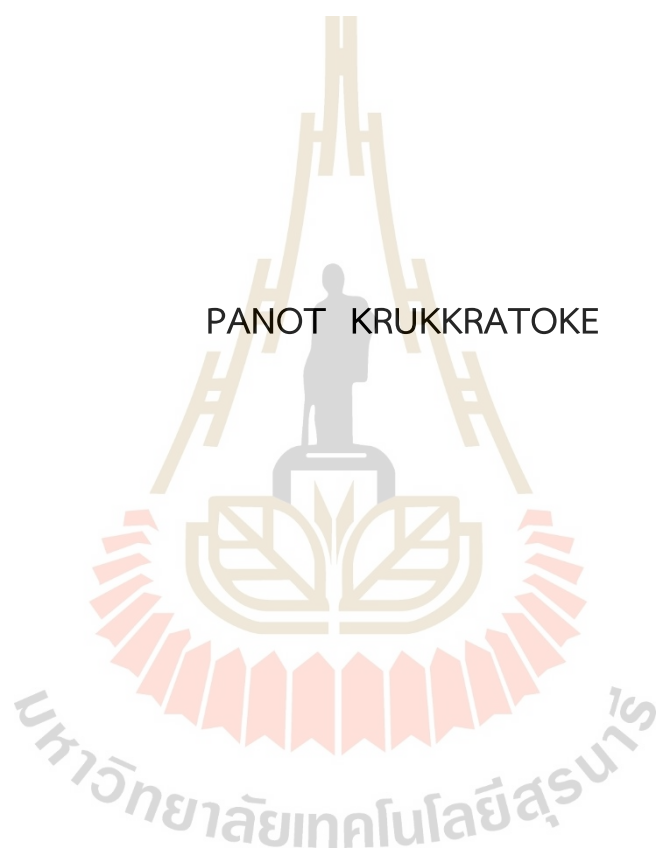# PARAMETERS AFFECTING STABILITY OF FAUJASITE ZEOLITE-SUPPORTED CATALYSTS FOR TRANSESTERIFICATION OF PALM OIL

PANOT KRUKKRATOKE

A Thesis Submitted in Partial Fulfillment of the Requirements for the
Degree of Doctor of Philosophy in Chemistry
Suranaree University of Technology
Academic Year 2023

ปัจจัยที่มีผลต่อความเสถียรของตัวเร่งปฏิกิริยาบนซีโอไลต์ฟูจาไซต์สำหรับปฏิกิริยาทรานส์เอสเทอร์ริฟิเคชันของน้ำมันปาล์ม

นายปณต ครึกกระโทก

วิทยานิพนธ์นี้เป็นส่วนหนึ่งของการศึกษาตามหลักสูตรปริญญาวิทยาศาสตรดุษฎีบัณฑิต
สาขาวิชาเคมี
มหาวิทยาลัยเทคโนโลยีสุรนารี
ปีการศึกษา 2566

PARAMETERS AFFECTING STABILITY OF FAUJASITE ZEOLITE-SUPPORTED CATALYSTS FOR TRANSESTERIFICATION OF PALM OIL
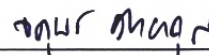
Suranaree University of Technology has approved this submitted in partial fulfillment of the requirements for the Degree of Doctor of Philosophy.

Thesis Examining Committee

_____

(Prof. Dr. Nurak Grisdanurak)

Chairperson

_____

(Prof. Dr. Jatuporn Wittayakun)

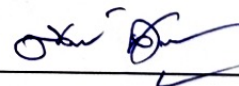Member (Thesis Advisor)

_____

(Assoc. Prof. Dr. Sanchai Prayoonpokarach)

Member (Thesis Co-Advisor)

_____

(Assoc. Prof. Dr. Kamonwad Ngamchuea)

Member

_____

(Asst. Prof. Dr. Natkanin Supamathanon)

Member

_____

(Assoc. Prof. Dr. Yupaporn Ruksakulpiwat)

Vice Rector for Academic Affairs

and Quality Assurance

_____

(Prof. Dr. Santi Maensiri)

Dean of Institute of Science

ปณต ครึกกระโทก : ปัจจัยที่มีผลต่อความเสถียรของตัวเร่งปฏิกิริยาบนซีโอไลต์ฟูจาไซต์ สำหรับปฏิกิริยาทรานส์เอสเทอร์ริฟิเคชันของน้ำมันปาล์ม (PARAMETERS AFFECTING STABILITY OF FAUJASITE ZEOLITE-SUPPORTED CATALYSTS FOR TRANSESTERIFICATION OF PALM OIL). อาจารย์ที่ปรึกษา : ศาสตราจารย์ ดร.จตุพร วิทยาคุณ, 129 หน้า

คำสำคัญ : ซีโอไลต์ FAU ตัวเร่งปฏิกิริยาวิวิธพันธ์ ปฏิกิริยาทรานส์เอสเทอร์ริฟิเคชัน ไบโอดีเซล

ตัวเร่งปฏิกิริยาวิวิธพันธ์ที่ประกอบด้วยโพแทสเซียมวัสดุรองรับซีโอไลต์ฟูจาไซต์ ได้แก่ NaX และ NaY โดยใช้โพแทสเซียม 12% (12K/NaX และ 12K/NaY) สามารถเร่งปฏิกิริยาทรานส์เอสเทอร์ ริฟิเคชันของน้ำมันปาล์มได้และให้ผลผลิตไบโอดีเซลมากกว่า 90% อย่างไรก็ตามบทบาทของโพรง FAU ในตัวเร่งปฏิกิริยาดังกล่าวยังไม่ชัดเจน และประสบปัญหาการพังเชิงโครงสร้างของซีโอไลต์ เพื่อ ศึกษาบทบาทของโพรงซีโอไลต์จึงใช้กระบวนการดูดซับด้วยพาราควอตเพื่อปิดกั้นโพรงซีโอไลต์ก่อน ทำให้เอิบชุ่มด้วยสารตั้งต้นโพแทสเซียม จากนั้นจึงนำตัวเร่งปฏิกิริยาที่ได้ไปทดสอบด้วยปฏิกิริยา ดังกล่าว ผลการศึกษาแสดงให้เห็นว่ายังไม่สามารถยืนยันบทบาทของโพรง FAU ได้ นอกจากนี้การปิด กั้นซีโอไลต์ด้วยพาราควอตยังไม่สามารถป้องกันการพังเชิงโครงสร้างของซีโอไลต์

การที่บทบาทของโพรง FAU จากการทดลองด้วยโพแทสเซียมเข้มข้น 12% ยังไม่ชัดเจนอาจ เนื่องมาจากปริมาณโพแทสเซียมสูงเกินไป ดังนั้นจึงทำการทดลองโดยลดปริมาณเป็น 8% โดยน้ำหนัก พบว่า 8K/NaX-PQ และ 8K/NaY-PQ สามารถผลิตน้ำมันไบโอดีเซลได้ 35.6% และ 7.1% ตามลำดับ ผลผลิตที่มากกว่าบน 8K/NaX-PQ เกิดจากซีโอไลต์ NaX มีการดูดซับพาราควอตน้อยกว่า ส่งผลให้เกิดผลึกโพแทสเซียมอะซิเตตขนาดใหญ่ในตัวเร่งปฏิกิริยาก่อนเผา และเมื่อผ่านกระบวนการ เผาทำให้เกิดการพังเชิงโครงสร้างซีโอไลต์ ในทางกลับกันซีโอไลต์ NaY ที่มีการดูดซับพาราควอตสูงนั้น จะมีการกระจายตัวที่ดี (กล่าวคือขนาดผลึกโพแทสเซียมอะซิเตตเล็ก) โดยไม่มีการพังเชิงโครงสร้าง ซีโอไลต์อย่างมีนัยสำคัญ ดังนั้นบทบาทของโพรง FAU คือการกระจายสารตั้งต้นโพแทสเซียมอะซิเตต

อย่างไรก็ตามการเตรียม K/NaX จากสารละลายบัฟเฟอร์โพแทสเซียมอะซิเตตจำเป็นต้องเผา เพื่อเปลี่ยนให้เป็นคาร์บอเนต การเผาเป็นการใช้พลังงานซึ่งทำให้เกิดการพังเชิงโครงสร้างและทำให้ไม่ สามารถนำกลับมาใช้ใหม่ได้ เพื่อลดการใช้พลังงานและปกป้องโครงสร้างซีโอไลต์ จึงได้เตรียมตัวเร่ง ปฏิกิริยาโดยการทำให้เอิบชุ่มด้วยเกลือโพแทสเซียมคาร์บอเนต (K₂CO₃) ลงบนซีโอไลต์ NaX โดยตรง ผลการทดลองพบว่ายังคงรักษาโครงสร้างซีโอไลต์ไว้ได้ ตัวเร่งปฏิกิริยา K₂CO₃/NaX ให้แนวโน้มการ ผลิตไบโอดีเซลเช่นเดียวกับตัวเร่งปฏิกิริยาที่เตรียมโดยใช้สารละลายบัฟเฟอร์อะซิเตต ดังนั้นตัวเร่ง ปฏิกิริยา K₂CO₃/NaX ซึ่งเตรียมได้ด้วยการใช้พลังงานที่น้อยลงนี้จึงมีศักยภาพในการพัฒนาต่อไป

ยิ่งไปกว่านั้น ได้ศึกษาการปรับปรุงการนำกลับมาใช้ใหม่โดยใช้ตัวเร่งปฏิกิริยา Na_2CO_3/NaX เนื่องจาก Na_2CO_3 มีความสามารถในการละลายได้น้อยในสารผสมของผลิตภัณฑ์ การศึกษาพบว่า Na_2CO_3/NaX มีประสิทธิภาพการเร่งปฏิกิริยาน้อยกว่า K_2CO_3/NaX แต่สามารถนำกลับมาใช้ใหม่ได้ดีกว่า
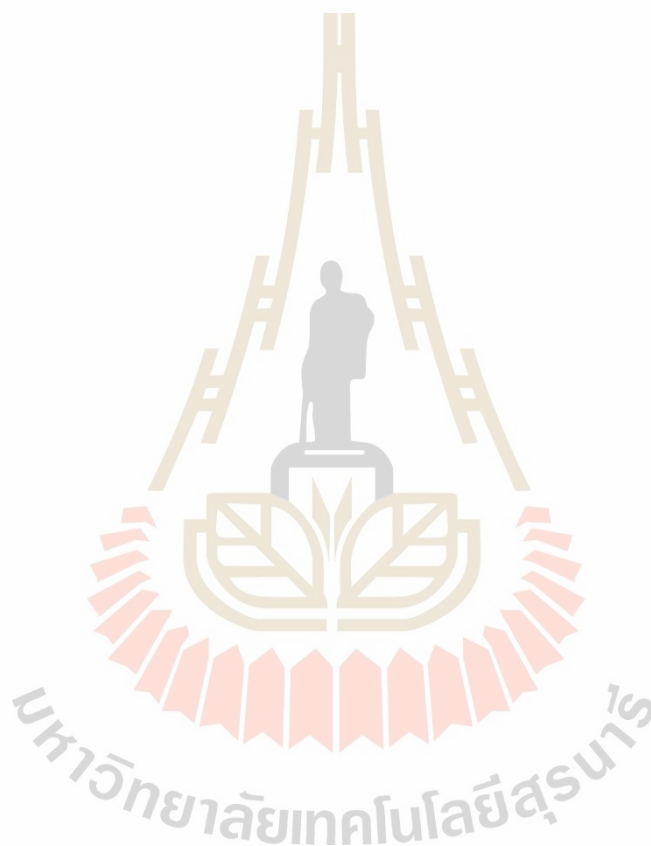
สาขาวิชาเคมี

ปีการศึกษา 2566

ลายมือชื่อนักศึกษา_____

ลายมือชื่ออาจารย์ที่ปรึกษา_____

ลายมือชื่ออาจารย์ที่ปรึกษาร่วม_____

PANOT KRUKKRATOKE : PARAMETERS AFFECTING STABILITY OF FAUJASITE ZEOLITE-SUPPORTED CATALYSTS FOR TRANSESTERIFICATION OF PALM OIL. THESIS ADVISOR : PROF. JATUPORN WITTAYAKUN, Ph.D. 129 PP.

Keywords : FAU Zeolite; Heterogeneous catalyst; Transesterification; Biodiesel

Heterogeneous catalysts comprised of potassium supported on faujasite (FAU) zeolites including NaX and NaY with 12% potassium (12K/NaX and 12K/NaY) were prepared to catalyze the transesterification of palm oil, producing more than 90% biodiesel yields. However, the role of FAU cavities in such catalysts was unclear and the catalysts suffered problems from the collapse of zeolitic structure. To understand the role of FAU cavities, zeolite pores were blocked by paraquat via adsorption before the impregnation of potassium precursor. The obtained catalysts (12K/NaX-PQ and 12K/NaY-PQ) were characterized and used for transesterification of palm oil. The study showed that the role of FAU cavities is not resolved. Moreover, blocking the zeolite cavities with paraquat could not prevent the zeolite collapse.

The effect of FAU cavities was not clearly understood presumably due to high potassium loading. Thus, the same experiment was repeated using potassium 8 wt.%. The biodiesel yields of transesterification on 8K/NaX-PQ and 8K/NaY-PQ were 35.6% and 7.1%, respectively. The higher yield from 8K/NaX-PQ was due to the lower PQ adsorption on NaX, leading to a large crystal size of potassium acetate in the as-prepared sample and more collapse on the zeolite structure. On the other hand, NaY with higher PQ adsorption had good dispersion (namely, small crystal size) of the acetate without significant collapse of zeolite structure. Thus, the role of FAU cavities is proposed to disperse potassium acetate precursor.

The preparation of K/NaX from potassium acetate buffer requires calcination to convert the precursor to carbonate. The calcination process consumes energy and causes structural collapse of the zeolite, resulting in poor reusability. To reduce energy consumption and protect the zeolite structure, the catalyst was prepared by direct impregnation of potassium carbonate salt (K_2CO_3) onto zeolite NaX. The

zeolite structure of the prepared catalysts was still preserved. The K_2CO_3/NaX catalyst had the same results of biodiesel production as the catalyst prepared by using acetate buffer solution. Therefore, the K_2CO_3/NaX catalyst, prepared with less energy consumption, has the potential for further development. Furthermore, Na_2CO_3/NaX catalyst was investigated to improve the reusability due to the less solubility of Na_2CO_3 in the product mixture. The K_2CO_3/NaX catalyst showed a very high biodiesel yield (95.9%) with poor reusability, while the Na_2CO_3/NaX catalyst showed only 70.6% with a gradual drop. The study revealed that Na_2CO_3/NaX was less effective than K_2CO_3/NaX but showed better reusability.
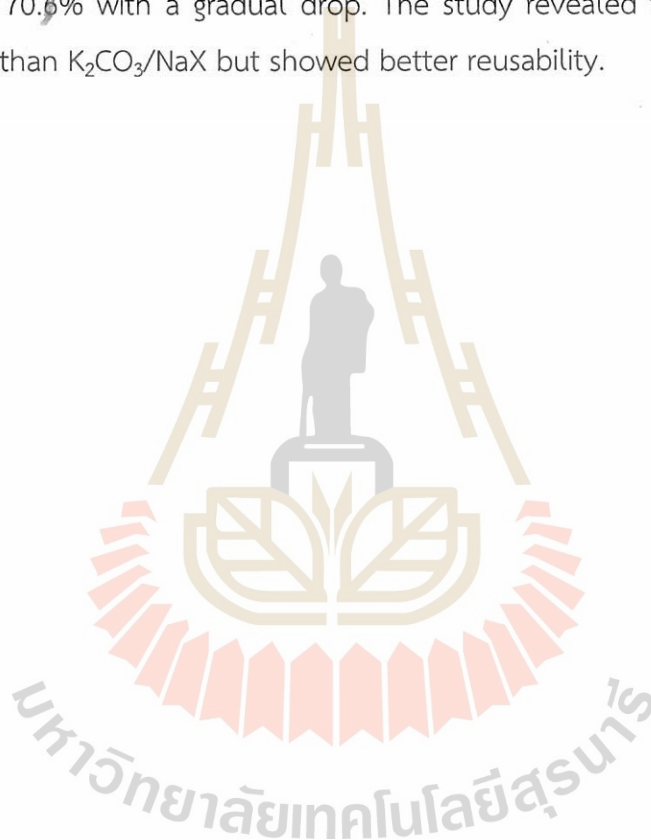
School of Chemistry

Academic Year 2023

Student's Signature_____

Advisor's Signature_____

Co-Advisor's Signature_____

ACKNOWLEDGEMENTS

CONTENTS

CONTENTS (Continued)

CONTENTS (Continued)

LIST OF TABLES

LIST OF FIGURES

LIST OF FIGURES (Continued)

LIST OF FIGURES (Continued)

LIST OF FIGURES (Continued)

LIST OF ABBREVIATIONS

ATR	=	Attenuated total reflectance
DTG	=	Differential thermogravimetry
FAU	=	Faujasite
FID	=	Flame ionization detector
FTIR	=	Fourier Transform Infrared Spectrometer
GC	=	Gas chromatography
GIS	=	Gismondine
HMB	=	3-hydroxy-3-methyl-2-butanone
MBOH	=	2-Methyl-3-butyn-2-ol
MBYNE	=	3-methyl-3-buten-1-yne
MIPK	=	3-methyl-3-buten-2-one
PP	=	Polypropylene
PQ	=	Paraquat (1,1'-dimethyl-4,4'-bipyridinium dichloride)
Prenal	=	3-methyl-2-buten-1-al
SEM	=	Scanning electron microscope
TGMS	=	Thermogravimetric mass-spectrometer
TLC	=	Thin-layer chromatography
UV-Vis	=	Ultraviolet–visible
XRD	=	X-ray diffraction
XRF	=	X-ray Fluorescence

CHAPTER I

INTRODUCTION

Nowadays, there is an international effort for sustainable alternatives for energy sources due to the rising energy demand as well as the environmental issues involving fossil fuels. One promising solution is biodiesel, a renewable and biodegradable fuel derived from plant oils or animal fats and methanol via a reaction called transesterification. Among various feedstocks, palm oil offers a particularly attractive option due to the mass manufacturing in the ASEAN region including Thailand.

A general procedure for transesterification requires a homogeneous base catalyst such as a solution of KOH and NaOH. The catalyst is mixed directly with the feedstock oil and methanol under heat treatment. In the end, the catalyst must be removed by washing it with a large amount of water to produce biodiesel that meets the standards. Such a process produces a large amount of wastewater which requires further treatment.

Heterogeneous catalysts have gained attention to minimize the washing process. Heterogeneous catalysts are commonly solid, a different phase from the reactants and products. They can be separated easily from the biodiesel product. Under optimal conditions, heterogeneous catalysts could be regenerated and reused in subsequent reaction cycles, minimizing waste generation and making the transesterification process more sustainable.

There is a diverse array of heterogeneous catalysts that were recently explored for the transesterification of palm oil including potassium (K) supported on the FAU zeolites (NaX and NaY). Initially, KOH was impregnated on NaY to produce catalysts for the transesterification of palm oil. The catalysts gave high biodiesel yields but the zeolite structure collapsed (Intarapong et al., 2011). To protect the zeolite structure, a milder precursor, CH_3COOK buffer solution was impregnated on zeolite NaY (Supamathanon et al., 2011) to produce catalyst with 4, 8 and 12 wt.% of

potassium. After calcination, the obtained K/NaY samples still showed characteristics of zeolite support. They were tested in the transesterification of jatropha seed oil. The activity increased with potassium loading and the best catalyst was 12K/NaY. This approach was further improved by using zeolite NaX which has a stronger basicity than NaY (Manadee et al., 2017). 12K/NaX gave a higher biodiesel yield than 12K/NaY (Manadee et al., 2017; Supamathanon et al., 2011). Furthermore, the dispersion of potassium species was improved by ultrasound-assisted impregnation (Rakmae et al., 2016). It was confirmed that potassium acetate was transformed to carbonate after calcination. The catalyst had higher basicity and more effective in transesterification of palm oil, reaching equilibrium faster than the catalyst prepared without sonication.

Recently, 12K/NaX and 12K/NaY catalysts from the same preparation method, ultrasound-assisted impregnation were compared and tested under the same conditions (Kosawatthanakun et al., 2022). Almost 100% biodiesel yields were obtained from both catalysts in the first cycle. However, the yields dropped significantly in the second cycle with more decrease from 12K/NaY. They suggested that the deactivation was due to the collapse of zeolite structure by the hydrolysis of the zeolitic bonds with the assistance of potassium ion. They also reported the leaching of potassium into the products.

From the works on 12K/NaX and 12K/NaY mentioned above, the role of zeolite cavity and the cause of collapse are still not clear. Those doubts led to the investigation in Chapter III. To understand the role of zeolite cavities, the catalysts were prepared by impregnation on cavity-blocked zeolites. The compound that could block the cavities of zeolite NaX and NaY is paraquat (Keawkumay et al., 2019; Rongchapo et al., 2017). Thus, Chapter III reports the catalyst preparation by impregnation of potassium acetate buffer on paraquat-adsorbed zeolites, characterization and testing in transesterification of palm oil. When the potassium species are outside the cavities, the collapse of the zeolite structure could be avoided.

From Chapter III, the potassium loading was too high to observe the effect of the zeolite cavity and understand the collapse. Thus, in Chapter IV, a similar investigation was performed with a lower potassium content, namely 8 wt.%.

However, the calcination was considered as the energy consumption. It generated waste of chemicals and time as well as cost. To minimize wastes, the catalysts in Chapter V were prepared by direct impregnation of K_2CO_3 solution without calcination. However, K_2CO_3 had a very high solubility in the mixture of methanol and glycerol (Malins, 2018), resulting in poor reusability. To reduce the solubility, Na_2CO_3, a lower solubility compound, was introduced as another catalyst for transesterification of palm oil. Thus, this chapter also studied the solubility of precursors between K_2CO_3 and Na_2CO_3. This proposed hypothesis did not only eliminate the risk of structural collapse, but the improvement of reusability was also proposed.

1.1   Research objectives

This study employs various experimental techniques to clarify the factors contributing to the structural collapse of potassium-based heterogeneous catalysts used in the transesterification of palm oil, which ultimately hinders their reusability as well as the presence of the synthesis methods for novel heterogeneous catalysts. The first objective is to understand the influence of the FAU cavity on the NaY-supported potassium catalyst by using paraquat-adsorbed zeolite. The second objective is to synthesize a carbonate heterogeneous catalyst on NaX in order to prevent the structural collapse, study the effect of the solubility of precursor (K_2CO_3 and Na_2CO_3) on the heterogeneous catalyst, and improve the recycle ability of the heterogeneous catalyst for transesterification of palm oil. The last objective is to propose the new active species that catalyze the transesterification of palm oil.

1.2   Scope and limitation of the study

This work uses refined palm oil from Sime Darby Oils Morakot Public Co., Ltd., Thailand, paraquat from the farmer shop in Nakhon Ratchasima, and other chemicals with the laboratory grade. The influence of zeolite cavity on transesterification was

studied by impregnation of potassium precursor on paraquat-adsorbed zeolite NaX and NaY. The carbonate catalyst (K_2CO_3/NaX and Na_2CO_3/NaX) was synthesized and studied in the aspect of improvement of the catalyst synthesis as well as the reusability, solubility of the precursor, and indication of the new active species.

1.3   References

Intarapong, P., Luengnaruemitchai, A., and Jai-In, S. (2011). Transesterification of palm oil over KOH/NaY zeolite in a packed-bed reactor. *Int. J. Renew. Energy Res.*, *1*(4), 271–280. doi: https://doi.org/10.20508/ijrer.v1i4.81.g66

Keawkumay, C., Rongchapo, W., Sosa, N., Suthirakun, S., Koleva, I. Z., Aleksandrov, H. A., Vayssilov, G. N., and Wittayakun, J. (2019). Paraquat adsorption on NaY zeolite at various Si/Al ratios: A combined experimental and computational study. *Mater. Chem. Phys.*, *238*, 121824. doi: https://doi.org/10.1016/j.matchemphys.2019.121824

Kosawatthanakun, S., Pansakdanon, C., Sosa, N., Chanlek, N., Roessner, F., Prayoonpokarach, S., and Wittayakun, J. (2022). Comparative properties of K/NaX and K/NaY from ultrasound-assisted impregnation and performance in transesterification of palm oil. *ACS Omega*, *7*(11), 9130–9141. doi: https://doi.org/10.1021/acsomega.1c04912

Malins, K. (2018). The potential of K_3PO_4, K_2CO_3, Na_3PO_4 and Na_2CO_3 as reusable alkaline catalysts for practical application in biodiesel production. *Fuel Process. Technol.*, *179*, 302–312. doi: https://doi.org/10.1016/j.fuproc.2018.07.017

Manadee, S., Sophiphun, O., Osakoo, N., Supamathanon, N., Kidkhunthod, P., Chanlek, N., Wittayakun, J., and Prayoonpokarach, S. (2017). Identification of potassium phase in catalysts supported on zeolite NaX and performance in transesterification of Jatropha seed oil. *Fuel Process. Technol.*, *156*, 62–67. doi: https://doi.org/10.1016/j.fuproc.2016.09.023

Rakmae, S., Keawkumay, C., Osakoo, N., Montalbo, K. D., de Leon, R. L., Kidkhunthod, P., Chanlek, N., Roessner, F., Prayoonpokarach, S., and Wittayakun, J. (2016). Realization of active species in potassium catalysts on zeolite NaY prepared by ultrasound-assisted impregnation with acetate buffer and improved performance

in transesterification of palm oil. *Fuel*, *184*, 512–517. doi: https://doi.org/10.10 16/j.fuel.2016.07.035

Rongchapo, W., Keawkumay, C., Osakoo, N., Deekamwong, K., Chanlek, N., Prayoonpokarach, S., and Wittayakun, J. (2017). Comprehension of paraquat adsorption on faujasite zeolite X and Y in sodium form. *Adsorpt. Sci. Technol.*, *36*(1–2), 684–693. doi: https://doi.org/10.1177/0263617417715394

Supamathanon, N., Wittayakun, J., and Prayoonpokarach, S. (2011). Properties of Jatropha seed oil from Northeastern Thailand and its transesterification catalyzed by potassium supported on NaY zeolite. *J. Ind. Eng. Chem.*, *17*(2), 182–185. doi: https://doi.org/10.1016/j.jiec.2011.02.004

CHAPTER II

LITERATURE REVIEW

Nowadays, there are a lot of green energies to develop for environmentally friendly processes such as solar, wind, geothermal, hydropower, ocean energy, and bioenergy. Among them, biofuel, which is manufactured via an ecologically benign process, is the global source of green energy (Al-Ani et al., 2019). The most intriguing fuels in bioenergy aspect is biodiesel, which is potentially produced by the reaction of transesterification, a chemical reaction between alcohols and triglycerides (TGs), such as vegetable oils or animal fats. In this chapter, the process of biodiesel production through transesterification is described, accompanied with a detail of the history of potassium catalyst for the catalysis of this reaction as well as the related problems. At the end, an objective is proposed to clarify such a problem.

2.1 Transesterification and biodiesel

Transesterification, a reversible reaction, is the exchange of alkyl groups from esters with alkyl groups from alcohols (Tajuddin et al., 2016), as depicts in **Figure 2.1**. Briefly, this reaction, with the help of a catalyst, leads to the formation of fatty acid methyl or ethyl esters (FAMEs or FAEEs, known as biodiesel) and glycerol. It also involves the interaction of methanol or ethanol onto the carbonyl groups from TGs, respectively, and the protonation of the ester oxygen. Ester products are thought of as environmentally friendly diesel fuel for vehicles. Importantly, in order to maximize the product yield and quantity of FAMEs, a higher concentration of excess amount of alcohol is needed. Inevitably, several kinds of lipases or other enzymes, as well as basic or acidic catalysts, must be employed to speed up this process (Zhao et al., 2014).

$$R_1COOCH_2$$
$$R_2COOCH \quad + \quad 3CH_3OH \quad \underset{\longleftarrow}{\xrightarrow{\text{Catalyst}}} \quad HOCH \quad + \quad R_2COOCH_3$$
$$R_3COOCH_2 \qquad\qquad\qquad\qquad\qquad\qquad HOCH_2 \qquad R_3COOCH_3$$

| Triglyceride | Alcohol | Glycerol | Esters |
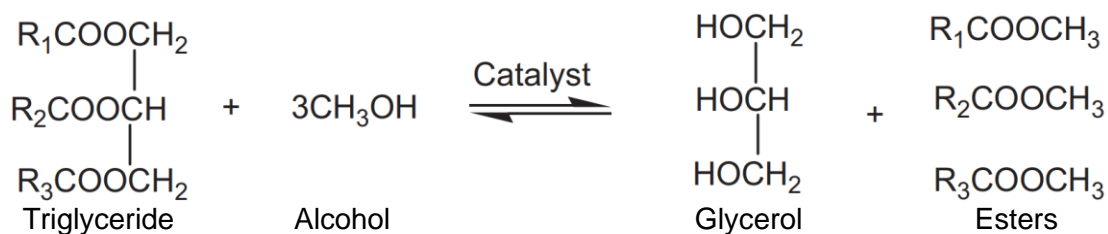
Figure 2.1 The overall transesterification reaction of triglyceride and alcohol.

$$R_1COOCH_2 \qquad\qquad\qquad\qquad\qquad HOCH_2$$
$$R_2COOCH \quad + \quad CH_3OH \quad \xrightarrow{\text{Catalyst}} \quad R_2COOCH \quad + \quad R_1COOCH_3$$
$$R_3COOCH_2 \qquad\qquad\qquad\qquad\qquad R_3COOCH_2$$

Triglyceride · Diglyceride

$$HOCH_2 \qquad\qquad\qquad\qquad\qquad HOCH_2$$
$$R_2COOCH \quad + \quad CH_3OH \quad \xrightarrow{\text{Catalyst}} \quad HOCH \quad + \quad R_2COOCH_3$$
$$R_3COOCH_2 \qquad\qquad\qquad\qquad\qquad R_3COOCH_2$$

Diglyceride · Monoglyceride

$$HOCH_2 \qquad\qquad\qquad\qquad\qquad HOCH_2$$
$$HOCH \quad + \quad CH_3OH \quad \xrightarrow{\text{Catalyst}} \quad HOCH \quad + \quad R_3COOCH_3$$
$$R_3COOCH_2 \qquad\qquad\qquad\qquad\qquad HOCH_2$$

Monoglyceride · Glycerol
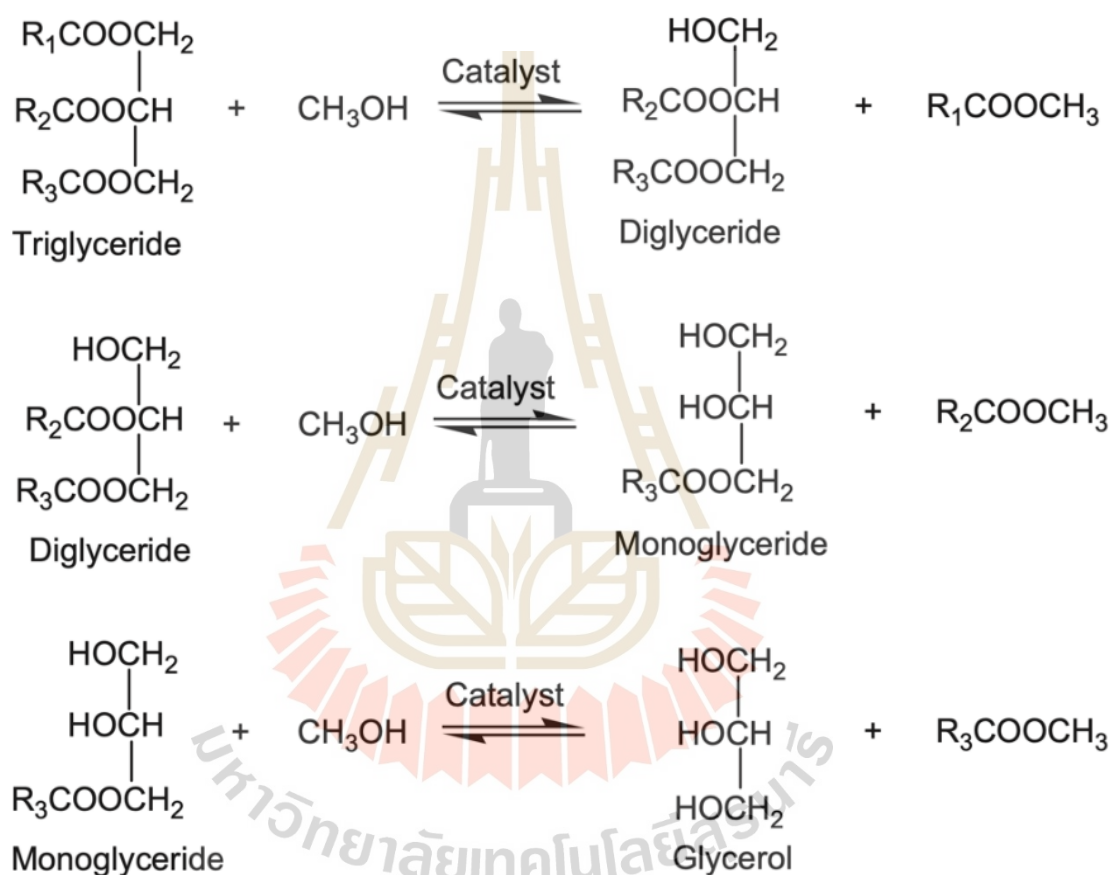
Figure 2.2 The step-by-step mechanism of the transesterification reaction of triglyceride and methanol.

Meanwhile, this process could actually use of several kinds of alcohols, for example, butanol, propanol, ethanol, and methanol (Demirbas, 2005). However, methanol (CH_3OH) is applied popularly. Since it is renewable, extracted from agricultural resources, and naturally less hazardous to the surrounding, ethanol (CH_3CH_2OH) is preferred over other kinds of alcohol (Aransiola et al., 2014). Although methanol is more harmful, it is still the most frequently employed alcohol source for

transesterification owing to its outstanding physical and chemical characteristics and its affordability (Demirbas, 2005).

2.2 Catalysts for transesterification

Transesterification is a step-by-step reversible reaction in which the alkyl group of an alcohol is substituted for the alkyl group of an ester (Tajuddin et al., 2016), as shown in **Figure 2.2**. Alcohol and triglycerides react to produce intermediates that are diglycerides and monoglycerides. Following those interactions with alcohol lead to the production of glycerol and biodiesel. The reaction requires a catalyst. The two primary categories of catalysts used in this manufacturing process are homogeneous and heterogeneous.

2.2.1 Homogeneous catalyst

Homogeneous catalysis is the process that catalyst molecules and reaction substrates exist in a single phase, usually liquid phase. Although homogeneous catalysts offer excellent activities, their separation from the final product presents significant economic and environmental drawbacks due to the large quantities of chemicals, energy, and costs required during the process.

2.2.2 Heterogeneous catalyst

Heterogeneous catalysis is a system where the catalyst and the reacting molecules (reagents) exist in distinct phases. Usually, the catalyst is a solid, while the reactants are in a liquid or gas phase. These catalysts often consist of two key parts: an active component that performs the main reaction and a support material that provides a platform and enhances the activity or stability of the active component (Mardhiah et al., 2017). This process indicates that heterogeneous catalysis improves the separation process as well as the reusability. Heterogeneous catalysts utilized in the production of biodiesel are categorized as acidic and alkaline similar to the homogeneous catalysts (Tan et al., 2015).

In case of the acid-catalyzed transesterification, the catalysts have an ability to control the type of biodiesel produced or tailored biofuels (Kiss, 2009). This allows for adjusting the fatty acid components (esters) in the final product to achieve

specific properties for the biodiesel. However, this difference in reaction speed might be attributed to the ability of the deprotonation of the triglyceride molecule, leading to a more favorable reaction pathway compared to the step of protonation involved in acid catalysis. Such process, which usually found by using basic catalyst, is quicker than an acid-catalyzed reaction. Thus, this thesis focuses on base catalysts.

On the other hand, the fundamental principle of the basic-catalyzed transesterification lies in the formation of a nucleophilic alkoxide from the alcohol molecule, as depicts in **Figure 2.3**. This alkoxide, with its electron-rich oxygen atom, acts as a powerful nucleophile, readily attacking the electrophilic carbon atom in the carbonyl group of the triglyceride molecule. This attack initiates the reaction pathway for biodiesel production (Schuchardt et al., 1998). Similar to acid catalysis, the base-catalyzed mechanism operates on a branch-by-branch basis, meaning that it targets each individual fatty acid chain attached to the glycerol molecule in the triglyceride (Tajuddin et al., 2016). The first step in this process involves a base removing a proton (hydrogen ion) from an alcohol molecule. This deprotonation reaction results in the formation of an alkoxide ion. A common example is the conversion of methanol (an alcohol) into methoxide ion by a base substance (B symbol in **Figure 2.3**). This methoxide ion becomes a strong nucleophile, indicating to has a high affinity for attacking positively charged regions. Then, the resulting alkoxide ion plays a key role. Due to its negative charge, the alkoxide attracted to the positively charged carbonyl carbon atom in the triglyceride. This nucleophilic attack leads to the formation of a tetrahedral carbon intermediate, as shown in the middle of **Figure 2.3**. After that, first fatty acid methyl ester is detached, producing a diglyceride anion (Aransiola et al., 2014). Diglyceride is eventually generated by protonating the diglyceride anion from protonated base substance, and the catalyst subsequently recovers the alkali characteristic (Aransiola et al., 2014; Trejo-Zárraga et al., 2018).
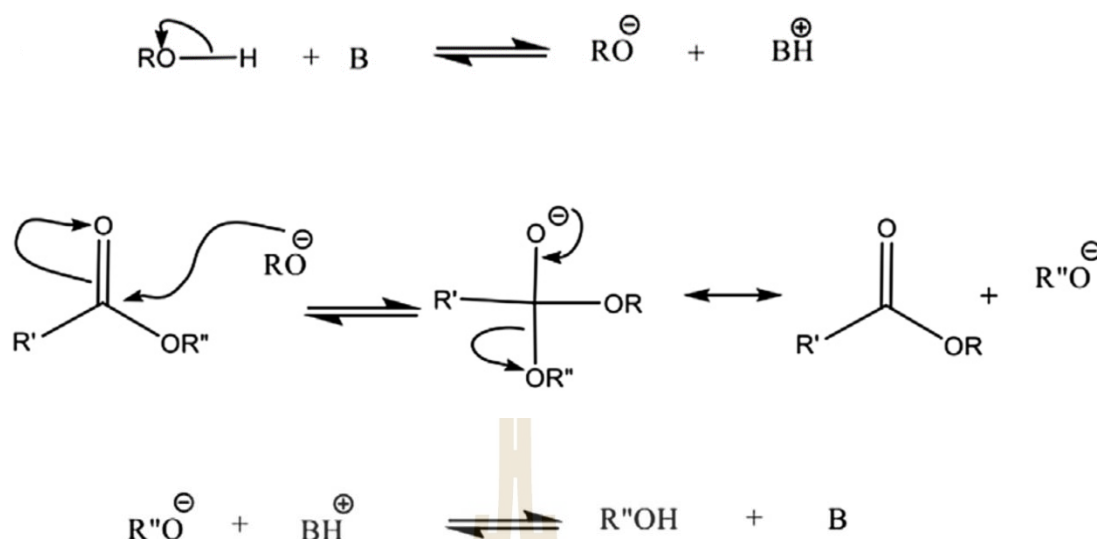
Figure 2.3 Homogeneous base-catalyzed transesterification reaction mechanism
(modified from Aransiola et al., 2014 with permission).

Here is an example of homogeneous base catalysts for the reaction of transesterification (Aransiola et al., 2014; Atadashi et al., 2013; Bohlouli et al., 2021; Ma et al., 1999; Mohandass et al., n.d.). This reaction could be facilitated by such materials. Some research studied metal methoxides, where a metal atom is bonded to a methoxide group ($^-OCH_3$) (Chen et al., 2012; Dias et al., 2008; Sharma et al., 2009). Another example is sodium ethoxide ($NaOC_2H_5$), which is a specific type of metal alkoxide derived from sodium and ethanol. It could also consider broader categories of catalysts such as alkali metal hydroxides (MOH, where M is an alkali metal), which were commonly used in the industrial scale (Demirbas, 2008; Intarapong et al., 2011; Keera et al., 2011; Noiroj et al., 2009; Rashid et al., 2008; Sharma et al., 2009) and alkali metal alkoxides (containing an alkoxide group ^-OR instead of hydroxide) (Behzadi et al., 2009). Even certain carbonate salts, like sodium carbonate (Na_2CO_3) and potassium carbonate (K_2CO_3), could exhibit basic character and act as catalysts under specific reaction conditions (Baroi et al., 2009). As these catalysts are affordable to manufacture while still exhibiting excellent performance. For many years, homogeneous alkali catalysts have been the go-to method for transesterification, from small lab experiments to large-scale industrial production of biodiesel (Frascari et al., 2008; Noureddini et al., 2005). While acidic catalysts can be

used, however, alkaline catalysts are generally more effective. They achieve a higher conversion of triglycerides to the products in a shorter reaction time (Fukuda et al., 2001).

As stated previously, although homogeneous basic catalysts show excellent catalysis, their separation from the product still presents drawbacks. To overcome such problems, an example of basic heterogeneous catalyst is introduced. This includes supporting metal hydroxides or oxides, like those derived from sodium or potassium hydroxide on alumina ($Na/NaOH/Al_2O_3$, (Kim et al., 2004)). Additionally, impregnating Y-zeolites with calcium oxide, calcium carbonate, or calcium hydroxide (CaO/NaY, $CaCO_3/NaY$, and $Ca(OH)_2/NaY$) shows potential for transesterification reaction (Di Serio et al., 2008). Besides, studies are investigating loading metal oxides like calcium oxide, magnesium oxide, and strontium oxide (CaO, MgO, and SrO) onto natural zeolites (Mierczynski et al., 2021). Here are the examples of heterogeneous basic catalysts that are used for transesterification, which derived from the impregnation of KOH or NaO_x on the aluminosilicate support such as $\gamma–Al_2O_3$, zeolite NaY, and zeolite NaX (Noiroj et al., 2009; Suppes et al., 2004). These heterogeneous basic catalysts offer the potential benefits of reusability and potentially milder reaction conditions compared to their homogeneous counterparts.

Biodiesel manufacturing could be costly. The cost of preparing the catalyst and purchasing the raw components as well as the disposal catalysts could cause the process of manufacturing biodiesel costly (Aransiola et al., 2014). Loading a homogeneous catalyst onto the solid supporting material—also referred to as a heterogeneous catalyst—is an alternative approach of inventing an effective catalyst for transesterification, as mentioned previously. Outstanding qualities as similar with the reusability lead to less material being used and lower expenses for manufacturing. (Aransiola et al., 2014).

2.3 Heterogeneous basic catalysts and yield of biodiesel

While homogeneous catalysts could be highly effective for transesterification, heterogeneous catalysts offer distinct advantages. Their reusability eliminates the need for constant replenishment, leading to significant cost savings. In addition, a basic heterogeneous catalyst that achieves comparable performance to a homogeneous catalyst would also offer a significant cost advantage. Such pros was obtained from the structure of heterogeneous catalyst that consists of two parts: the active species and support. For active species, the basic compounds were interested in this work, which was supported by their advantage, as stated in **Section 2.2.2**. For, support, there are plenty materials that housed for the active species. The numerous examples were showed previously. In this work, FAU zeolite was interested.

Zeolites are a fascinating family of materials with microporous crystalline structures made of aluminum (Al) and silicon (Si) sharing tetrahedral units connected by oxygen atoms. The tetrahedral framework of zeolite incorporates aluminum atoms positioned to create a negatively charged framework. This is called primary building unit, as shown in **Figure 2.4a**. These negative charges are balanced by cations such as sodium (Na^+) residing within the pores. Among the various zeolite frameworks, faujasite (FAU) zeolite (**Figure 2.4b**) stands out for its unique properties and broad range of applications. They could not only be easily and economically synthesized but also has a high thermal stability, which is considered to be a suitable material for catalyst preparation. Moreover, the largest pore width is 0.74 nm, which is wide enough for precursor incorporation, compared to other zeolites.

Primary building unit   **FAU structure**
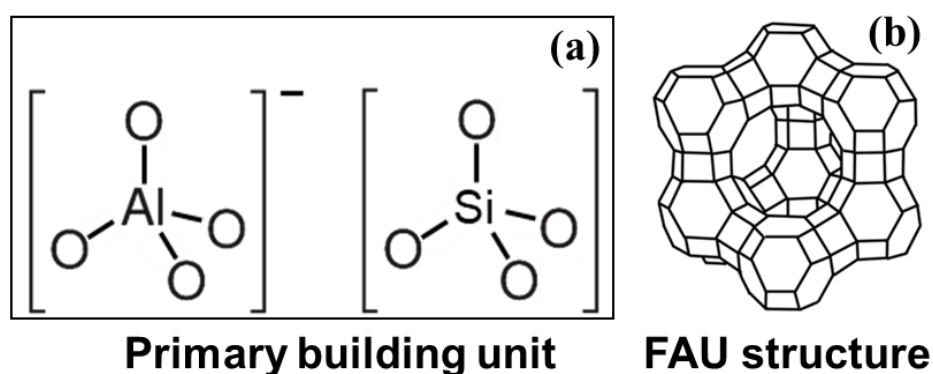
Figure 2.4 The primary building unit of zeolite (a) and FAU structure (b).

FAU zeolite includes two types with different Si/Al ratio (zeolite NaX and NaY). Both types have been used as support for catalyst in the transesterification. Here is the review about the catalyst development that FAU zeolite was used as supporting material. The development of a heterogeneous catalyst crafted by zeolite NaY with the impregnation of potassium hydroxide (KOH) solutions of varying concentrations was presented (Noiroj et al., 2009). The 10%K/NaY catalyst achieved the highest biodiesel yield, exceeding 91%. The researchers further explored the gamma alumina (γ–Al_2O_3) as an alternative support material and discovered that the 25%K/Al_2O_3 catalyst yielded comparable results. Interestingly, X-ray fluorescence (XRF) analysis revealed that potassium (K) species were leached less extensively from zeolite NaY (10%K/NaY: decrease from 5.0% to 4.9%) compared to alumina (25%K/Al_2O_3: decrease 10.7% to 5.2% decrease). However, impregnating zeolite NaX with KOH solution also yielded a promising catalyst, with the 10%K/NaX formulation, demonstrating the highest conversion rate for soybean oil. (Xie et al., 2007). Consistently, both Xie's (KOH/NaX) and Intarapong's (KOH/NaY) studies in 2011 observed a consistent trend, which was the increasing the amount of KOH solution impregnated into the zeolite support initially led to higher biodiesel yields. However, exceeding an optimal precursor loading resulted in a dwindle in oil conversion. (Intarapong et al., 2011; Xie et al., 2007). However, an excessive KOH loading can obstruct the pores of the support material, hindering the accessibility of reactants to the catalytic sites and thereby limiting the effectiveness of the catalyst.

Several studies have documented that exceeding the optimal catalyst loading capacity of a support could lead to structural collapsing problem (Intarapong et al., 2011; Ketzer et al., 2020; Noiroj et al., 2009; Xie et al., 2007). Their results showed that the structural collapsing sample from KOH (very low XRD intensity) produced a high biodiesel yield in the first cycle. However, the poor reusability was still observed (Intarapong et al., 2011). This probably leads to it being uneconomical to use heterogeneous catalysts instead of homogenous. In order to relieve the structural collapse monitored with an excessive catalyst loading, Supamathanon et al. and Manadee et al. explored the use of buffer solutions instead of strong base compounds. Supamathanon and collegues impregnated zeolite NaY with potassium

acetate buffer (CH_3COOK/CH_3COOH), while the same buffer solution with zeolite NaX was employed (Manadee et al., 2017; Supamathanon et al., 2011). Although such precursor seems to be an acidic compound; however, the calcination was carried out after impregnation to produce potassium carbonate, which has a basic property. Besides, utilizing an ultrasound assistance during the impregnation process could significantly enhance the dispersion of active species throughout the support material (Rakmae et al., 2016). In theory, ultrasonic radiation—a sound wave with a frequency higher than that of waves normally audible to humans—was what caused bubbles to form in liquids (Born and Wolf, 1980; Mohammadnezhad et al., 2017). The bubbles keep growing until they explode, resulting in high pressure and temperatures (Soltani et al., 2018).

The literature review reveals several studies exploring the application of ultrasonic radiation in catalyst preparation for transesterification. For example, Ketzer et al. applied the ultrasound-assisted impregnation to synthesize WO_3/USY zeolites, demonstrating their potential as heterogeneous acidic catalysts for transesterification (Ketzer et al., 2020). Their characterizations included the following three advantages of utilizing ultrasound technology. First advantage was the modification of the zeolite framework, which the ultrasound might alter the zeolite structure, effectively creating more accessible sites for reactant molecules. The second benefit of the utilization of the ultrasonic radiation was the preservation of textural properties: compared to conventional methods, ultrasound might lead to a less significant reduction in the zeolite's textural properties, such as pore size and surface area. These textural properties are crucial for reactant diffusion within the catalyst. Additionally, the enhanced interaction between active sites and support was considered as a third advantage of the application of the ultrasonic radiation. Briefly, ultrasound could promote a stronger interaction between the active phase (WO_3) and the zeolite support (USY). However, excessively strong interactions might block some moderate and weak acid sites on the zeolite, potentially reducing overall catalytic activity. Rakmae et al. investigated the impact of ultrasound during catalyst preparation by comparing two methods for creating a potassium acetate buffer catalyst (CH_3COOK-CH_3COOH/NaY) (Rakmae et al., 2016). The catalyst prepared with the ultrasound

assistance also demonstrated several advantages. Firstly, ultrasound facilitated a more uniform distribution of potassium throughout the zeolite (NaY) support material. Secondly, this catalyst achieved a biodiesel yield of 72.0% in just 2 hours, indicating a significant improvement in reaction speed compared to conventional methods. Lastly, analyses using X-ray photoelectron spectroscopy (XPS) and atomic absorption spectroscopy (AAS) revealed that the composition of the active phase remained stable throughout the reaction and during leaching tests. Kosawatthanakun et al. explored the use of ultrasound-assisted impregnation to prepare CH_3COOK-CH_3COOH catalysts using both zeolite NaX and NaY (Kosawatthanakun et al., 2022). Those researches suggested that the ultrasound helped to minimize pore blockage within the support materials (zeolites). This experiment reduced blockage, which contributed to the achievement of higher biodiesel yields. However, even with the application of a gentler precursor and ultrasound, their XRD pattern is still not high compared to bare zeolite, resulting in poor reusability.

According to the structural collapsing catalyst, those materials usually were accompanied by high concentration of precursor (>10% potassium), leading to a high biodiesel yield. Unfortunately, it came together with poor reusability. However, the catalyst containing a lower concentration of precursor also produced low yield. It could be implied that the development of catalysts containing a high concentration of precursor is still necessary.

2.4 Influence of basic compound loading on catalytic performance

As mentioned previously, the potassium carbonate (base substance) was produced after calcination. It implies that higher concentration of potassium acetate buffer results in the higher basicity, leading to better catalysis. So, the effectiveness of heterogeneous basic catalysts is linked to their basicity. **Table 2.1** provides an example of the catalysts, along with their corresponding basicity measurements. Intarapong et al. investigated the influence of KOH loading on zeolite NaY catalysts by impregnating it with varying KOH contents (5, 10, 15, and 20 wt%) (Intarapong et al., 2011). Their research highlights the critical role of basicity in catalyst

performance. They observed a progressive increase in basicity measured using the Hammett titration technique, from 2.47 to 2.70%, as the KOH content increased from 5% to 15% wt. However, exceeding this optimal level (15K/NaY) with 20% KOH resulted in framework collapse. This underlines the importance of finding the optimal basicity for a catalyst. It indicates that the determination of the basicity of heterogeneous catalysts was crucial for optimizing transesterification. A consistent trend was observed in the catalysts listed in **Table 2.1**: regardless of the preparation method, increasing the amount of the basic active phase loaded onto the solid support material generally led to an enhancement in catalyst basicity.

Table 2.1 Examples of heterogeneous catalyst with the basicity measurement.

Catalysts	Quantity of the precursor (% wt)	Technique for basicity measurement	Reference
KOH/NaY	5, 10, 15, and 20	CO_2-TPD, Hammett titration	(Intarapong et al., 2011)
KOH/Al_2O_3	10, 15, 20, 25, 30, and 35	CO_2-TPD	(Noiroj et al., 2009)
KOH/NaY	8, 9, 10, 13, and 15		
CH_3COOK-CH_3COOH/NaY	4, 8, and 12	Pyrrole-TPD and MBOH conversion	(Nuttinee et al., 2012)
$CaNO_3$/Al-MCM-41	10, 20, and 30	XRD	(Vardast et al., 2019)
Bi_2O_3/La_2O_3	1, 2, 3, 5, and 7	CO_2-TPD	(Rabiah Nizah et al., 2014)
CH_3COOK-CH_3COOH/NaX	4, 8, 12, and 16	CO_2-TPD	(Manadee et al., 2017)

In the transesterification research, a significant body of work has investigated the link between a catalyst's basicity and its activity. To assess this crucial property, researchers have used various techniques, including carbon dioxide temperature-programmed desorption (CO_2-TPD), 2-Methyl-3-butyn-2-ol (MBOH) conversion,

Hammett titration, Fourier Transform Infrared Spectrometry (FTIR), and X-ray diffraction (XRD) (Intarapong et al., 2011; Kosawatthanakun et al., 2022; Manadee et al., 2017; Noiroj et al., 2009; Nuttinee et al., 2012; Rabiah Nizah et al., 2014; Vardast et al., 2019). However, each technique provides different accuracy depending on the principles. In this work, XRD analysis, FTIR technique, and MBOH conversion were applied to measure the basicity of the catalyst, which were described with examples below.

2.4.1 X-ray diffraction (XRD)

X-ray diffraction (XRD) has applied as a promising technique for briefly detecting potassium acetate (basic compound). Kosawatthanakun and Rakmae's study employed the XRD analysis to investigate the transformation of the precursor inside their $CH_3COOK-CH_3COOH/FAU$ zeolite catalyst. Interestingly, their analysis revealed that the initially phase converted into K_2CO_3, a basic compound, during catalyst preparation, suggested by Fourier Transform Infrared Spectrometer (FTIR) technique (Kosawatthanakun et al., 2022; Rakmae et al., 2016). Their findings also displayed the bands at 1397 and 1493 cm^{-1}, which was the character of carbonate. Analysis of the as-prepared catalyst using X-ray diffraction (XRD) revealed a diminished signature of the parent FAU zeolite material. Conversely, new peaks emerged at 8.88°, 14.26°, and 27.18°, which corresponded to potassium acetate. Notably, these peaks disappeared after the calcination process. This observation suggested a successful distribution of K_2CO_3, the product of calcination, throughout the zeolite support. In addition, Vardast et al. employed XRD to investigate the crystallinity and presence of impurities in their Al-MCM-41 and CaO samples. They noticed a correlation between sharper peaks in the diffractograms corresponded with an increased calcium content. This suggested that higher calcium loading led to enhanced catalyst alkalinity, effectively transforming into improved catalytic activity for biodiesel production (Vardast et al., 2019).

2.4.2 Fourier Transform Infrared Spectrometer (FTIR)

Fourier Transform Infrared Spectrometer (FTIR) is utilized to determine functional groups in catalysts. The $CH_3COOK-CH_3COOH/FAU$ precursor was changed to K_2CO_3, which is a base, (Kosawatthanakun et al., 2022; Manadee et al., 2017;

Rakmae et al., 2016). Initially, an infrared spectroscopy (likely used) band indicated the presence of acetate, a characteristic signature of an acidic group from precorsor. Interestingly, this band disappeared after calcination, while a new band emerged corresponding to carbonate. Furthermore, the intensity of this new band increased as the concentration of the precursor solution used in catalyst preparation went up. This phenomenon suggests that the intensity of the carbonate band could be a potential tool for measuring the basicity of these catalysts.

2.4.3 MBOH conversion

2-Methyl-3-butyn-2-ol (MBOH) serves as a probe molecule to assess the basic strength of the solid materials. Lauren-Pernot et al. employed MBOH in a dehydration reaction catalyzed by acidic materials like activated alumina or P_2O_5/SiO_2 (Lauron-Pernot et al., 1991). This reaction converts MBOH into 3-methyl-3-buten-1-yne (MBYNE). They tested MBOH decomposition in concentrated sulfuric acid. Their analysis revealed the formation of two byproducts: 3-hydroxy-3-methyl-2-butanone (HMB) and 3-methyl-3-buten-2-one (MIPK). The reaction pathways for MBOH transformation depending on the acidity or basicity of the surrounding environment (**Figure 2.5**). These pathways likely categorize acidic, basic, and amphoteric (having both acidic and basic properties) areas (Alsawalha et al., 2004). The dehydration of MBOH to MBYNE is a reaction that preferentially occurs on surfaces containing weak acidic sites (Supamathanon et al., 2012). The formation of 3-methyl-2-buten-1-al (Prenal) is the result of the isomerization of MBOH through strong acidic sites. Conversely, amphoteric or coordinatively unsaturated (defect) sites contribute to the synthesis of HMB and MIPK. Acetone and acetylene are produced as MBOH degrades at each of the fundamental sites. This technique is coupled with gas chromatography (GC) analysis. By analyzing the peak areas of the resulting chromatogram, researchers can obtain a precise estimation of the catalyst's basicity (Kosawatthanakun et al., 2022). This study employed MBOH conversion, armed with GC analysis, to assess the basicity of zeolite NaX and K/NaX catalysts. The conversion of MBOH for NaX was significantly lower (0.93%) compared to K/NaX (85.90%), as determined by the presence of acetylene and acetone in the GC analysis. These results highlight the sensitivity of the MBOH conversion technique in detecting basicity differences

between catalysts. Among the various methods available, this technique appears to offer a highly accurate approach for basicity measurement.
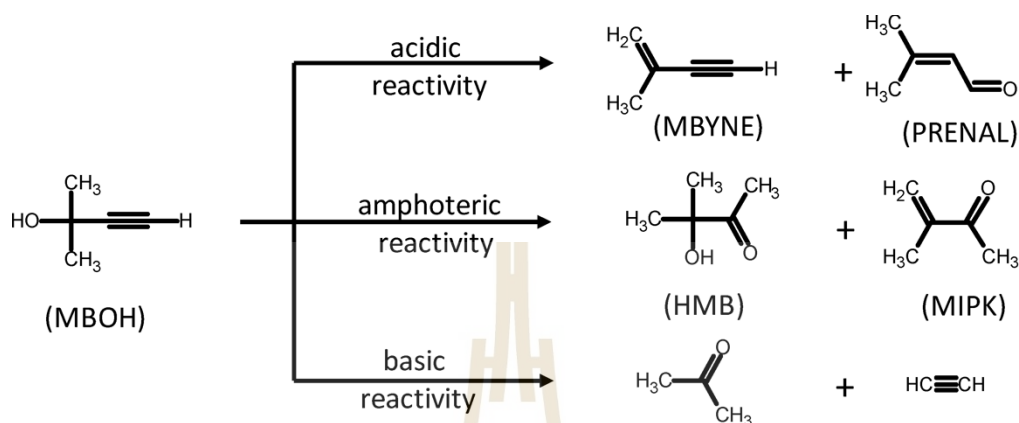
Figure 2.5 The pathway of MBOH conversion depended on characteristic surface of catalyst including acidic, amphoteric, and basic reactivity.

Figure 2.6 demonstrates the example of basicity measurement on potassium catalysts received from MBOH conversion (Kosawatthanakun et al., 2022). The results showed that non-conversion was obtained from bare zeolite. After the catalyst preparation, the MBOH was catalyzed by their potassium catalysts significantly. In addition, potassium supported on zeolite NaX exhibited a higher conversion than on NaY. Besides, this technique could report about the surface properties (acid or base) as mentioned previously. Both catalysts provided 100% basic product (acetylene and acetone). Therefore, these results could confirm the fact that the potassium acetate was calcined to produce potassium carbonate, which corresponds to the FTIR results. Moreover, a higher conversion from K/NaX means that this catalyst had a higher basicity than K/NaY.
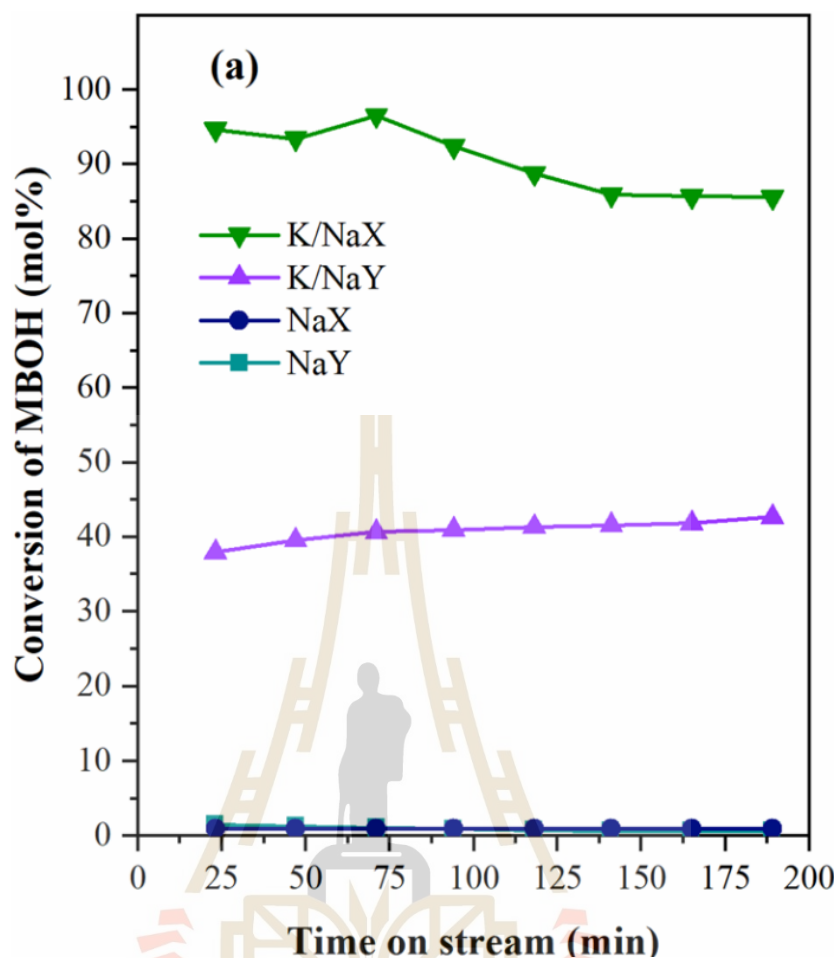
Figure 2.6 MBOH conversion at various times on stream of calcined K/NaX and K/NaY compared to the bare zeolite (Kosawatthanakun et al., 2022).

Despite achieving high biodiesel yields with CH_3COOK buffer/FAU catalysts, Kosawattanakun et al. identified a potential discrepancy. The reactant molecules used in transesterification (26-240 nm in size) are significantly larger than the pores within the FAU zeolite (0.74 nm). However, the transesterification reaction still occurs effectively. This notice led to the researchers to conclude that the active potassium species responsible for catalysis are most likely located on the external surface of the zeolite, rather than within its internal cavities, suggested by XRD. This indicates that K_2CO_3, the active phase for the reaction, resides on the outer surface of the zeolite. Moreover, as stated previously, the structural collapse of support was still a problem in the aspect of reusability. To clarify this concern, this research aims to

investigate such drawbacks by using paraquat-adsorbed zeolites (NaX and NaY) as a support for catalyst preparation in transesterification of palm oil. This investigation was involved the creating of potassium catalysts by first exchanging ions within the FAU zeolite structure with paraquat molecules. However, this initial ion exchange step is expected to cause the paraquat molecules to become trapped inside the zeolite cages, potentially leading to clogged pores and hindering the effectiveness of the catalyst (Keawkumay et al., 2019). Moreover, the precursor was then forced to locate at the external surface of FAU zeolite.

In addition, the preparation of a catalyst for the transesterification of palm oil was also proposed and presented in Chapter V. As mentioned previously, the utilization of potassium acetate buffer solution with calcination exhibited the structural collapse issue, accompanied by poor recyclability. To overcome such problems, potassium carbonate and sodium carbonate were used as precursors instead of potassium acetate buffer solution without calcination. This work related with the solubility of the precursor between potassium carbonate (K_2CO_3) and sodium carbonate (Na_2CO_3). The high reusability was observed by mixing the potassium carbonate into the mixture between methanol and glycerol while sodium carbonate showed poor reusability (Malins, 2018). This observation probably due to an extremely high biodiesel yield in the first cycle, then dramatically dropped in the second run, as reported in the previous literature (Kosawatthanakun et al., 2022). It could be assumed the potential deactivation of catalyst. Therefore, the sodium carbonate might be the outstanding candidate in the aspect of precursor. Although poor recycling ability was received in the sodium carbonate, it indicates that this precursor provided a high recovery ability, resulting in higher yield in the further run. Also, this work was studied to confirm the alkali-catalytic mechanism by carbonate species, as describes in **Figures 2.2** and **2.3**. To address these knowledge gaps, this thesis delves into two key areas: identifying the root causes of collapsing problem of the potassium catalyst and attempting to acquire the potential of carbonate-based catalysts to improve reusability in the transesterification of palm oil.

2.5 References

Al-Ani, A., Mordvinova, N. E., Lebedev, O. I., Khodakov, A. Y., and Zholobenko, V. (2019). Ion-exchanged zeolite P as a nanostructured catalyst for biodiesel production. *Energy Reports*, *5*, 357–363. doi: https://doi.org/10.1016/j.egyr.2019.03.003

Aransiola, E. F., Ojumu, T. V, Oyekola, O. O., Madzimbamuto, T. F., and Ikhu-Omoregbe, D. I. O. (2014). A review of current technology for biodiesel production: State of the art. *Biomass & Bioenergy*. *61*, 276–297. doi: https://doi.org/10.1016/j.biombioe.2013.11.014

Atadashi, I. M., Aroua, M. K., Abdul Aziz, A. R., and Sulaiman, N. M. N. (2013). The effects of catalysts in biodiesel production: A review. *J. Ind. Eng. Chem.*, *19*(1), 14–26. doi: https://doi.org/10.1016/j.jiec.2012.07.009

Baroi, C., Yanful, E., and Bergougnou, M. (2009). Biodiesel production from Jatropha *curcas* oil using potassium carbonate as an unsupported catalyst. *Int. J. Chem. React. Eng.*, *7*(1), 1–18. doi: https://doi.org/10.2202/1542-6580.2027

Behzadi, S. and Farid, M. M. (2009). Production of biodiesel using a continuous gas–liquid reactor. *Bioresour. Technol.*, *100*(2), 683–689. doi: https://doi.org/10.1016/j.biortech.2008.06.037

Bohlouli, A. and Mahdavian, L. (2021). Catalysts used in biodiesel production: a review. *Biofuels*, *12*(8), 885–898. doi: https://doi.org/10.1080/17597269.2018.1558836

Born, M. A. X. and Wolf, E. (1980). Chapter XIII - Optics of Metals. in M. A. X. Born & E. Wolf (Eds.), Principles of Optics (Sixth Edition) (pp. 611–664). Pergamon. doi: https://doi.org/10.1016/B978-0-08-026482-0.50020-7

Chen, K.-S., Lin, Y.-C., Hsu, K.-H., and Wang, H.-K. (2012). Improving biodiesel yields from waste cooking oil by using sodium methoxide and a microwave heating system. *Energy*, *38*(1), 151–156. doi: https://doi.org/10.1016/j.energy.2011.12.020

Demirbas, A. (2005). Biodiesel production from vegetable oils via catalytic and non-catalytic supercritical methanol transesterification methods. *Prog. Energy Combust. Sci.*, *31*(5), 466–487. doi: https://doi.org/10.1016/j.pecs.2005.09.001

Demirbas, A. (2008). Comparison of transesterification methods for production of biodiesel from vegetable oils and fats. *Energy Convers. Manag.*, *49*(1), 125–130. doi: https://doi.org/10.1016/j.enconman.2007.05.002

Alsawalha, M., Rößner, F., and Al-Shamery, K. (2004). Characterization of acidic and basic properties of heterogeneous catalysts by test reactions.

Di Serio, M., Tesser, R., Pengmei, L., and Santacesaria, E. (2008). Heterogeneous catalysts for biodiesel production. *Energy & Fuels*, *22*(1), 207–217. doi: https://doi.org/10.1021/ef700250g

Dias, J. M., Alvim-Ferraz, M. C. M., and Almeida, M. F. (2008). Comparison of the performance of different homogeneous alkali catalysts during transesterification of waste and virgin oils and evaluation of biodiesel quality. *Fuel*, *87*(17), 3572–3578. doi: https://doi.org/10.1016/j.fuel.2008.06.014

Frascari, D., Zuccaro, M., Pinelli, D., and Paglianti, A. (2008). A pilot-scale study of alkali-catalyzed sunflower oil transesterification with static mixing and with mechanical agitation. *Energy & Fuels*, *22*(3), 1493–1501. doi: https://doi.org/10.1021/ef700584h

Fukuda, H., Kondo, A., and Noda, H. (2001). Biodiesel fuel production by transesterification of oils. *J. Biosci. Bioeng.*, *92*(5), 405–416. doi: https://doi.org/10.1016/S1389-1723(01)80288-7

Intarapong, P., Luengnaruemitchai, A., and Jai-In, S. (2011). Transesterification of palm oil over KOH/NaY zeolite in a packed-bed reactor. *Int. J. Renew. Energy Res.*, *1*(4), 271–280. doi: https://doi.org/10.20508/ijrer.v1i4.81.g66

Keawkumay, C., Rongchapo, W., Sosa, N., Suthirakun, S., Koleva, I. Z., Aleksandrov, H. A., Vayssilov, G. N., and Wittayakun, J. (2019). Paraquat adsorption on NaY zeolite at various Si/Al ratios: A combined experimental and computational study. *Mater. Chem. Phys.*, *238*, 121824. doi: https://doi.org/10.1016/j.matchemphys.2019.121824

Keera, S. T., El Sabagh, S. M., and Taman, A. R. (2011). Transesterification of vegetable oil to biodiesel fuel using alkaline catalyst. *Fuel*, *90*(1), 42–47. doi: https://doi.org/10.1016/j.fuel.2010.07.046

Ketzer, F., Celante, D., and de Castilhos, F. (2020). Catalytic performance and ultrasonic-assisted impregnation effects on WO$_3$/USY zeolites in esterification of oleic acid with methyl acetate. *Microporous & Mesoporous Mater*, *291*, 109704. doi: https://doi.org/10.1016/j.micromeso.2019.109704

Kim, H.-J., Kang, B.-S., Kim, M.-J., Park, Y. M., Kim, D.-K., Lee, J.-S., and Lee, K.-Y. (2004). Transesterification of vegetable oil to biodiesel using heterogeneous base catalyst. *Catal. Today*, *93–95*, 315–320. doi: https://doi.org/10.1016/j.cattod.2004.06.007

Kiss, A. A. (2009). Novel process for biodiesel by reactive absorption. *Sep. Purif. Technol.*, *69*(3), 280–287. doi: https://doi.org/10.1016/j.seppur.2009.08.004

Kosawatthanakun, S., Pansakdanon, C., Sosa, N., Chanlek, N., Roessner, F., Prayoonpokarach, S., and Wittayakun, J. (2022). Comparative properties of K/NaX and K/NaY from ultrasound-assisted impregnation and performance in transesterification of palm oil. *ACS Omega*, *7*(11), 9130–9141. doi: https://doi.org/10.1021/acsomega.1c04912

Lauron-Pernot, H., Luck, F., and Popa, J. M. (1991). Methylbutynol: a new and simple diagnostic tool for acidic and basic sites of solids. *Appl. Catal.*, *78*(2), 213–225. doi: https://doi.org/10.1016/0166-9834(91)80107-8

Ma, F. and Hanna, M. A. (1999). Biodiesel production: a review1Journal Series #12109, Agricultural Research Division, Institute of Agriculture and Natural Resources, University of Nebraska–Lincoln.1. *Bioresour. Technol.*, *70*(1), 1–15. doi: https://doi.org/10.1016/S0960-8524(99)00025-5

Malins, K. (2018). The potential of K$_3$PO$_4$, K$_2$CO$_3$, Na$_3$PO$_4$ and Na$_2$CO$_3$ as reusable alkaline catalysts for practical application in biodiesel production. *Fuel Process. Technol.*, *179*, 302–312. doi: https://doi.org/10.1016/j.fuproc.2018.07.017

Manadee, S., Sophiphun, O., Osakoo, N., Supamathanon, N., Kidkhunthod, P., Chanlek, N., Wittayakun, J., and Prayoonpokarach, S. (2017). Identification of potassium phase in catalysts supported on zeolite NaX and performance in transesterification of Jatropha seed oil. *Fuel Process. Technol.*, *156*, 62–67. doi: https://doi.org/10.1016/j.fuproc.2016.09.023

Mardhiah, H. H., Ong, H. C., Masjuki, H. H., Lim, S., and Lee, H. V. (2017). A review on latest developments and future prospects of heterogeneous catalyst in biodiesel production from non-edible oils. *Renew. Sustain. Energy Rev., 67*, 1225–1236. doi: https://doi.org/10.1016/j.rser.2016.09.036

Mierczynski, P., Szkudlarek, L., Chalupka, K., Maniukiewicz, W., Wahono, S. K., Vasilev, K., and Szynkowska-Jozwik, M. I. (2021). The effect of the activation process and metal oxide addition (CaO, MgO, SrO) on the catalytic and physicochemical properties of natural zeolite in transesterification reaction. *Materials, 14*(9), 2415. doi: https://doi.org/10.3390/ma14092415

Mohammadnezhad, G., Abad, S., Soltani, R., and Dinari, M. (2017). Study on thermal, mechanical and adsorption properties of amine-functionalized MCM-41/PMMA and MCM-41/PS nanocomposites prepared by ultrasonic irradiation. *Ultrason. Sonochem., 39*, 765–773. doi: https://doi.org/10.1016/j.ultsonch.2017.06.001

Mohandass, R., Ashok, K., Selvaraju, A., and Rajagopan, S. (n.d.). *Homogeneous Catalysts used in Biodiesel Production: A Review*. Retrieved from http://www. ijert.org

Noiroj, K., Intarapong, P., Luengnaruemitchai, A., and Jai-In, S. (2009). A comparative study of KOH/Al_2O_3 and KOH/NaY catalysts for biodiesel production via transesterification from palm oil. *Renew. Energy, 34*(4), 1145–1150. doi: https://doi.org/10.1016/j.renene.2008.06.015

Noureddini, H., Gao, X., and Philkana, R. S. (2005). Immobilized pseudomonas *cepacia* lipase for biodiesel fuel production from soybean oil. *Bioresour. Technol., 96*(7), 769–777. doi: https://doi.org/10.1016/j.biortech.2004.05.029

Nuttinee, S., Jatuporn, W., Sanchai, P., Wojciech, S., and Frank, R. (2012). Basic properties of potassium oxide supported on zeolite Y studied by pyrrole-TPD and catalytic conversion of methylbutynol. *Quim. Nova, 35*(9), 1719-1723. doi: https://doi.org/10.1590/S0100-40422012000900003

Rabiah Nizah, M. F., Taufiq-Yap, Y. H., Rashid, U., Teo, S. H., Shajaratun Nur, Z. A., and Islam, A. (2014). Production of biodiesel from non-edible Jatropha *curcas* oil via transesterification using Bi_2O_3–La_2O_3 catalyst. *Energy Convers. Manag., 88*, 1257–1262. doi: https://doi.org/10.1016/j.enconman.2014.02.072

Rakmae, S., Keawkumay, C., Osakoo, N., Montalbo, K. D., de Leon, R. L., Kidkhunthod, P., Chanlek, N., Roessner, F., Prayoonpokarach, S., and Wittayakun, J. (2016). Realization of active species in potassium catalysts on zeolite NaY prepared by ultrasound-assisted impregnation with acetate buffer and improved performance in transesterification of palm oil. *Fuel*, *184*, 512–517. doi: https://doi.org/10.1016/j.fuel.2016.07.035

Rashid, U., Anwar, F., Moser, B. R., and Ashraf, S. (2008). Production of sunflower oil methyl esters by optimized alkali-catalyzed methanolysis. *Biomass & Bioenergy*, *32*(12), 1202–1205. doi: https://doi.org/10.1016/j.biombioe.2008.03.001

Schuchardt, U., Sercheli, R., and Matheus, V. (1998). Transesterification of vegetable oils: A review. *J. Braz. Chem. Soc.*, *9*(1), 199–219. doi: https://doi.org/10.1590/S0103-50531998000300002

Sharma, Y. C. and Singh, B. (2009). Development of biodiesel: Current scenario. *Renew. Sustain. Energy Rev.*, *13*(6), 1646–1651. doi: https://doi.org/10.1016/j.rser.2008.08.009

Soltani, R., Dinari, M., and Mohammadnezhad, G. (2018). Ultrasonic-assisted synthesis of novel nanocomposite of poly(vinyl alcohol) and amino-modified MCM-41: A green adsorbent for Cd(II) removal. *Ultrason. Sonochem.*, *40*, 533–542. doi: https://doi.org/10.1016/j.ultsonch.2017.07.045

Supamathanon, N., Wittayakun, J., and Prayoonpokarach, S. (2011). Properties of Jatropha seed oil from Northeastern Thailand and its transesterification catalyzed by potassium supported on NaY zeolite. *J. Ind. Eng. Chem.*, *17*(2), 182–185. doi: https://doi.org/10.1016/j.jiec.2011.02.004

Suppes, G. J., Dasari, M. A., Doskocil, E. J., Mankidy, P. J., and Goff, M. J. (2004). Transesterification of soybean oil with zeolite and metal catalysts. *Appl. Catal. A Gen.*, *257*(2), 213–223. doi: https://doi.org/10.1016/j.apcata.2003.07.010

Tajuddin, N. A., Lee, A. F., and Wilson, K. (2016). 6 - Production of biodiesel via catalytic upgrading and refining of sustainable oleagineous feedstocks. In R. Luque, C. S. K. Lin, K. Wilson, & J. Clark (Eds.), Handbook of Biofuels Production (Second Edition) (pp. 121–164). Woodhead Publishing. doi: https://doi.org/10.1016/B978-0-08-100455-5.00006-0

Tan, Y. H., Abdullah, M. O., Nolasco-Hipolito, C., and Taufiq-Yap, Y. H. (2015). Waste ostrich- and chicken-eggshells as heterogeneous base catalyst for biodiesel production from used cooking oil: Catalyst characterization and biodiesel yield performance. *Appl. Energy*, *160*, 58–70. doi: https://doi.org/10.1016/j.apenergy. 2015.09.023

Trejo-Zárraga, F., Hernández-Loyo, F. de J., Chavarría-Hernández, J. C., and Sotelo-Boyás, R. (2018). Kinetics of Transesterification Processes for Biodiesel Production. In K. Biernat (Ed.), Biofuels (p. Ch. 8). Rijeka: IntechOpen. doi: https://doi.org/10.5772/intechopen.75927

Vardast, N., Haghighi, M., and Dehghani, S. (2019). Sono-dispersion of calcium over Al-MCM-41 used as a nanocatalyst for biodiesel production from sunflower oil: Influence of ultrasound irradiation and calcium content on catalytic properties and performance. *Renewable Energy*, *132*, 979–988. doi: https://doi.org/10.1016/j.renene.2018.08.046

Xie, W., Huang, X., and Li, H. (2007). Soybean oil methyl esters preparation using NaX zeolites loaded with KOH as a heterogeneous catalyst. *Bioresour. Technol.*, *98*(4), 936–939. doi: https://doi.org/10.1016/j.biortech.2006.04.003

Zhao, T., No, D. S., Kim, Y., Kim, Y. S., and Kim, I.-H. (2014). Novel strategy for lipase-catalyzed synthesis of biodiesel using blended alcohol as an acyl acceptor. *J. Mol. Catal. B Enzym.*, *107*, 17–22. doi: https://doi.org/10.1016/j.molcatb.2014.05.002

CHAPTER III

COMPARISON OF 12% POTASSIUM ON PARAQUAT-MODIFIED ON ZEOLITE SODIUM X AND Y FOR TRANSESTERIFICATION OF PALM OIL

3.1 Abstract

Faujasite (FAU) zeolites including NaX and NaY have been used as supports to disperse potassium species of heterogeneous catalysts for transesterification. However, the role of the zeolite cavity is still not clear. Those catalysts still suffer the structural collapsing problem from the hydrolysis of the zeolitic bond assisted by potassium. In this work, paraquat (PQ) is adsorbed on both FAU zeolites to block the FAU cavity and force the potassium precursor outside the zeolite. The modified zeolites are then impregnated with potassium acetate buffer solution and calcined to give 12K/NaX and 12K/NaY catalysts with 12 wt% of potassium loading. The catalysts are presumed to have potassium carbonate dispersed mainly on zeolite external surface. In transesterification, both 12K/NaX-PQ and 12K/NaY-PQ produced biodiesel yields of 62.7% and 60.4%, respectively in the first cycle. The catalysts still suffer from the leaching of active species and structural collapse. This observation comes with minimal potassium loss, while sodium and carbonate content decreased after calcination. This suggests ion exchange, leading to structural collapse.

3.2 Introduction

The escalating demand for renewable and sustainable energy sources has propelled various developments including biodiesel production process. Biodiesel is a renewable energy source produced from transesterification, a reaction between triglycerides (fats/oils) and alcohol (often methanol). The industrial process generally employs a homogeneous catalyst which requires a large amount of water to wash out the catalyst from the biodiesel product. As a result, the homogeneous catalyst is very

difficult to recover and reuse. Such drawbacks of homogeneous catalysts lead to research to develop heterogeneous catalysts to increase the opportunity for a more environmentally friendly and sustainable approach.

Potassium (K) supported on faujasite (FAU) zeolites are among several heterogeneous catalysts. KOH was impregnated on zeolite NaY catalysts to create K/NaY with 15 weight percent K (Intarapong et al., 2011). The catalyst produced 92.18% of the biodiesel. Nevertheless, high potassium loading resulted in catalyst aggregation. Furthermore, the increased temperature and higher potassium loading caused the zeolite structure to collapse, which decreased activity. As a result, the precursor was changed to a potassium acetate buffer solution to lessen the collapse problem of NaY (Supamathanon et al., 2011). Their best catalyst was 12K/NaY with 12 wt.% potassium content. Furthermore, an ultrasound-assisted impregnation approach was applied to improve the dispersion of potassium species on 12K/NaY (Rakmae et al., 2016). The better dispersion resulted in a shorter reaction time to produce the highest biodiesel yield. However, the low crystallinity of zeolite NaY was still observed in their XRD pattern. An attempt to enhance the catalyst performance was made by using a more basic zeolite, NaX as a support for potassium (Manadee et al., 2017). The biodiesel yields increased with the catalyst basicity from the higher potassium content.

The variety of works on transesterification mentioned above includes the different types of oil feedstocks and zeolite, catalyst preparation methods and reaction conditions. A direct comparison between 12K/NaX and 12K/NaY from the same potassium precursor and reaction conditions (Kosawatthanakun et al., 2022). 12K/NaX catalyst gave a higher biodiesel yield and better reusability in the second cycle than 12K/NaY. They reported problems with catalyst stability due to the zeolite structural collapse after calcination and the leaching of potassium species to the glycerol and biodiesel product. The zeolite collapse could be from the presence of potassium in the zeolite cavity which could accelerate the breakdown of Si-O-Al bonds. However, such an assumption still needs further investigation.

This work aims to prove that the presence of potassium in zeolite cavity was responsible for the structural collapse. Zeolite NaX and NaY are pretreated with paraquat, 1,1'-dimethyl-4,4'-bipyridinium dichloride which is commonly referred to as

paraquat (PQ) to occupy the zeolite cavities. PQ could be adsorbed by NaX and NaY by ion exchange with sodium cations in the zeolite cavities (Rongchapo et al., 2017). The adsorption capacity of NaY is higher than that of NaX due to the weaker interaction between sodium cations and the negative zeolite framework charge. It was further confirmed that each supercage cavity of zeolite NaY could accommodate two PQ molecules (Keawkumay et al., 2019) as shown in Figure 3.1.
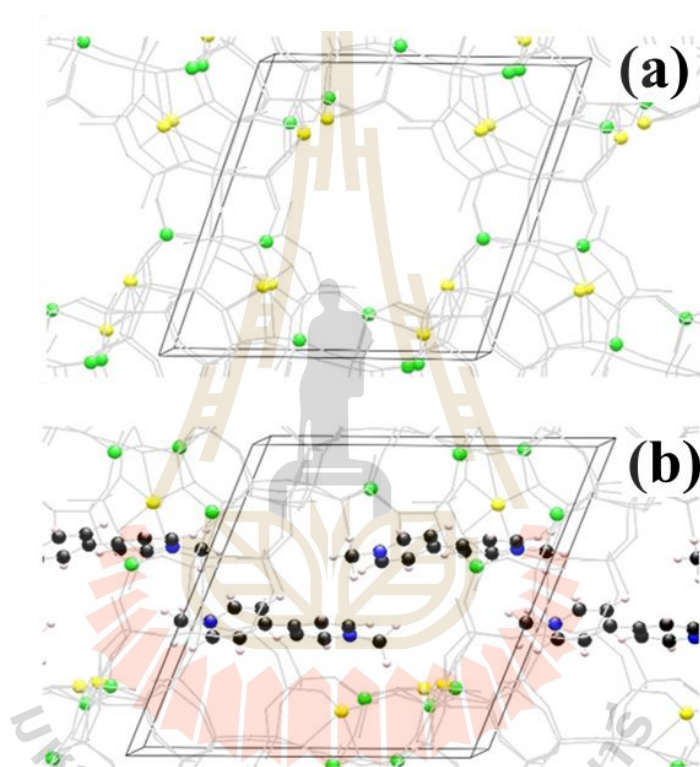
Figure 3.1   Simulated images of bare NaY zeolite (a) and zeolite with two adsorbed-paraquat molecules per unit cell (b). Color coding of different centers is shown in panel b: Al – green, Na – yellow, C – black, N – blue, H – light pink; Si and O centers are not shown. (Modified from (Keawkumay et al., 2019) with permission).

In this work, NaX and NaY are loaded with paraquat to occupy the zeolite supercages before impregnation with a potassium acetate buffer solution. The potassium precursor is presumed to be located only on the zeolite's external surface.

The as-prepared and calcined catalysts are characterized by XRD, FTIR, XRF, and MBOH conversion, and tested in transesterification of palm oil.

3.3 Experimental

3.3.1 Chemicals and Materials

The following chemicals were used for the synthesis of zeolites: fumed silica (SiO_2, CARLO ERBA, 99%), sodium aluminate ($NaAlO_2$, SIGMA-ALDRICH, Al-(Al_2O_3): 50-56% and Na-(Na_2O): 40-45%), sodium hydroxide (NaOH, CARLO ERBA, 97.0%). The marketable-grade paraquat (Masda, 27.6 %w/v) was purchased from a nearby agro shop in Nakhon Ratchasima, Thailand. Commercial zeolite NaX (SIGMA-ALDRICH with the powder form, ~2 μm average particle size) was obtained to compare synthesized zeolite NaX. Acetate buffer solution was prepared by using acetic acid (CH_3COOH, RCI Labscan Limited, 99.7%) and potassium acetate (CH_3COOK, CARLO ERBA, 99%). In transesterification, methanol (CH_3OH, Sigma-Aldrich, 99.8%), Hexane (C_6H_{14}, CARLO ERBA, 96%) and refined palm oil, used in this present research obtained from Sime Darby Oils Morakot Public Co., Ltd, Thailand, was used.

3.3.2 Synthesis of zeolite NaX and NaY

NaX was synthesized by a procedure modified from the literature (Jantarit et al., 2020) to produce the product with a Si/Al ratio of approximately 1.0 and an overall molar gel ratio of $NaAlO_2$: $4SiO_2$: $16NaOH$: $325H_2O$. In brief, 54.48 g of NaOH was dissolved in 527.7 g of DI water, 8.16 g of $NaAlO_2$ was then added. The mixture was stirred for 30 minutes; at that time, a clear solution was achieved. After that, the mixture was added by 87.72 g of Na_2SiO_3, stirred for 1 hour, capped and sealed, and hydrothermally crystallized at 90 °C for 24 hours. The sample was washed with DI water several times until neutral by centrifugation at 4000 rpm for 5 min. Finally, the sample was dried at 100 °C for overnight.

Zeolite NaY with a Si/Al ratio of approximately 2.0 was synthesized from an overall gel molar ratio of $4.62Na_2O$: $1Al_2O_3$: $10SiO_2$: $180H_2O$ with a method adapted from the literature (Keawkumay et al., 2019). Firstly, in a polypropylene (PP) bottle, 2.04 g of NaOH was dissolved in 9.974 g of DI water. Next, 1.045 g of anhydrous $NaAlO_2$ was added to the alkali solution. The mixture was stirred until the solution was

transparent. Then, 11.31 g of Na$_2$SiO$_3$ solution was poured. After that, the mixture, so-called a seed gel, was stirred for 10 minutes before being covered and aged for 24 hours at room temperature.

The process for creating a feedstock gel was thereafter the same as that used to generate a seed gel, with the exception that it was used immediately and not aged. Briefly, 6.547 g of NaAlO$_2$ was added and stirred until the solution becomes clear after 0.07 g of NaOH has been dissolved in 65.485 g of DI water in a PP bottle. Then, 71.205 g of Na$_2$SiO$_3$ was added dropwise. After that, the overall gel was produced by pouring feedstock gel to seed gel, capping, and sealing the mixture, and hydrothermally crystallizing it at 90 °C for 24 hours. Finally, the sample was washed and dried with the same procedure zeolite NaX.

3.3.3 Preparation of paraquat-modified zeolites

The PQ adsorption on NaX and NaY was carried out according to the previous work (Keawkumay et al., 2019). In a beaker filled with 1000 ppm of paraquat solution (1:400 w/v), 7 g of each adsorbent was added. At room temperature (25 °C), the mixture was stirred for 3 hours at a speed of 500 rpm. To prevent the excess PQ crystal deposited on the external surface of zeolite, the PQ-adsorbed powder was washed with DI water five times at 4000 rpm for 10 minutes, and the concentration of PQ is determined by UV-Vis spectrophotometer. The powder was dried at 100 °C for overnight. A UV-Vis spectrophotometer (Varian CARY 300) was used to calculate the remaining paraquat concentration. The amount of PQ adsorbed at equilibrium (q_e) was estimated by the equation below

$$q_e = \frac{(C_0 - C_e) \times V}{w} \tag{1}$$

where C_0 and C_e are the initial and equilibrium concentration of paraquat (mg/L). V and w are the volume of paraquat solution (L) and the amount of adsorbent (g).

Figure 3.2a shows the scanning UV-Vis spectrum of 10 ppm commercial PQ solution, and DI water was employed as solvent and blank solution. The maximum wavelength was at 191 nm and 257 nm, which the position at 257 nm was able to be

utilized for the measurement of PQ concentration. The calibration curve was prepared between 2 to 10 ppm, which is depicted in **Figure 3.2b**. Moreover, the linear regression from these points was y = 0.08014x + 0.00129 with R^2 = 0.99926. This equation was also used for calculation of equilibrium adsorption capacity (q_e). The synthesized zeolite NaX and NaY exhibited 46.7 and 146.4 $mg_{paraquat}/g_{zeolite}$, respectively. This adsorption result was consistent with the literature that the paraquat adsorption by using zeolite NaY as as adsorbent performed better than zeolite NaX (Rongchapo et al., 2017). Moreover, the low capacity might be caused by the zeolite NaP. GIS structure of zeolite NaP had only 3.32 Å of pore width, which was lower than the FAU structure (7.35 Å), resulting in inability to enter the zeolite. This finding corresponded with 3 credit Krukkratoke's thesis in Bachelor degree, 2018, Suranaree University of Technology (SUT), which reported that the maximum PQ adsorption capacity (q_m) reduced significantly when the zeolite phase transferred from NaY to NaP.

Figure 3.2c provides the scanning UV-Vis spectrum of PQ solution collected from the liquid layer after centrifugation. All spectra were compared to DI water (purple line with no peak). The strong peak with the light blue shade in the liquid layer were still observed after the second washing of the PQ-adsorbed zeolite. Note that the blue was not the color of paraquat. The liquid was then colorless after centrifugation for the 3rd time. Finally, the low intensity at 257 nm was exhibited at the last washing, which was ready for the catalyst synthesis.

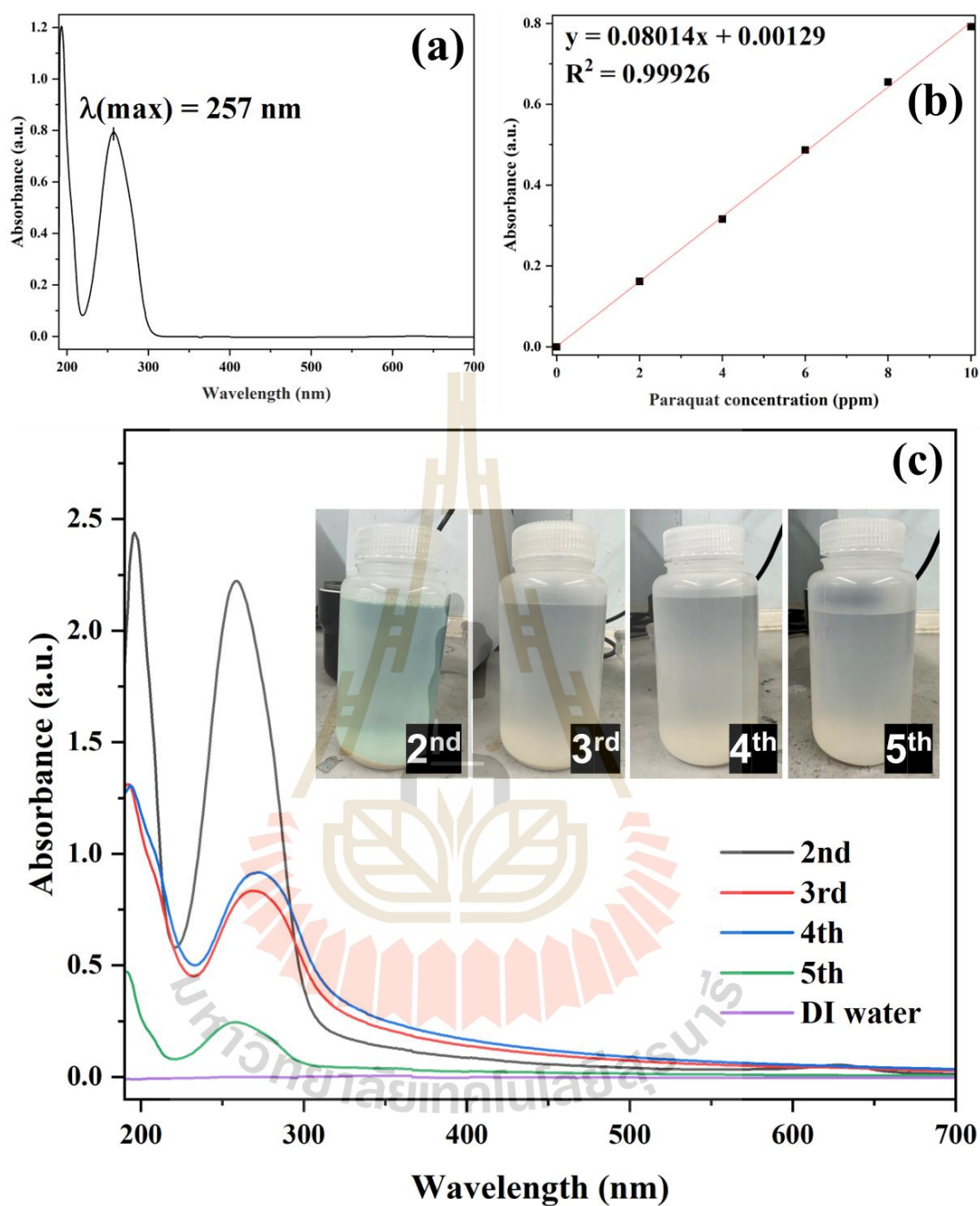**Figure 3.2**   The scanning UV-Vis spectrum of 10 ppm commercial PQ solution (a), PQ calibration curve (b), and the scanning UV-Vis spectrum of PQ solution collected from the liquid after centrifugation (c).

3.3.4 Synthesis of potassium catalyst on PQ-modified zeolite

The synthesis of this heterogeneous catalyst for transesterification of palm oil was modified from the literature (Kosawatthanakun et al., 2022). The dried

support was impregnated by CH_3COOK/CH_3COOH buffer solution with a concentration of 12% w/w potassium. The drop was continued until a slurry was obtained. Then, the mixture was stirred at 350 rpm for 10 minutes before being treated in an ultrasonic bath for another 10 minutes. After that, the mixture was slowly dried using a hot air oven, which gradually increased the temperature starting at 40 °C and then increments of 10 °C, holding each temperature for an hour until 80 °C was then completely dried for 24 hours. Finally, the as-prepared catalyst, which dried, was calcined at 500 °C for 3 hours in an environment of air with a heating rate of 1 °C/min to convert the acetate form to carbonate form. The samples were named as 12K/NaX-PQ and 12K/NaY-PQ.

3.3.4 Transesterification of palm oil

The transesterification reaction was done according to our prior research (Kosawatthanakun et al., 2022). In short, a 100-milliliter one-neck round bottom flask fitted with a Graham condenser was utilized to mix 0.2 g of catalyst, 2.9 g of methanol, and 5 g of palm oil. The reaction was conducted in paraffin bath at 60 °C for 3 hours and 500 rpm of stirring. The finished mixture was separated by suction filtration and rinsed with 5 mL of methanol. The liquid phase was evaporated to eliminate methanol using a rotary evaporator at 50 °C at a rotation speed of 60 cycles/min. The evaporated liquid was transferred to a vial and left to separate overnight. The produced biodiesel in the top layer was gathered to find the quantitative content of fatty acid methyl esters (FAMEs). The solid phase was washed by methanol and hexane alternatingly. Finally, the solid sample was overnight dried at 100 °C and designated as a spent catalyst.

The biodiesel test method EN 14103 was conclusively evaluated for the desired amount of FAMEs, followed by gas chromatography (GC, Agilent HP 5890) armed with a flame ionization detector (FID) using a capillary column (CHROMPACK from Netherlands, 7700 WCOT Fused Silica, CP-sil-5 CB, 100% dimethylpolysiloxane) with a length of 10 m, a film thickness of 0.12 µm, and an internal and external diameter of 0.25 and 0.39 mm, respectively. The flow with 2.9 mL/min of hydrogen was employed as a carrier gas. An automatic injector was included with the chromatogram and the injections with a sample size of 1 µL will be performed with an "on-column" system. Both inlet and detection temperatures of 300 °C were used

with a split of 1.10 mL/min at 0.5 bar of pressure and a velocity of 31.1 cm/s. The temperature program was started at 80 ℃, held for 1 minute, then ramped up to 180 ℃ at a rate of 4 ℃/min, continuing for 8 minutes. In the second step, the oven was heated to 220 ℃ at a rate of 10 ℃/min and maintained for 2 minutes. Finally, the oven temperature was elevated to 260 ℃ with a ramp rate of 20 ℃/min and kept for 2 minutes. The internal standard was methyl dodecanoate, commonly known as "methyl laurate," $C12:0$ ($CH_3(CH_2)_{10}COOCH_3$, Cognis, 99%). The content of FAMEs (x_{FAMEs}) and the percentage of biodiesel yield in the obtained product was acquired from an equation, respectively:

$$x_{FAMEs} = \left[\frac{(\sum A_{C16:0-C18:2}) - A_{C12:0}}{A_{C12:0}} \right] \times \left[\frac{[C12:0]V_{C12:0}}{m_{sample}} \right] \quad (2)$$

where A, $[C12:0]$, $V_{C12:0}$, and m_{sample} was determined as a peak area from the chromatogram ($\sum A_{C16:0-C18:2}$ was gathered $C16:0$ (methyl hexadecanoate, known as methyl palmitate), $C18:0$ (methyl octadecanoate, known as methyl stearate), $C18:1$ n9e (methyl 9(E) octadecanoate, known as methyl elaidate), and $C18:2$ n6e (methyl $cis,cis - 9,2 -$ hexadecanoate, known as methyl linoleate)), concentration, volume of $C12:0$ concentration, and mass of the analyzed biodiesel sample, respectively.

$$biodiesel \; yield \; (\%mol) = \left[\frac{m_{biodiesel}}{m_{palm \; oil}} \right] \times \left[\frac{x_{FAMEs}}{x_{triglycerides}} \right] \times \left[\frac{M_{triglycerides}}{3M_{FAMEs}} \right] \times 100 \quad (3)$$

where the terms "$m_{biodiesel}$" and "$m_{palm \; oil}$" refer to the mass of biodiesel and palm oil, respectively. Triglyceride content as a percentage was designated as $x_{triglycerides}$. The average molecular weights of triglycerides and FAMEs, respectively, was denoted as $M_{triglycerides}$ and M_{FAMEs}. The stoichiometric value for the number 3 that is multiplied at M_{FAMEs} was imposed from the balanced chemical equation for the transesterification of triglycerides with methanol.

3.3.5 Characterization

Phases of the catalysts were analyzed by X-ray diffraction (XRD) on a Bruker D8 ADVANCE (Bruker AXS GmbH, Karlsruhe, Germany) with Cu Cu Kα radiation

(λ=1.5406 Å) operated at a voltage and current of 40 kV and 40 mA, respectively. The scan speed and increment were used as 0.2 s/step and 0.02 s/step, respectively. The 2θ range of 5–50° was applied to gather the diffractions.

Functional groups on catalysts were analyzed by Fourier transform infrared spectroscopy (FTIR, Bruker Tensor 27) using ATR mode with a resolution of 2 cm^{-1}. The wavenumber range and number of scans for this experiment were used from 400 to 2400 cm^{-1} and 64, respectively.

Elemental compositions of samples were determined by X-ray fluorescence spectroscopy (ED-XRF, Horiba XGT-5200). The X-ray source was a Rh X-ray tube with 50 kV/mA and Mono-capillary guide tubes. The Fluorescence detector was a Peltier-cooled silicon drift detector (SDD) with an energy range of 0-40 keV.

The degradation of 2-methylbut-3-yn-2-ol (MBOH) in a fixed-bed, automated bench unit reactor was performed to assess the basicity of the prepared catalysts. Briefly, 200 mg of catalyst was placed into a U-like stainless-steel tubular reactor with quartz wool at the head and tail of the sample, followed by a 4-hour pretreatment period at 350 °C in N_2 atmosphere. Subsequently, the reactor was cooled to 135 °C and purged with gaseous MBOH (LONZA, 99%) using N_2 as a carrier gas at a flow rate of 20 mL/min. The MBOH conversion and product selectivity were computed according to the equations published in the literature which were calculated on the basis of the sum peak areas as demonstrated in equation (4):

$$MBOH\ conversion\ (\%mol) = \left[1 - \frac{A_{MBOH}rRF_{MBOH}/Mw_{MBOH}}{\sum_i(A_i rRF_i/Mw_i)}\right] \times 100 \quad (4)$$

where A, rRF, and Mw were peak area ratio, relative response factor, and molecular weight. The MBOH and all products were determined by an "i" symbol, which was a mathematical variable for all components.

$$Product\ selectivity\ (\%mol) = \frac{A_p rRF_p/M_p}{\sum(A_x rRF_x/M_x)} \times 100 \quad (5)$$

where the subscriptions of p and x were abbreviated from the parameters of the preferred and each obtained product, respectively. The methodology was attributed to the rRF defined by the effective carbon number concept (ECN).

3.4 Results and Discussion

3.4.1 Properties of zeolite NaX and NaY

Figures 3.3a and **3.3b** present the photographs of the synthesized zeolite NaX and NaY. Both samples are fine white powder similar to the commercial zeolite NaX and NaY (not shown), respectively.

Figure 3.3 Physical appearances of zeolite NaX (a) and NaY (b).

Figures 3.4 and **3.5** show the XRD patterns and FTIR spectra of the synthesized zeolite NaX and NaY, respectively. The main peaks are observed in both patterns including the peaks at 6°, 10°, 11.6°, 15.4°, 20°, 23.2°, 26.5°, and 30.8° corresponding to FAU framework characteristics (Ch. Baerlocher, Darren Brouwer, Bernd Marler and L.B. McCusker, Database of Zeolite Structures, https://www.iza-structure.org/databases/). However, alien peaks were noticed in both samples, especially zeolite NaX. Those five peaks at 12.4°, 17.6°, 21.6°, 28°, and 33.3° are the character of the zeolite NaP, Gismondine (GIS) framework (Baerlocher et al.) The mixed phase was obtained likely because the amount of chemicals and size of containers in the synthesis procedure were doubled, leading to different conditions during crystallization. Normally, both types of zeolite NaX and zeolite NaY usually transform the phase to the zeolite NaP when the crystallization temperature is increased from

90 °C to 110 °C and 100 °C for zeolite NaX and NaY, respectively (Arshad, 2016; Nakhaei Pour and Mohammadi, 2021).

The functional groups of zeolites are confirmed by FTIR. The broad band around 3500 cm^{-1} is the stretching vibration (ν) of the hydroxyl group (O-H) probably from the adsorbed moisture along with the peak at 1650 cm^{-1} from bending mode (δ) on the external zeolite surface. Also, the peak at 2360 cm^{-1} corresponds to asymmetric stretching vibration (ν_3) of adsorbed carbon dioxide (CO_2). The strong peak at 979 cm^{-1} with a small shoulder, a couple of spikes at 777 cm^{-1} and 698 cm^{-1}, 567 cm^{-1} and the sharp last-right peak at 450 cm^{-1} are assigned to asymmetric stretching vibration (ν_{as}) in the internal tetrahedra of Si–O–T bond (when T atoms are Si or Al), the symmetric stretching vibration (ν_s) of Si–O–T bond, T–O bending vibration (δ) at external linkages, and the internal tetrahedral bending of O–T–O bond, respectively (Karge, 2001; Keawkumay et al., 2019).
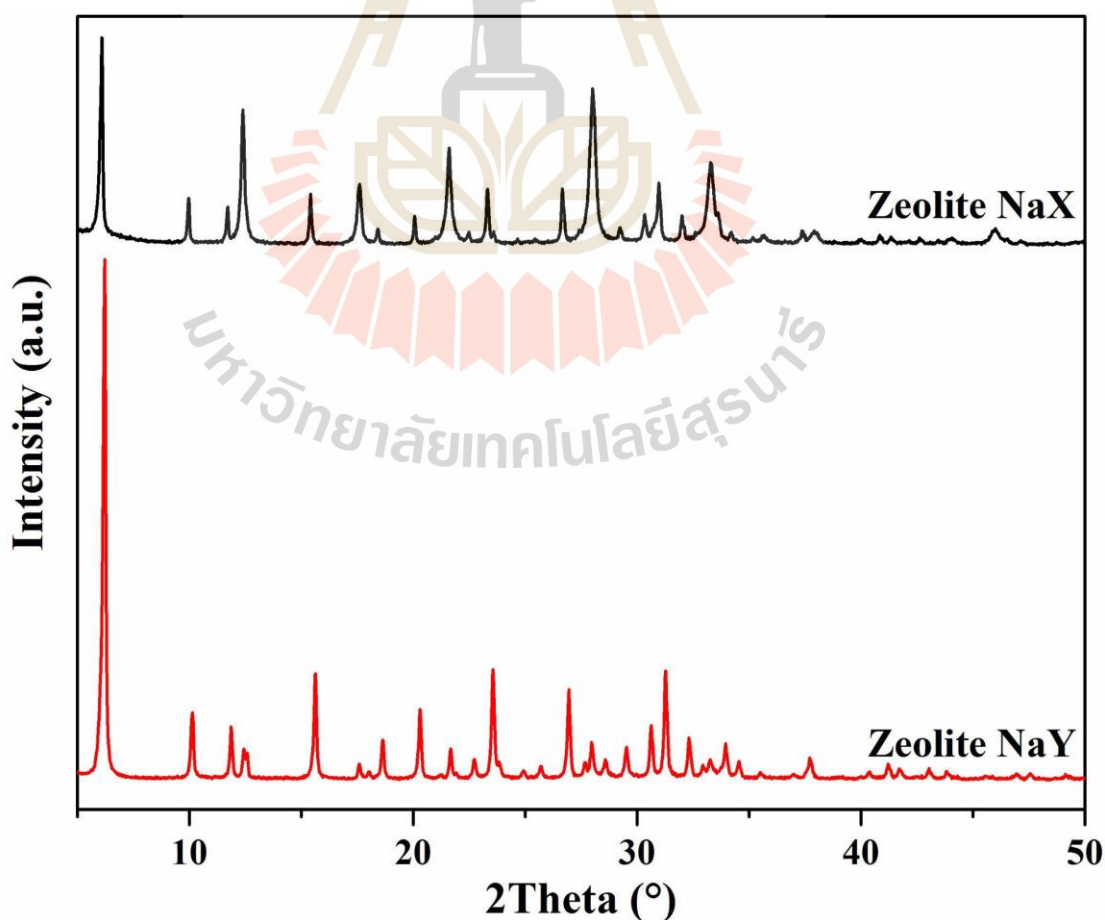
Figure 3.4 XRD patterns of the synthesized zeolite NaX and zeolite NaY.
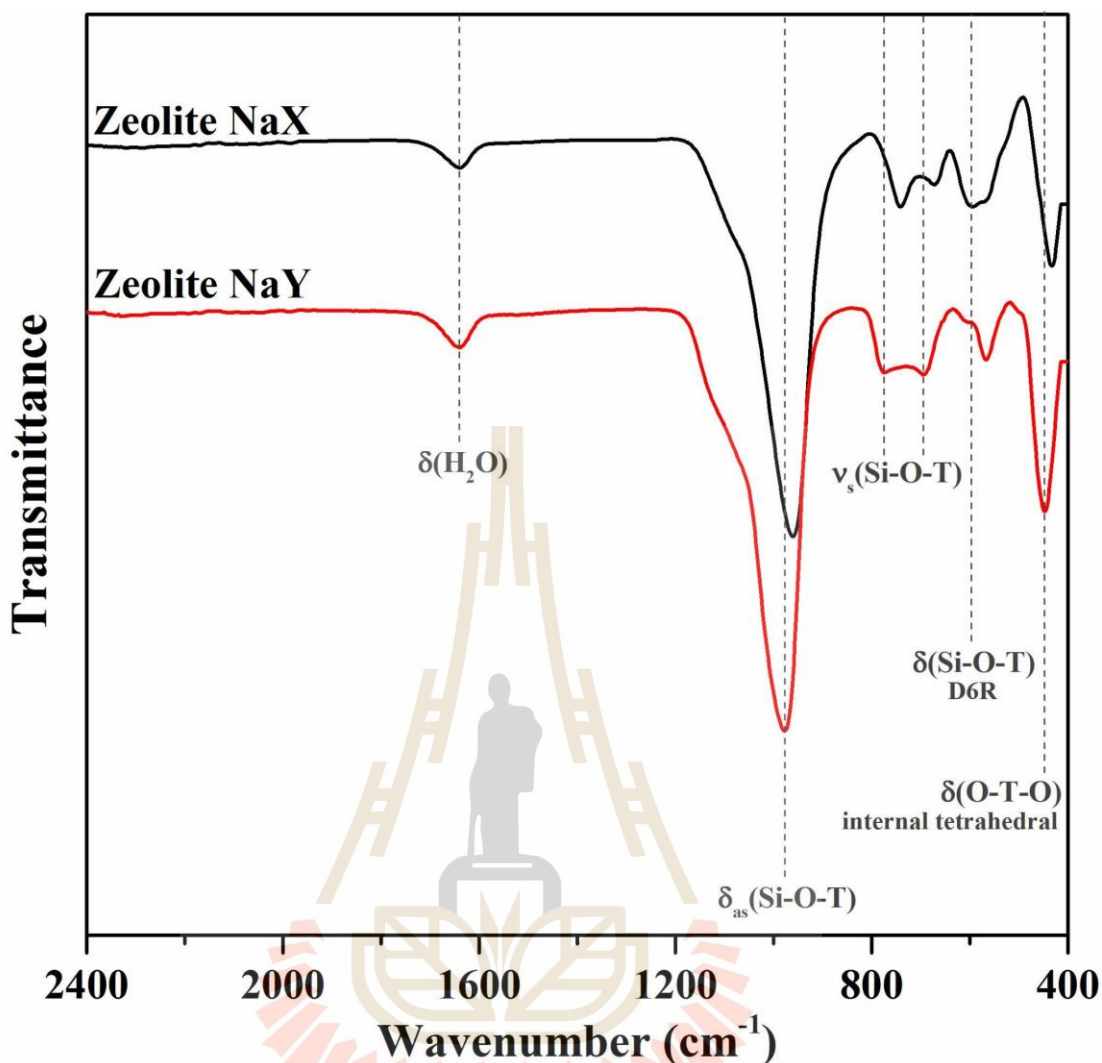
Figure 3.5 FTIR spectra of the synthesized zeolite NaX and zeolite NaY.

The elemental compositions of the synthesized zeolite NaX and NaY including Si, Al, Na, and K from X-ray fluorescence (XRF) are displayed in **Table 3.1**. The proportion was detected in the percent atomic unit. The Si/Al ratio which relates directly to hydrophobicity and hydrophilicity of the samples. The Si/Al ratios in the synthesized zeolite NaX and NaY are 1.7 and 2.5, respectively. The low Si/Al ratio indicates high contents of Al atoms and sodium charge-balancing cations. Although the high sodium content reflects a high ability to ion exchange, NaY has a higher PQ adsorption capacity than NaX due to the weaker electrostatic interaction between Na^+ and the negative area on the zeolite framework (Rongchapo et al., 2017). The Si/Al

ratios and the paraquat adsorption capacities of NaX and NaY from this work are similar to the literature (Rongchapo et al., 2017).

Table 3.1 Elemental compositions from XRF in the %atomic unit of synthesized zeolite NaX and NaY.

Samples	%atomic				Si/Al ratio
	Si	Al	Na	K	
Zeolite NaX	19.4	11.3	9.0	N/A	1.7
Zeolite NaY	22.0	8.8	7.9	N/A	2.5

3.4.2 PQ-adsorbed zeolite NaX and NaY

Figures 3.6a and **3.6b** are photographs of the PQ-adsorbed zeolite NaX and NaY, respectively. After PQ adsorption, the white zeolite powder turned light brown. The light brown color in PQ-adsorbed samples indicates the presence of organic compounds in the zeolite samples.

Figure 3.6 Physical appearances of PQ-adsorbed zeolite NaX (a) and NaY (b).

Figure 3.7 shows the XRD patterns of the PQ-adsorbed samples. The zeolite character peaks remain after the adsorption of PQ. However, the intensity of the peak at 10° from both NaX-PQ and NaY-PQ decreased when compared with the peak around 12°. This trait was also noticed in the literature due to the incorporation behavior of the PQ at the (220) plane (Keawkumay et al., 2019).
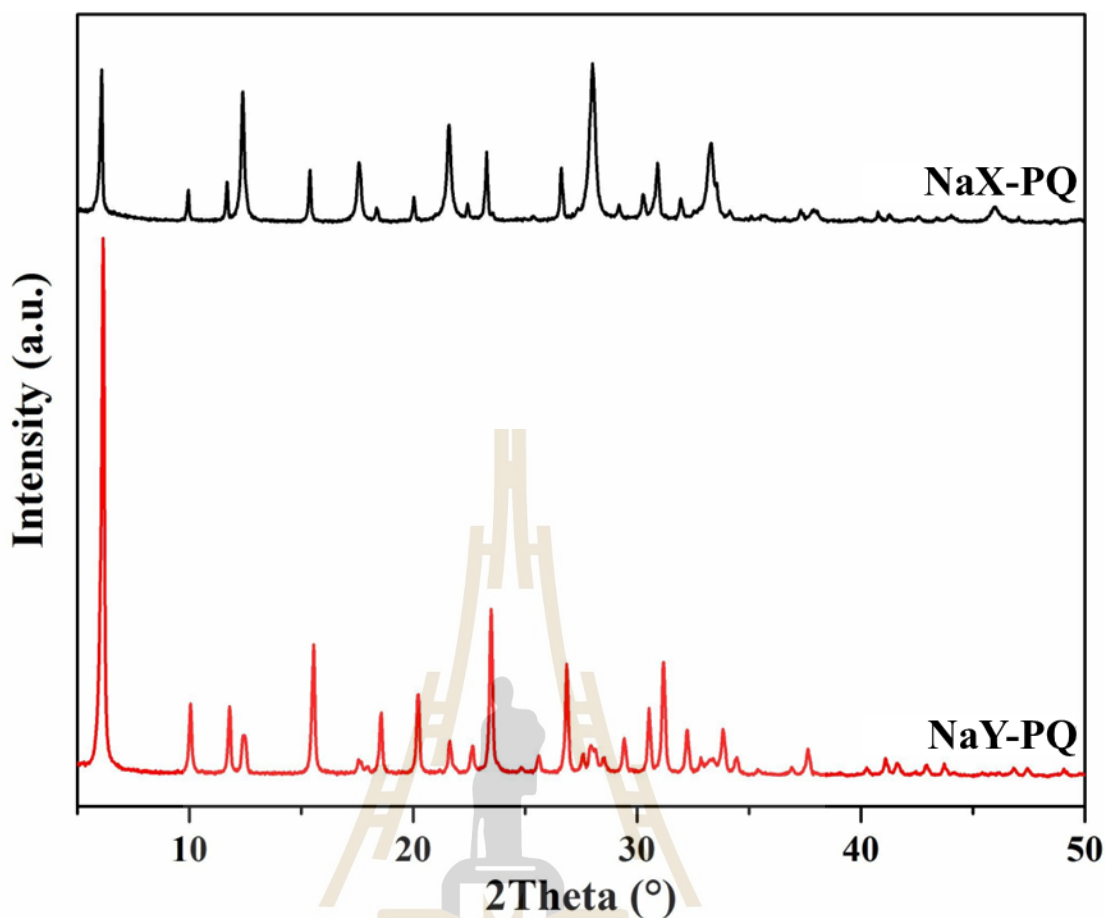
Figure 3.7 XRD patterns of PQ-adsorbed zeolite NaX and NaY.

Figure 3.8a illustrates FTIR spectra of PQ-adsorbed zeolite NaX and NaY. Several tiny peaks between 1600 cm^{-1} to 800 cm^{-1} are observed from the spectra of NaX-PQ and NaY-PQ, which corresponded to the vibration of PQ. The zoom-in infrared spectra in **Figures 3.8b** and **3.8c** show the peaks at 1571, 1512, 1454, 1340, 1272, 1226, 1191 and 833 cm^{-1}. Those peaks were consistent with the FTIR spectrum of laboratory-grade solid paraquat in the literature (Dinis-Oliveira et al., 2008; Hennessy et al., 1999; Hsu and Pan, 2007; Keawkumay et al., 2019; Rongchapo et al., 2017). The peak at 1571 cm^{-1} is from the symmetric stretching (ν_{ring}) in the aromatic ring of PQ, according to the peak at 1562 cm^{-1} reported in the literature (Hennessy et al., 1999). The peak at 1512 cm^{-1} indicates an ν_{ring} in the aromatic C=C bond associated with δ_{C-H}. The weak peak at 1506 cm^{-1} is assigned to the vibration of H$_3$C–N$^+$ bonds (Hsu and Pan, 2007). Besides, the peak at 1454 cm^{-1} confirms the same vibration at 1562 cm^{-1}, but different position

in the pyridyl ring. In addition, the peaks at 1272, 1226, and 1191 cm^{-1} were $\delta_{C-H} + \nu_{ring}$ and $\nu(H_3C-N^+)$ vibration, respectively.
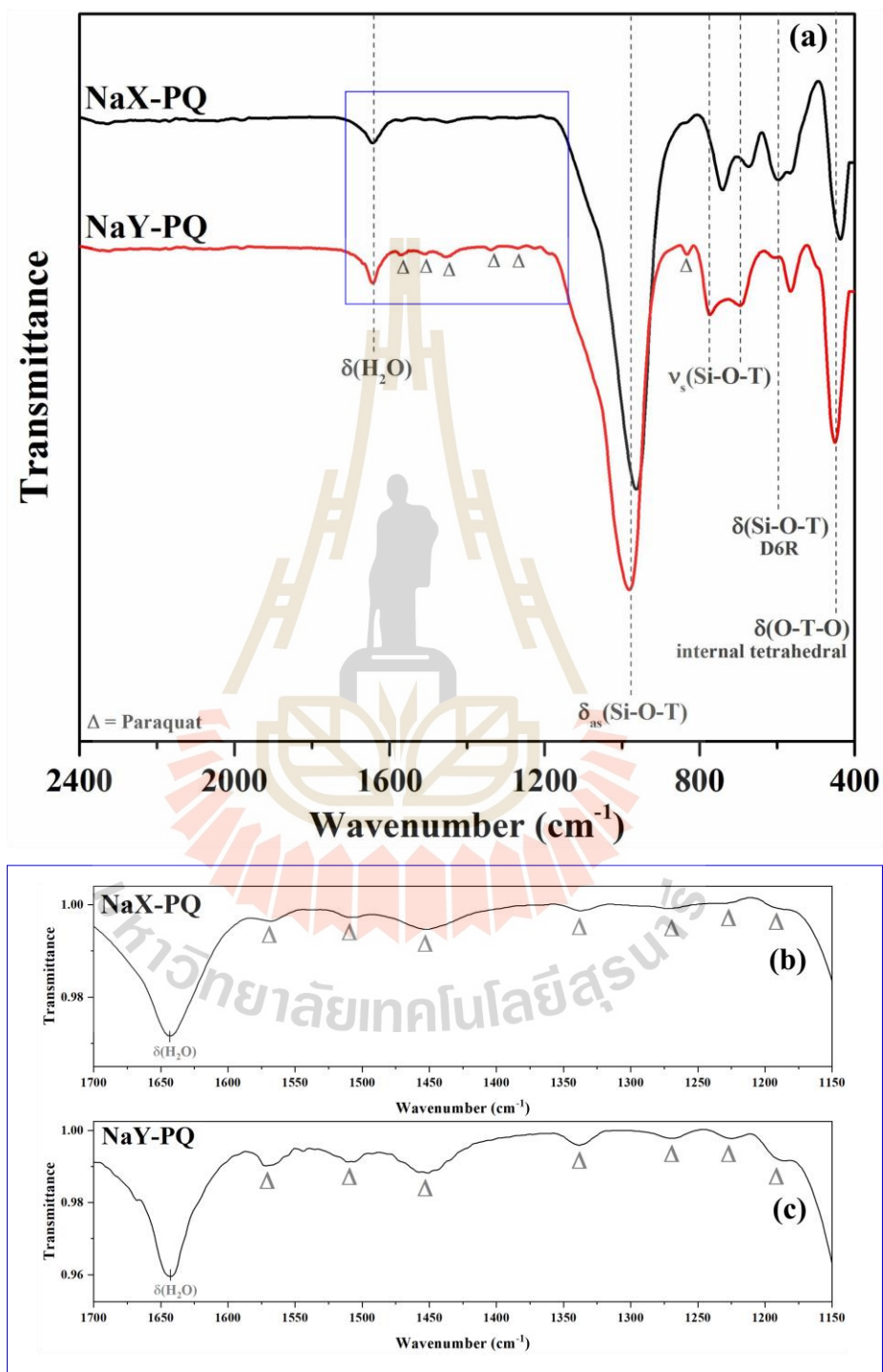
Figure 3.8 The normalized FTIR spectra (a) of PQ-adsorbed zeolite NaX and NaY and the zoom-in FTIR spectra of NaX-PQ (b) and NaY-PQ (c).

To compare the functional groups after PQ adsorption, the normalized FTIR spectra of NaX-PQ and NaY-PQ were investigated, as shown in **Figures 3.9**. Even though the strongest peak was equal, the PQ peaks on zeolite NaY were higher than those on NaX. This observation is in line with the publications that NaY had higher adsorption than NaX (Keawkumay et al., 2019; Rongchapo et al., 2017).
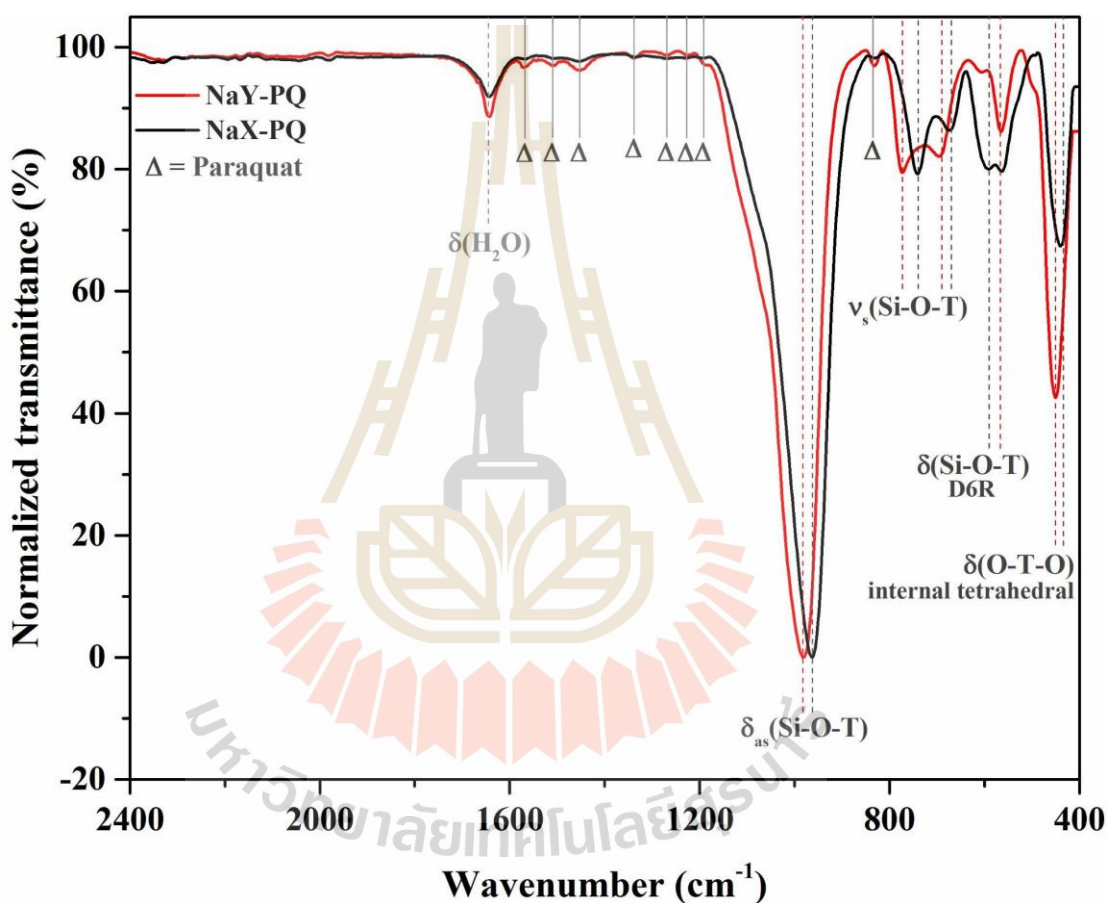
Figure 3.9 Normalized FTIR spectra of PQ-adsorbed zeolite NaX and NaY.

3.4.3 Characterization of potassium on PQ-adsorbed NaX and NaY

Figures 3.10a and **3.10b** show the photographs of as-prepared 12K/NaX-PQ and 12K/NaY-PQ, respectively. 12K/NaY-PQ shows a darker color than 12K/NaX-PQ, consistent with their PQ adsorption capacities. **Figures 3.10c** and **3.10d** are the

photographs of calcined samples. Both samples turned white after calcination at 500 °C for 3 h in the air atmosphere, implying the decomposition of organic compounds.
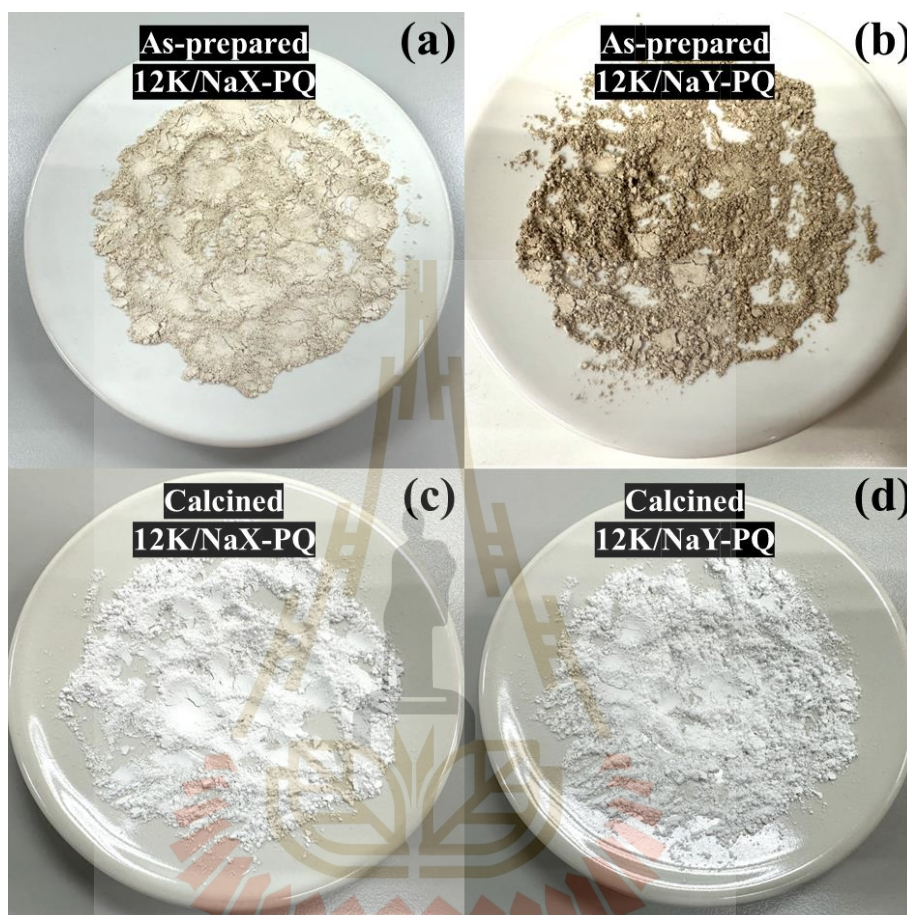
Figure 3.10 Physical appearances of as-prepared 12K/NaX-PQ (a), as-prepared 12K/NaY-PQ (b), 12K/NaX-PQ (c), 12K/NaX-PQ (d).

**Figures 3.11** and **3.12** display the XRD patterns and FTIR spectra of the as-prepared samples, respectively. Firstly, a slight decrease in the zeolite peaks was observed after impregnation, especially the plane (111) reported in the recent work (Kosawatthanakun et al., 2022). Moreover, the acetate peaks on NaX are stronger than those on NaY. This might be caused by the higher PQ adsorption capacity of zeolite NaY that allows the precursor to reside at the external surface. In the case of zeolite NaX, the lower PQ adsorption ability resulted in more acetate dispersion on the zeolite external surface, supported by the stronger acetate peaks. In the FTIR analysis, a couple of strong acetate peaks were shown. Small peaks between bands 1600 to 800

cm^{-1} were observed in the as-prepared 12K/NaY-PQ. This was due to the higher ability of PQ adsorption in zeolite NaY, as mentioned above. Moreover, the zeolite character remained after the impregnation, which could be noticed between bands 800 to 400 cm^{-1}.
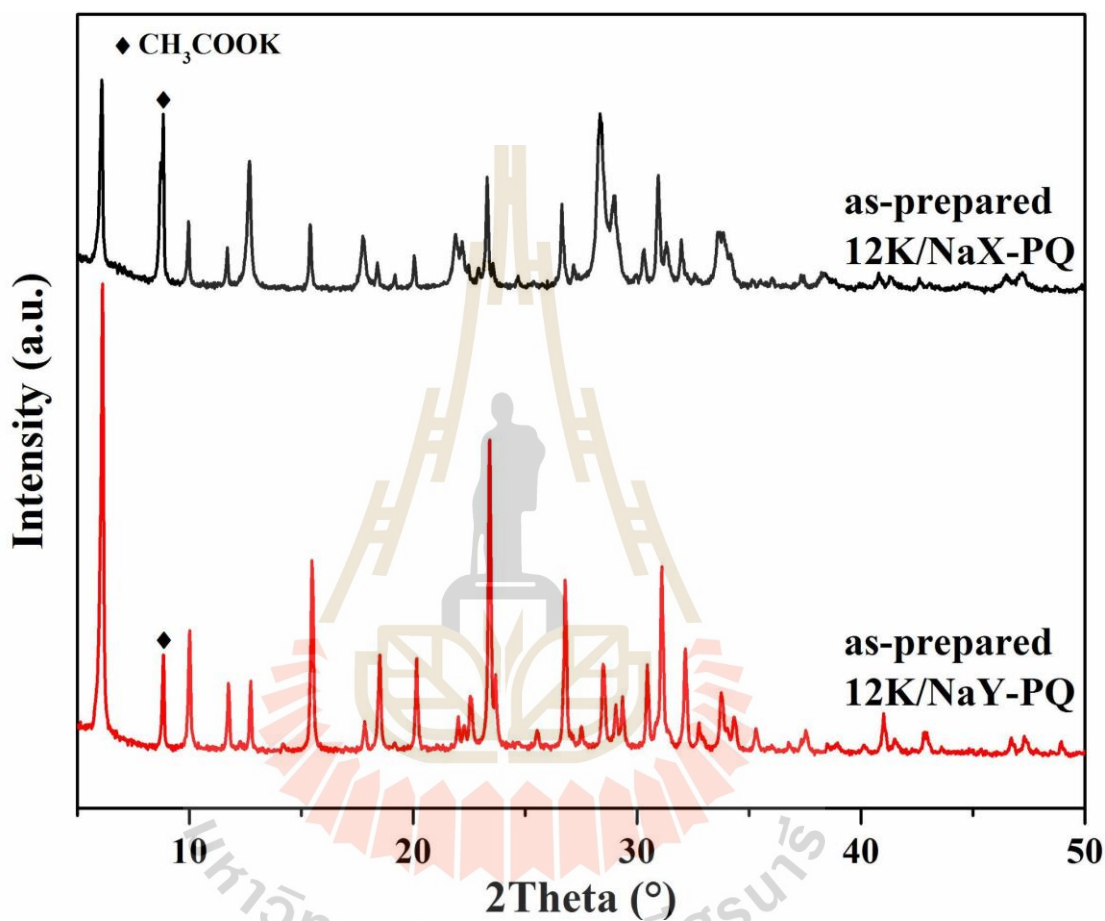
Figure 3.11 XRD patterns of the as-prepared 12K/NaX-PQ and 12K/NaY-PQ.
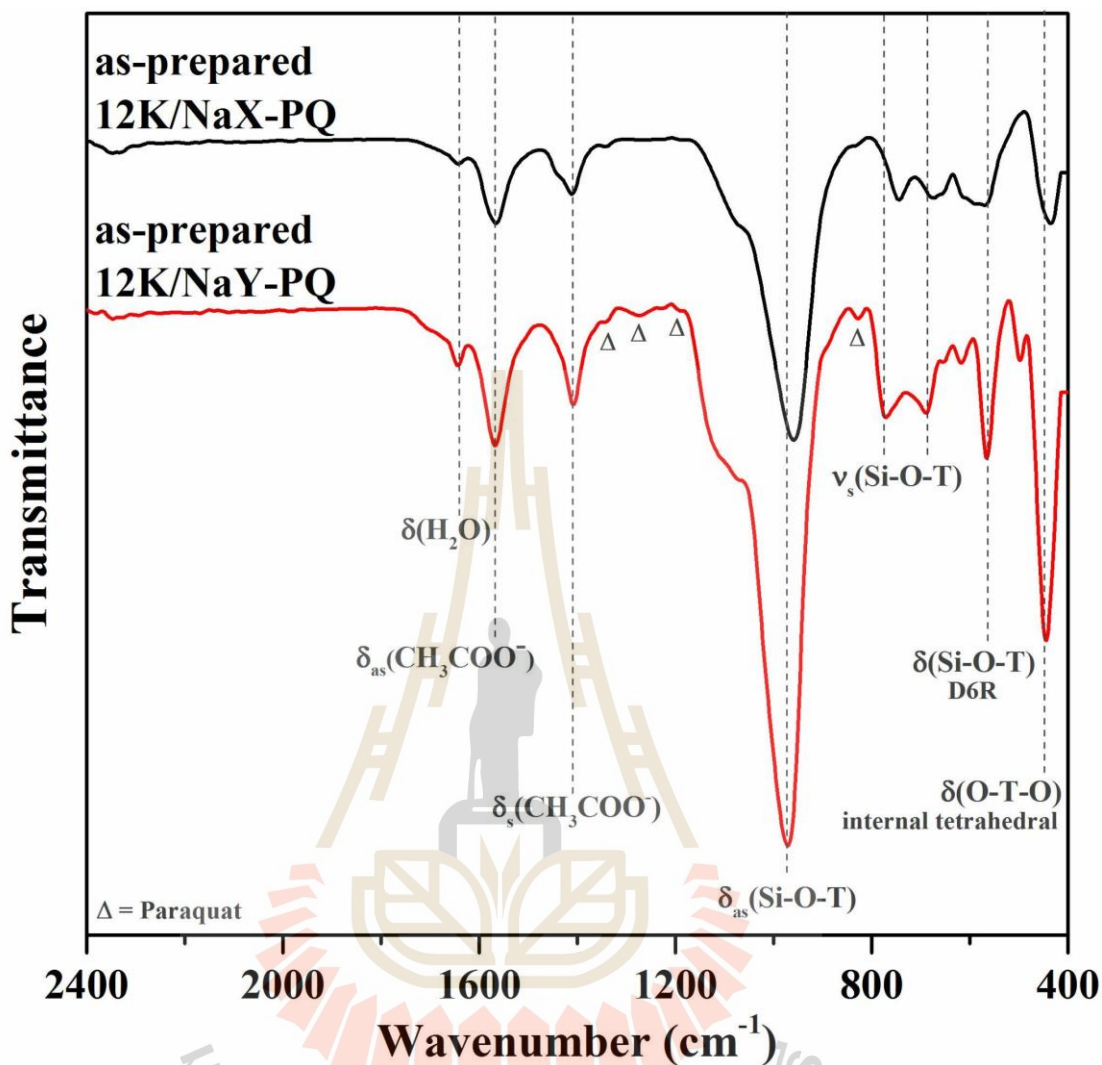
Figure 3.12 FTIR spectra of the as-prepared 12K/NaX-PQ and 12K/NaY-PQ.

       Figures 3.13 and **3.14** display the diffractograms and FTIR curves of the 12% potassium catalysts, respectively. Firstly, according to the high amount of precursor, the flat lines with tiny spikes were exhibited after calcination. In the case of the 12K/NaY-PQ, despite the fact that the acetate peak at 8.88° looked to be the short one, the XRD pattern of the calcined sample also produced a low intensity. Inevitably, the strong peak of acetate, which was exhibited in the as-prepared 12K/NaX-PQ, resulted in almost the none of zeolite nature after calcination. This was also observed in the literature (Kosawatthanakun et al., 2022). The strong acetate peaks disappeared after calcination and the peaks of carbonate species emerged. Moreover, the

carbonate peak in the 12K/NaX-PQ was stronger than 12K/NaY-PQ because of the lower q_m, which was accompanied by the larger degree of impregnation in the NaX-PQ. the larger amount of potassium acetate buffer impregnated in the NaX-PQ. The broad peaks of both zeolite types were also noticed, aligning with the XRD results. Therefore, this experiment still could not be used to study the effect of cavity of the support. The results could not confirm the blocking of zeolite cavity by PQ. However, the difference in the ability of precursor impregnation could be used to study the catalytic performance.
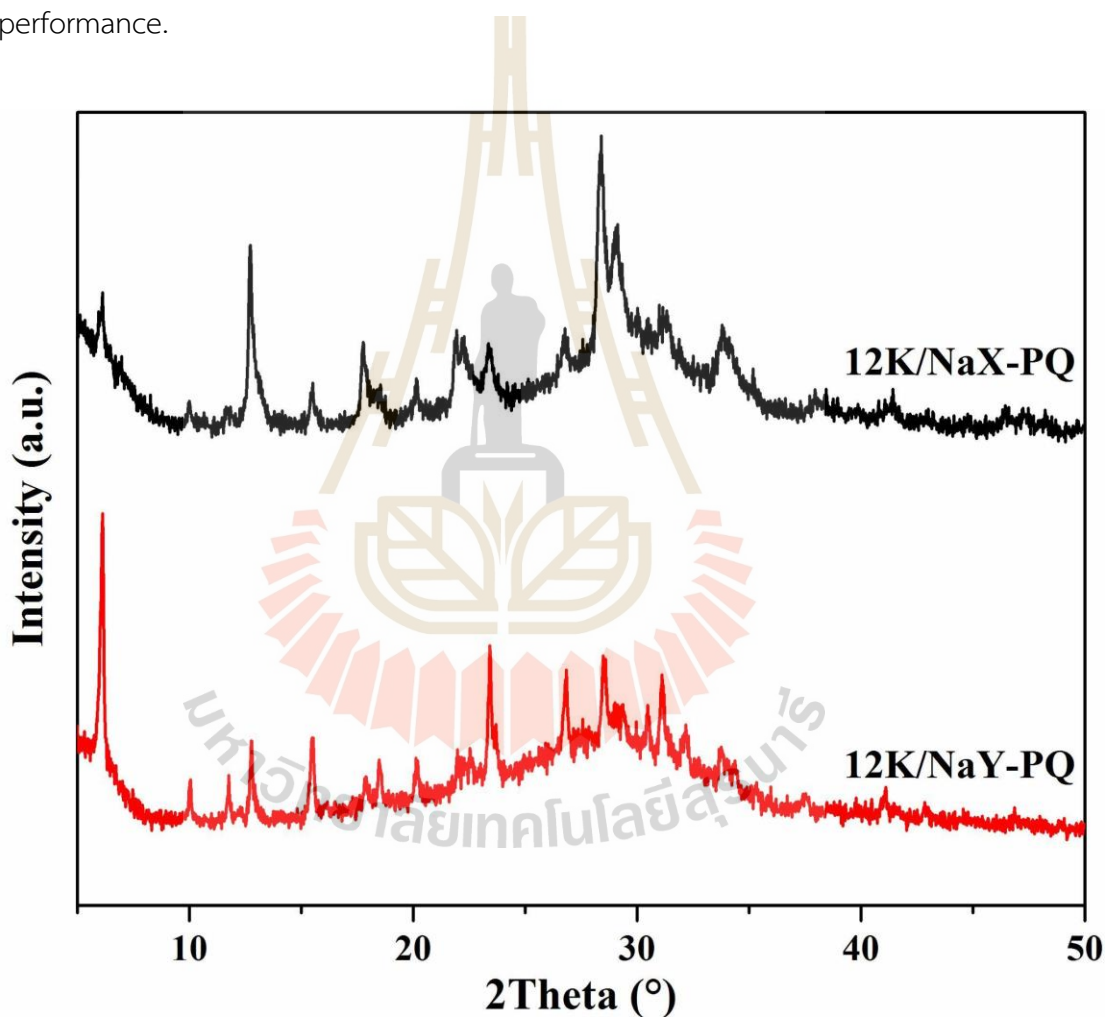
Figure 3.13 XRD patterns of 12K/NaX-PQ and 12K/NaY-PQ.
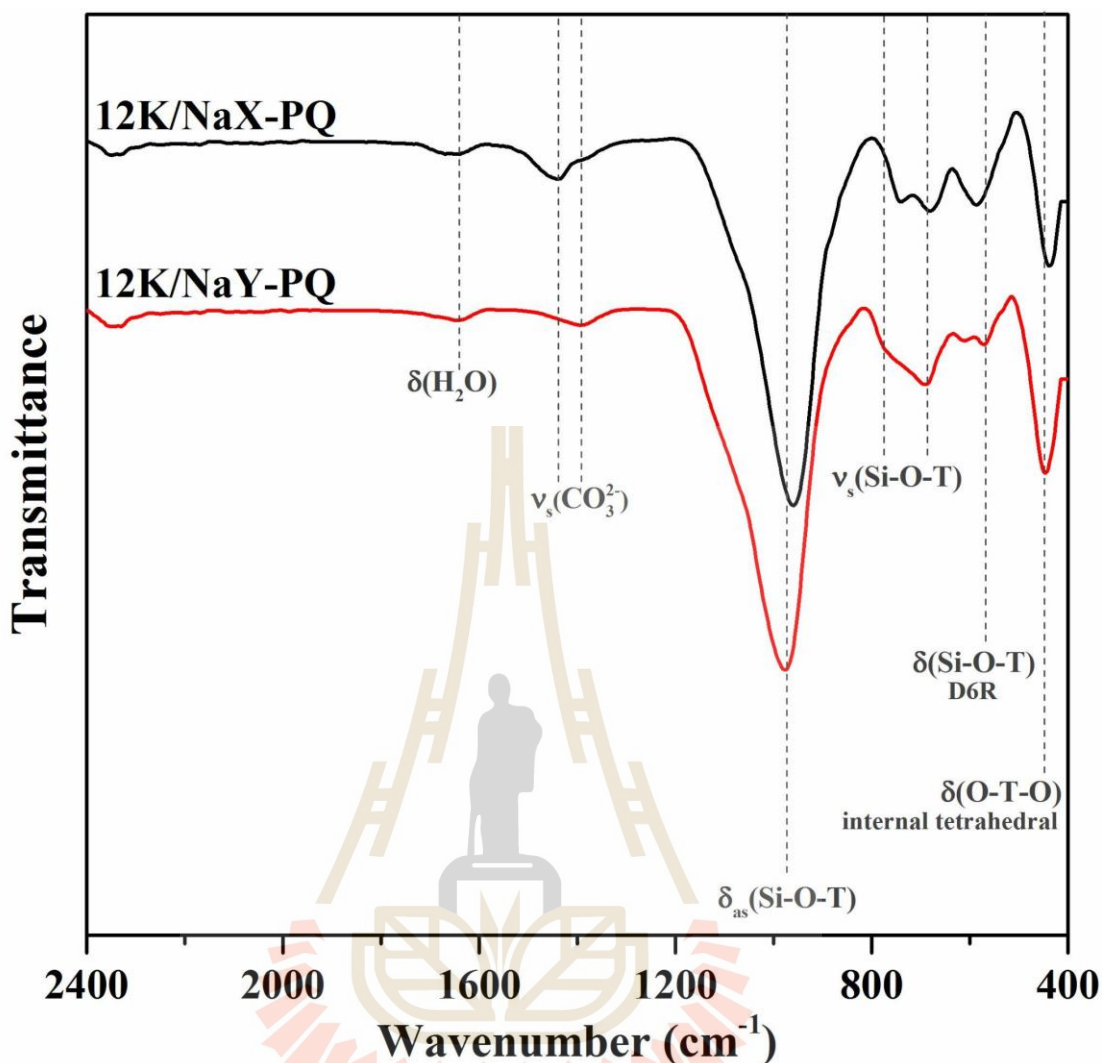
Figure 3.14 FTIR spectra of 12K/NaX-PQ and 12K/NaY-PQ.

Figure 3.15 shows that the MBOH conversions from 12K/NaX-PQ are lower than those from 12K/NaY-PQ. The conversions from both samples are nearly constant. These results are consistent with the previous papers (Kosawatthanakun et al., 2022; Nuttinee et al., 2012) that steady and high conversions are obtained from catalysts with 12 %wt of potassium. The numeric data of the MBOH conversions and product selectivity from the calcined samples in the mol% unit are compared in **Table 3.2**. The product selectivity indicates that both catalysts mainly contain base-catalyzed sites. The FTIR spectra suggest that those basic sites are carbonate.

In this work, 12K/NaX-PQ exhibited lower conversion than 12K/NaY-PQ, which opposed the literature (Kosawatthanakun et al., 2022). This result also was in

contrast with the FTIR spectra that 12K/NaX-PQ showed stronger carbonate bands than 12K/NaY-PQ (see **Figure 3.14**). This could imply that 12K/NaX-PQ had a poorer dispersion of active species. However, the XRD patterns in both literature and this work exhibited a flat line, which means that it the dispersion and accessibility could not be clearly compared (Kosawatthanakun et al., 2022; Nuttinee et al., 2012). Moreover, the BET surface area decreased dramatically, which was caused by the destroyed structure of zeolite NaX and NaY (Kosawatthanakun et al., 2022; Rakmae et al., 2016). Thus, the conversion of MBOH could be from a high concentration of carbonate on the collapsed supports.

Figure 3.15 MBOH conversion of 12K/NaX-PQ and 12K/NaY-PQ; reaction temperature, 120 ℃; amount of catalyst, 0.020 g.

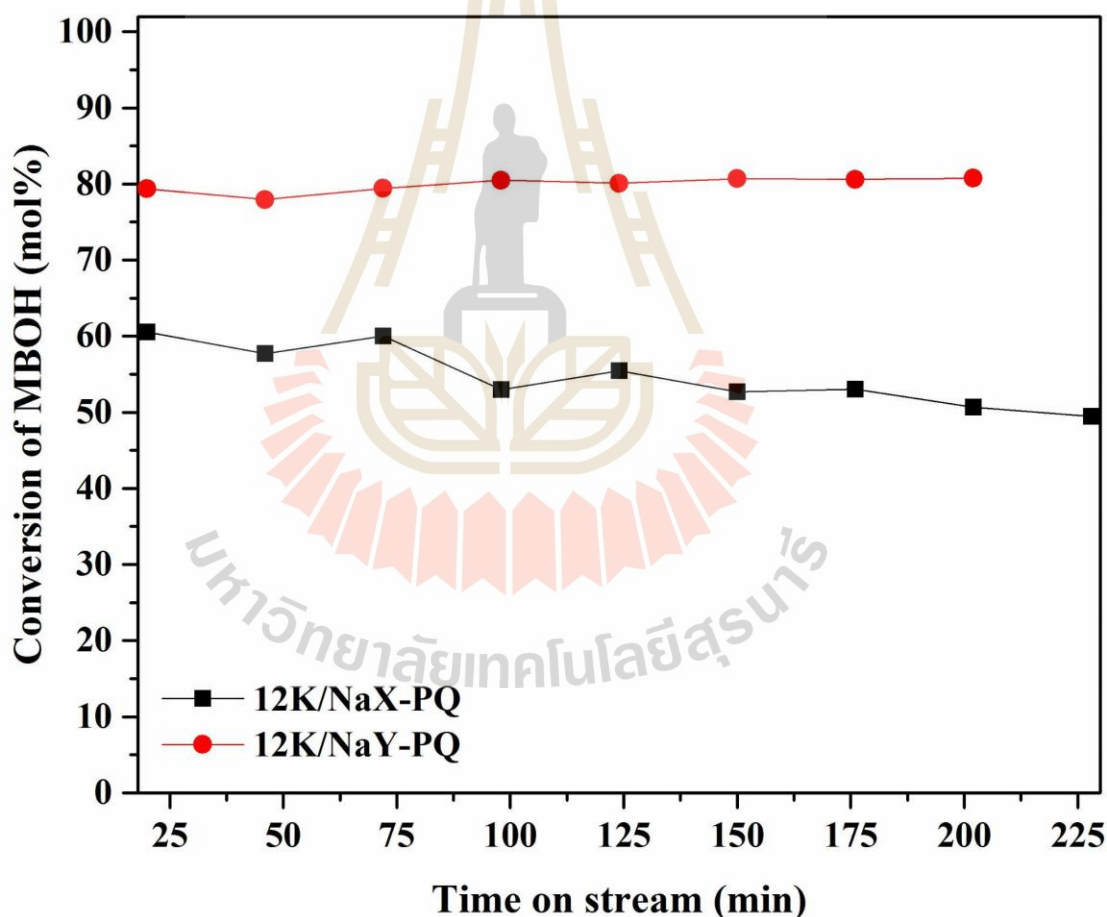**Table 3.2** MBOH conversion and product selectivity from the MBOH decomposition of 12% catalysts analyzed by gas chromatography.

Samples	MBOH conversion (mol%)		Product selectivity (mol%)			
			Base-catalyzed site		Acid-catalyzed site	
	1st injection	Last injection	Acetylene	Acetone	MBYNE	Prenal
12K/NaX-PQ	60.6	49.5	58.2	41.6	0.2	0
12K/NaY-PQ	79.4	80.7	57.7	42.2	0.1	0

3.4.4 Transesterification of palm oil catalyzed by 12K/FAU-PQ

Figure 3.16 illustrates the relationship between the percentage of biodiesel yield over the 12% w/w potassium catalysts (12K/NaX-PQ and 12K/NaY-PQ) for the first and second cycles (received from GC-FID and their chromatograms were shown in **Figures 3.17** and **3.18**, respectively). High biodiesel yields (62.7% and 60.4%) were obtained from 12K/NaX-PQ and 12K/NaY-PQ in the first cycle, respectively. These yields were lower than the literature. **Table 3.3** presents the examples of 12% CH_3COOK/CH_3COOH catalysts supported on FAU zeolite for transesterification and %yield, which was sorted by the published date. Most literatures provided a percentage of the biodiesel yield, catalyzed in different oil types, higher than 70% in the first cycle (Kosawatthanakun et al., 2022; Manadee et al., 2017; Maneechot et al., 2021; Montalbo et al., 2013; Rakmae et al., 2016; Supamathanon et al., 2011). This is probably due to the partial decomposition of the potassium buffer solution since it was at the external surface of the support, which was blocked by paraquat molecules. In the second cycle, approximately 3% biodiesel yields were obtained. This tendency was similar to 12K/NaY in the literature (Kosawatthanakun et al., 2022). In the case of 12K/NaX, the yields 97.9% and 61.3% were received in the first and second cycle, respectively (Kosawatthanakun et al., 2022). They concluded that the utilized catalysts, which exhibited more structural collapse, showed the leaching of potassium, an active species, into the products of glycerol and biodiesel (Kosawatthanakun et al., 2022).
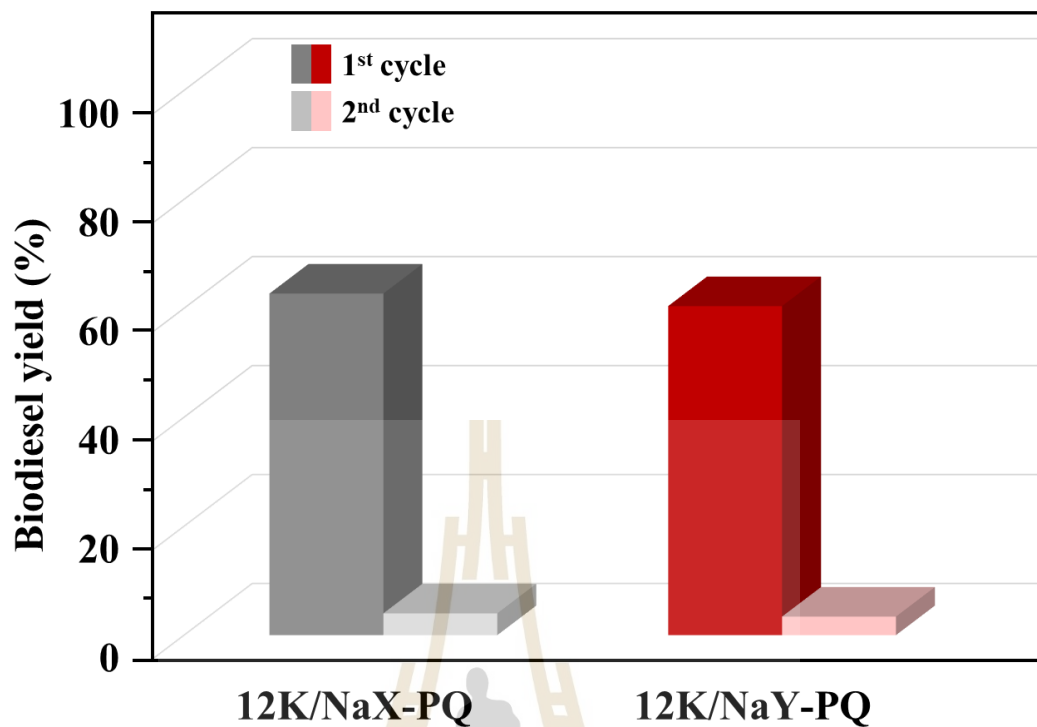
Figure 3.16 Biodiesel yield from transesterification reaction of palm oil catalyzed at 60 °C for 3 h by 0.2 g of 12K/NaX-PQ and 12K/NaY-PQ.
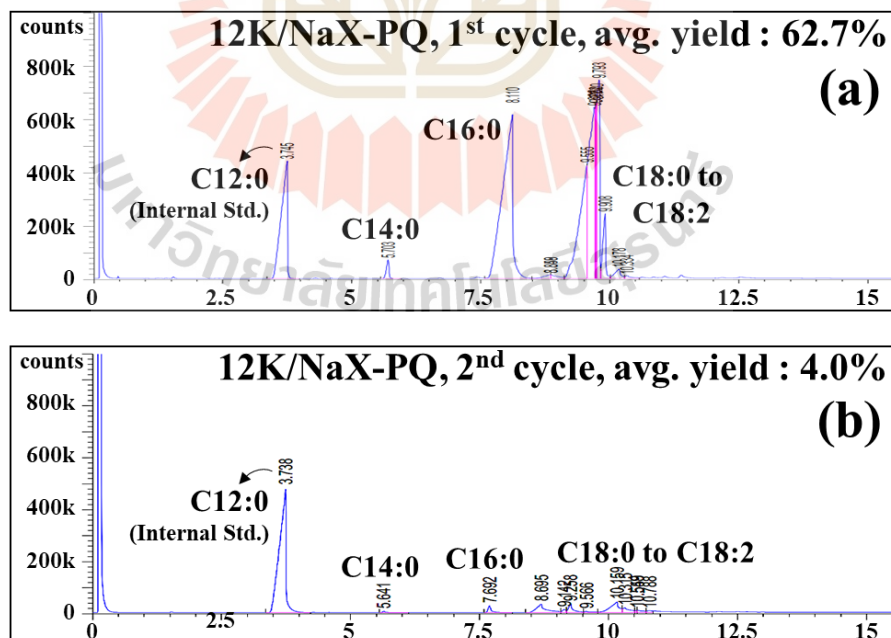
Figure 3.17 Chromatograms of biodiesel from the 1st (a) and 2nd (b) cycles catalyzed by 12K/NaX-PQ.
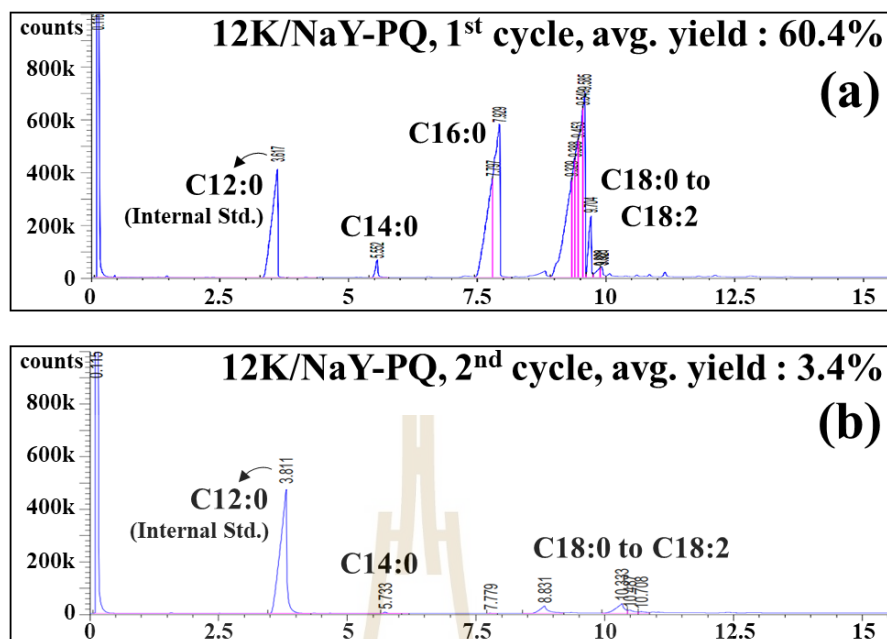
Figure 3.18 Chromatograms of biodiesel from the 1st (a) and 2nd (b) cycles catalyzed

by 12K/NaX-PQ.

Table 3.3 Examples of 12% CH_3COOK/CH_3COOH catalysts supported on FAU zeolite for transesterification and %yield, which was sorted by the published date.

Catalysts	Oil type	%yield		Ref.
		1st cycle	2nd cycle	
12K/NaY	Jatropha seed oil	73.4%	N/A	(Supamathanon et al., 2011)
12K/NaY	Jatropha seed oil	77.2%	N/A	(Montalbo et al., 2013)
12K/NaY-U	Palm oil	72.4%	N/A	(Rakmae et al., 2016)
12K/NaX	Jatropha seed oil	83%	N/A	(Manadee et al., 2017)
12K/NaY-hierarchical-U	Jatropha seed oil	97.3%	96.1%	(Maneechot et al., 2021)

*U was abbreviated for ultrasound assistance.

Table 3.3 Examples of 12% CH₃COOK/CH₃COOH catalysts supported on FAU zeolite for transesterification and %yield, which was sorted by the published date (continued).

Catalysts	Oil type	%yield		Ref.
		1st cycle	2nd cycle	
12K/NaX-U	Palm oil	97.9%	61.3%	(Kosawatthanakun et al., 2022)
12K/NaY-U	Palm oil	94.4%	2.7%	(Kosawatthanakun et al., 2022)
12K/NaX-PQ	Palm oil	62.7%	4.0%	This work
12K/NaY-PQ	Palm oil	60.4%	3.4%	This work

*U was abbreviated for ultrasound assistance.

Figure 3.19 and **Table 3.4** show the results from the analysis of spent catalysts by FTIR and XRF, respectively. The carbonate band vanished in the spent 12K/NaX-PQ and 12K/NaY-PQ catalysts. This reduction of carbonate peak was also observed in the 12K/NaX and 12K/NaY (Kosawatthanakun et al., 2022). They suggested that the active species, potassium ion, located at the external surface of the zeolite support, and then leached into glycerol and biodiesel products.

The fresh 12K/NaX-PQ and 12K/NaY-PQ as well as their spent materials were analyzed for the elemental compositions of Si, Al, Na, and K compared with the catalysts without paraquat modification. Firstly, the Si/Al ratio in 12K/NaX-PQ and 12K/NaY-PQ still remained the same (namely, 1.7 and 2.4–2.5, respectively) after the catalyst preparation (precursor loading and calcination). However, their zeolitic property was not available since the structural collapse was observed, as suggested by XRD and FTIR studies. The 12K/NaX-PQ contained 6.8% and 10.4% of sodium and potassium, respectively. Interestingly, when this catalyst was used in the transesterification of palm oil, the percentage of sodium dwindled by half while the potassium was nearly unchanged. This behavior was also noticed from the fresh and spent 12K/NaY-PQ catalyst. The possible phenomenon might be the exchange between the charge-balancing sodium cation and potassium ions from the precursor.

The catalyst without PQ modification, 12K/NaX had 4.6% sodium and 6.1% potassium. The contents in the spent sample were 4.9% and 5.4%, respectively. A similar trend was also observed in 12K/NaY samples. As proposed above, the ion exchange between potassium ions from the potassium acetate buffer solution and the charge-balancing sodium cation at the zeolite surface might represent a probable phenomenon that occurs in Na-zeolitic support. This results in the formation of sodium carbonate which is an active species to catalyze transesterification. This observation was consistent with the disappearance of carbonate bands in the FTIR spectra. So, the ion exchange between sodium and potassium probably occurred, then the sodium acetate might be generated before calcination. After that, both potassium and sodium carbonates were produced by thermal treatment, which might be the active species to accelerate the reaction. This hypothesis will be proved in **Chapter V**. Note that, only the influence of the structure of zeolite support was studied in this chapter by applying the PQ molecules before the catalyst preparation.
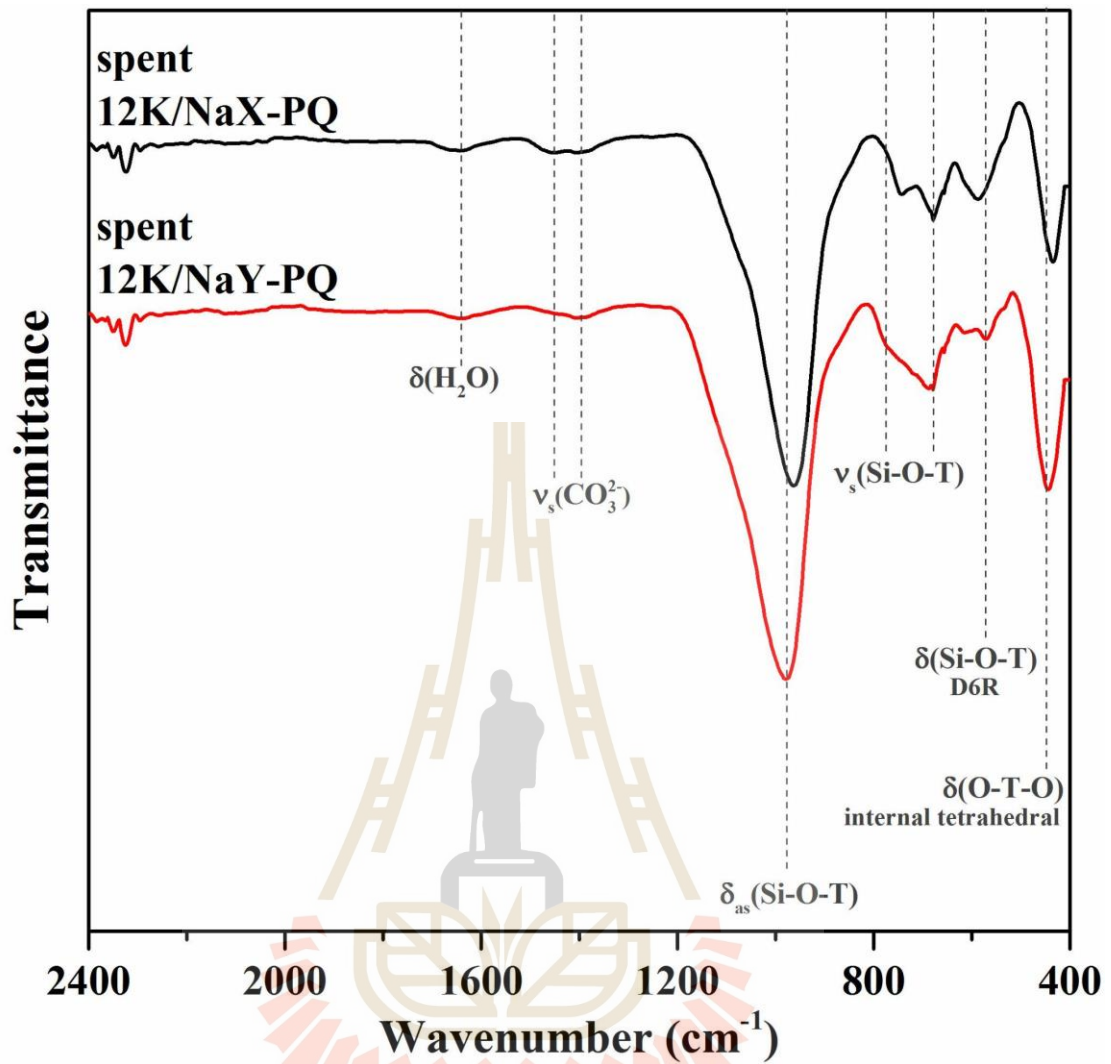
Figure 3.19 FTIR spectra of spent 12K/NaX-PQ and 12K/NaY-PQ.

Table 3.4 Elemental compositions from XRF in the %atomic unit of fresh and spent 12% w/w potassium catalysts.

Samples	%atomic				Si/Al ratio
	Si	Al	Na	K	
12K/NaX-PQ	18.1	10.8	6.8	10.4	1.7
Spent 12K/NaX-PQ	19.3	11.3	3.5	10.6	1.7
12K/NaX	18.9	10.9	4.6	6.1	1.7
Spent 12K/NaX	18.9	11.2	4.9	5.4	1.7
12K/NaY-PQ	20.7	8.6	5.6	9.8	2.4
Spent 12K/NaY-PQ	21.4	8.7	4.3	9.7	2.5
12K/NaY	20.1	8.4	7.6	4.8	2.4
Spent 12K/NaY	22.3	8.9	4.1	6.4	2.5

For more discussion, this result was similar to those literature (Kosawatthanakun et al., 2022). Both samples still showed structural collapse as well as the poor reusability. This means that 12% potassium was too high to investigate the effect of the FAU cavity. Paraquat molecules were flooded by precursors, resulting in the similar pattern of result. Thus, in the up-coming chapter, the concentration of the precursor was reduced from 12% to 8% in order to precisely study the effect of the zeolite cavity on the potassium catalyst preparation.

3.5 Conclusion

This study explored the influence of the zeolitic cavity on the potassium catalysts by adsorbing paraquat on the zeolites prior to catalyst preparation. The resulting catalysts still showed the collapse of zeolite structure, as normally seen in the literature. This might be due to the excess amount of precursor that could partially ion exchange into the cavities. In the transesterification, approximately 60% biodiesel yield was received in the first cycle. This catalytic performance was lower than in the literature (almost 100%) due to the partial decomposition of the precursor, which was a result of pore blocking by paraquat. Then, it dropped to about 3% in the second

cycle. This trend was also seen in the literature, which was caused by the leaching of potassium in the reaction. However, the potassium content of these catalysts almost maintained while the percentage of sodium as well as the carbonate bands were dropped. This result suggests the ion exchange between the potassium ion and the charge-balancing cation (sodium and paraquat), resulting in the structural collapse after calcination.

3.6 References

Arshad, S. (2016). The effect of crystallization time and temperature on hydrothermal synthesis of zeolite NaX from Bongawan kaolin. *Int. J. Eng. Technol.*, *13*(1), 33–39.

Dinis-Oliveira, R. J., Duarte, J. A., Sánchez-Navarro, A., Remião, F., Bastos, M. L., and Carvalho, F. (2008). Paraquat poisonings: Mechanisms of lung toxicity, clinical features, and treatment. *Crit. Rev. Toxicol.*, *38*(1), 13–71. doi: https://doi.org/10.1080/10408440701669959

Hennessy, B., Megelski, S., Marcolli, C., Shklover, V., Bärlocher, C., and Calzaferri, G. (1999). Characterization of Methyl Viologen in the Channels of Zeolite L. *J. Phys. Chem. B.*, *103*(17), 3340–3351. doi: https://doi.org/10.1021/jp984573y

Hsu, S. T. and Pan, T. C. (2007). Adsorption of paraquat using methacrylic acid-modified rice husk. *Bioresour. Technol.*, *98*(18), 3617–3621. doi: https://doi.org/10.1016/j.biortech.2006.11.060

Intarapong, P., Luengnaruemitchai, A., and Jai-In, S. (2011). Transesterification of palm oil over KOH/NaY zeolite in a packed-bed reactor. *Int. J. Renew. Energy Res.*, *1*(4), 271–280. doi: https://doi.org/10.20508/ijrer.v1i4.81.g66

Jantarit, N., Tayraukham, P., Osakoo, N., Föttinger, K., and Wittayakun, J. (2020). Formation of EMT/FAU intergrowth and nanosized SOD zeolites from synthesis gel of zeolite NaX containing ethanol. *Mater. Res. Express*, *7*(7), 075011. doi: https://doi.org/10.1088/2053-1591/aba55a

Karge, H. G. (2001). Chapter 15 - Characterization by IR spectroscopy. In H. Robson & K. P. Lillerud (Eds.), *Verified Syntheses of Zeolitic Materials* (pp. 69–71). Elsevier Science. doi: https://doi.org/10.1016/B978-044450703-7/50113-7

Keawkumay, C., Rongchapo, W., Sosa, N., Suthirakun, S., Koleva, I. Z., Aleksandrov, H. A., Vayssilov, G. N., and Wittayakun, J. (2019). Paraquat adsorption on NaY zeolite at various Si/Al ratios: A combined experimental and computational study. *Mater. Chem. Phys.*, *238*, 121824. doi: https://doi.org/10.1016/j.matchemphys.2019.121824

Kosawatthanakun, S., Pansakdanon, C., Sosa, N., Chanlek, N., Roessner, F., Prayoonpokarach, S., and Wittayakun, J. (2022). Comparative properties of K/NaX and K/NaY from ultrasound-assisted impregnation and performance in transesterification of palm oil. *ACS Omega*, *7*(11), 9130–9141. doi: https://doi.org/10.1021/acsomega.1c04912

Manadee, S., Sophiphun, O., Osakoo, N., Supamathanon, N., Kidkhunthod, P., Chanlek, N., Wittayakun, J., and Prayoonpokarach, S. (2017). Identification of potassium phase in catalysts supported on zeolite NaX and performance in transesterification of Jatropha seed oil. *Fuel Process. Technol.*, *156*, 62–67. doi: https://doi.org/10.1016/j.fuproc.2016.09.023

Maneechot, P., Sriprapakhan, P., Manadee, S., and Artkla, R. (2021). Improvement of potassium species dispersed on hierarchical zeolite NaY by using combined methods between ultrasound and microwave-assisted impregnation as catalysts for transesterification of refined Jatropha seed oil. *Biomass & Bioenergy*, *153*, 106202. doi: https://doi.org/10.1016/j.biombioe.2021.106202

Montalbo, K., de Leon, R., Sophiphun, O., Manadee, S., Prayoonpokarach, S., and Wittayakun, J. (2013). Characterization and catalytic performance of potassium loaded on rice husk silica and zeolite NaY for transesterification of Jatropha seed oil. *Quim. Nova*. 36(8), 1116–1120. doi: https://doi.org/10.1590/S0100-40422013000800007

Nakhaei Pour, A. and Mohammadi, A. (2021). Effects of synthesis parameters on organic template-free preparation of zeolite Y. *J. Inorg. Organomet. Polym. Mater.*, *31*(6), 2501–2510. doi: https://doi.org/10.1007/s10904-021-01926-1

Nuttinee, S., Jatuporn, W., Sanchai, P., Wojciech, S., and Frank, R. (2012). Basic properties of potassium oxide supported on zeolite Y studied by pyrrole-TPD and catalytic

conversion of methylbutynol. *Quim. Nova*, *35*(9), 1719-1723. doi: https://doi.org/ 10.1590/S0100-40422012000900003

Rakmae, S., Keawkumay, C., Osakoo, N., Montalbo, K. D., de Leon, R. L., Kidkhunthod, P., Chanlek, N., Roessner, F., Prayoonpokarach, S., and Wittayakun, J. (2016). Realization of active species in potassium catalysts on zeolite NaY prepared by ultrasound-assisted impregnation with acetate buffer and improved performance in transesterification of palm oil. *Fuel*, *184*, 512–517. doi: https://doi.org/10.1016/ j.fuel.2016.07.035

Rongchapo, W., Keawkumay, C., Osakoo, N., Deekamwong, K., Chanlek, N., Prayoonpokarach, S., and Wittayakun, J. (2017). Comprehension of paraquat adsorption on faujasite zeolite X and Y in sodium form. *Adsorp. Sci. Technol.*, *36*(1–2), 684–693. doi: https://doi.org/10.1177/0263617417715394

Supamathanon, N., Wittayakun, J., and Prayoonpokarach, S. (2011). Properties of Jatropha seed oil from Northeastern Thailand and its transesterification catalyzed by potassium supported on NaY zeolite. *J. Ind. Eng. Chem.*, *17*(2), 182–185. doi: https://doi.org/10.1016/j.jiec.2011.02.004

CHAPTER IV

COMPARISON OF 8% POTASSIUM ON PARAQUAT-MODIFIED ON
ZEOLITE SODIUM X AND Y FOR TRANSESTERIFICATION OF
PALM OIL

4.1 Abstract

In Chapter III, the 12 wt% potassium loading on paraquat-adsorbed FAU zeolite was too high to study the effect of the zeolite cavity. Both zeolite types showed over-impregnation, resulting in structural collapse. To clarify the effect of the zeolite cavity, the same experiment was carried out on 8K/NaX-PQ and 8K/NaY-PQ, with potassium loading 8 wt%. 8K/NaX-PQ gave 35.6% biodiesel yield in the first cycle while 8K/NaY-PQ provided only 7.1%. This difference was accompanied by the PQ adsorption along with the impregnation. As-prepared 8K/NaX-PQ exhibited higher acetate character, resulting in the collapse. However, the acetate was not found in as-prepared 8K/NaY-PQ, implying that the cavity was blocked by PQ and forced the precursor to locate at the external surface. Thus, the role of zeolite cavities is to confine the precursor for conversion to carbonate, crucial for initial high yield. However, conversion also leads to structural collapse, resulting in a sharp drop in reusability.

4.2 Introduction

The structure of zeolite in the potassium heterogeneous catalysts was still crucial for the reusability in transesterification of palm oil. The collapse of support usually came with poor reusability, as seen in both previous results and the literature (Intarapong et al., 2011; Kosawatthanakun et al., 2022). On the other hand, 12 wt% K/hierarchical NaY, which still exhibited high intensity of XRD peak intensities, produced excellent reusability for 5 cycles from 97.3% to 88.2% (Maneechot et al., 2021). This suggests that the zeolite support, which houses the active species, could only function effectively when its structural integrity is maintained.

According to Chapter III, the the impact of the zeolite cavity in 12K/FAU-PQ catalysts is still obscured probably due to the high concentration of potassium, 12 wt%. This excess amount could cause a structural collapse in both zeolite NaX and NaY even if both types had different paraquat adsorption capacities. Thus, the smaller amount of precursor might show more clearly the effect of zeolite cavity. The lower concentration of the potassium precursor might affect different degrees of impregnation on the zeolite containing different adsorbed paraquat. Hypothetically, zeolite NaX, with its lower paraquat adsorption capacity (46.7 mg/g), might allow for a larger amount of precursor impregnation. Conversely, zeolite NaY, which exhibits a higher paraquat adsorption capacity (146.4 mg/g), might have a smaller impregnation. This suggests that in zeolite NaY, most of the precursor molecules likely reside on the external surface of the zeolite support rather than within its cavities. Therefore, this chapter still aims to study the effect of zeolite cavity based on the different degrees of impregnation on the zeolite containing different adsorbed paraquat. The comparison included the synthesis of 8K/NaX-PQ and 8K/NaY-PQ as well as their catalytic performance and characterization.

4.3 Experimental

The catalyst preparation was similar to Chapter III except that the lower precursor concentration was used as to produce 8 wt%. The prepared catalysts were named 8K/NaX-PQ and 8K/NaY-PQ. The catalysts were characterized by XRD, FTIR, and MBOH conversion. The transesterification was performed and the biodiesel yields were determined with the same procedure described in Chapter III.

4.4 Results and Discussion

4.4.1 Appearance of 8% potassium catalysts

The appearances of as-prepared 8K/NaX-PQ and 8K/NaY-PQ are presented in **Figures 4.1a** and **4.1b**, respectively. The photographs of the calcined catalysts are displayed in **Figures 4.1c** and **4.1d**. Similar to the catalyst with 12 wt%

potassium, the powders of as-prepared samples were brown after impregnation and turned white after calcination, suggesting that paraquat decomposition.
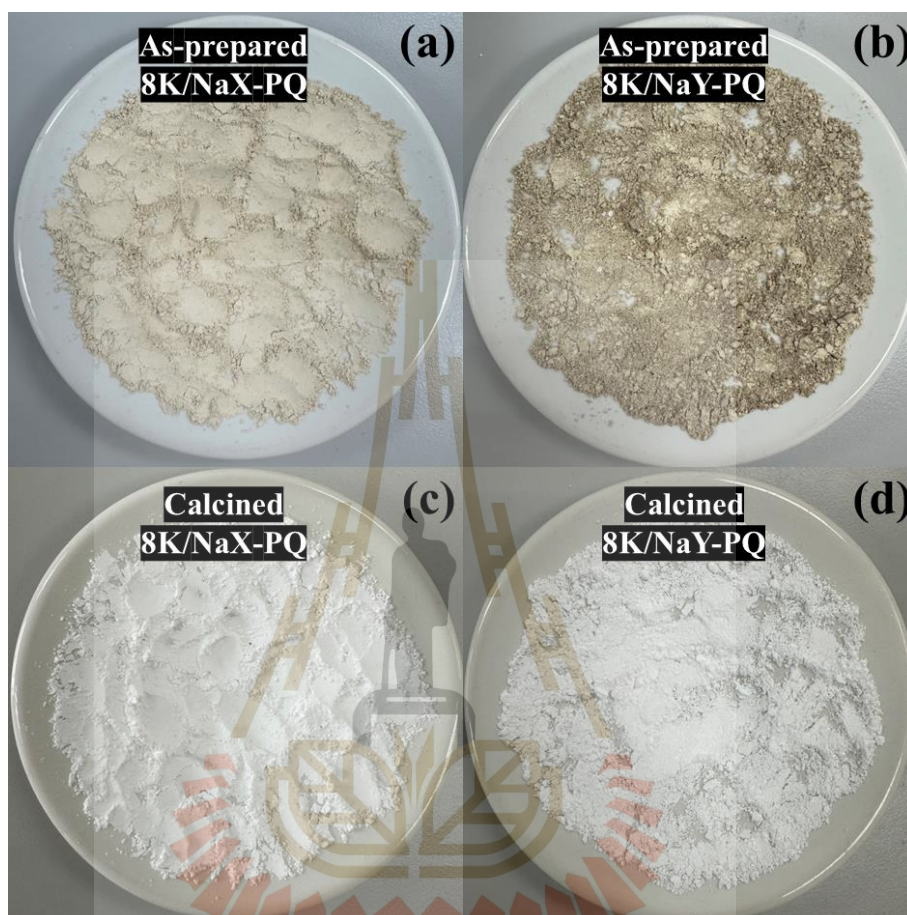

Figure 4.1 Physical appearances of as-prepared 8K/NaX-PQ (a), as-prepared 8K/NaY-PQ (b), 8K/NaX-PQ (c), 8K/NaY-PQ (d).

4.4.2 Transesterification of palm oil catalyzed by 8K/FAU-PQ

Figure 4.2 demonstrates the biodiesel yields from the first and second cycles from 8K/NaX-PQ and 8K/NaY-PQ. The chromatograms were shown in **Figures 4.3** and **4.4**, respectively. A biodiesel yield of 35.6% was obtained by the catalysis of 8K/NaX-PQ. Interestingly, only 7.1% was received by the 8K/NaY-PQ. Those catalysts were prepared with the identical concentration except the support material (PQ-adsorbed FAU zeolite). As stated in the previous chapter, zeolite NaY had a higher PQ adsorption capacity than zeolite NaX. This result led to different impregnation ability

of potassium acetate buffer solution. To understand the phenomenon of such catalysis, both as-prepared and calcined samples were studied.
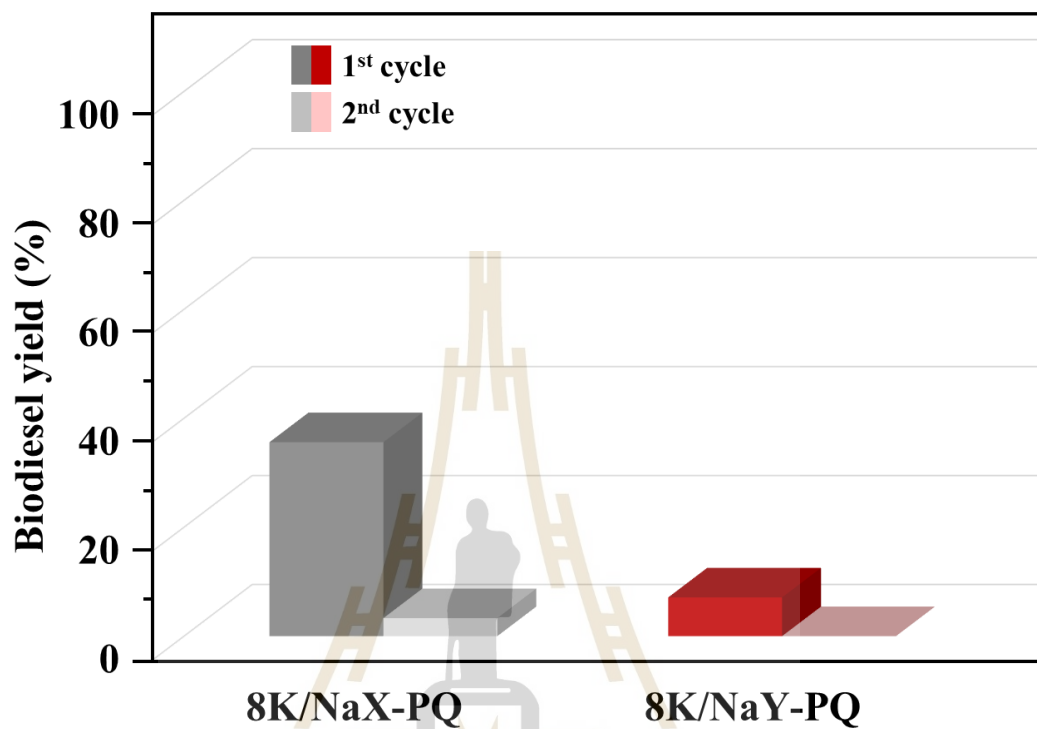

Figure 4.2 Biodiesel yield from transesterification reaction of palm oil catalyzed at 60 ℃ for 3 h by 0.2 g of 8K/NaX-PQ and 8K/NaY-PQ.
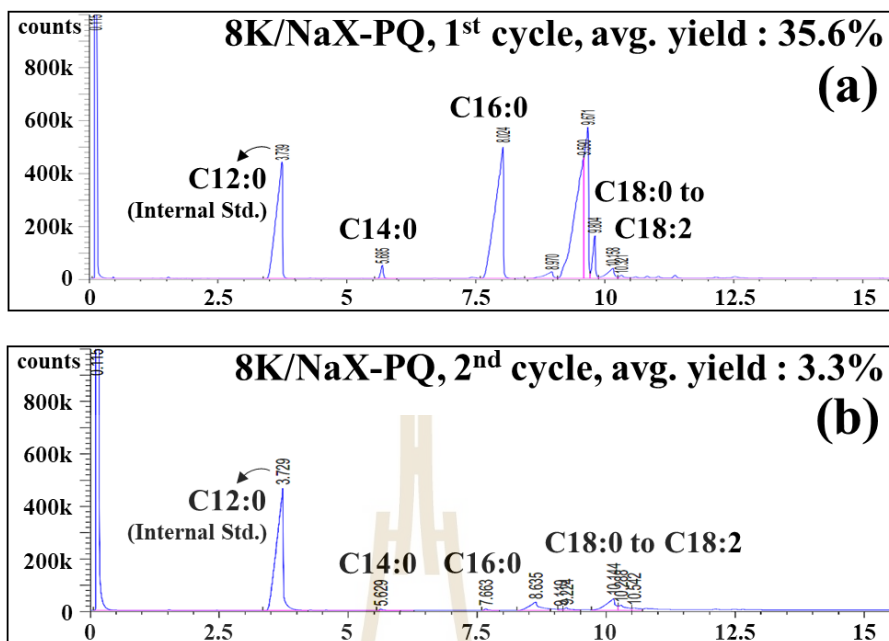
Figure 4.3 Chromatograms of biodiesel from the 1st (a) and 2nd (b) cycles catalyzed
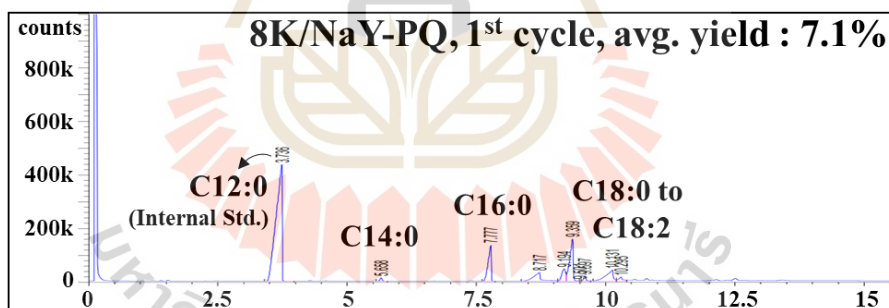
by 8K/NaX-PQ.

Figure 4.4 Chromatogram of biodiesel from the 1st cycle catalyzed by 8K/NaY-PQ.

4.4.3 Characterization of 8% potassium catalysts

Figures 4.5 and **4.6** display the diffractograms and FTIR spectra of the as-prepared samples, respectively. Firstly, in the as-prepared samples of 8% potassium acetate, the zeolite peaks in the 12% samples slightly decreased. Interestingly, the sharp peak at 8.88° and the tiny peak at 23.5° (diamond symbol) were majestically noticed in the only as-prepared 8K/NaX-PQ. This 2θ was indicated as the acetate (Kosawatthanakun et al., 2022). However, this finding was not observed in the 8K/NaY-

PQ. It indicated that zeolite NaX, a poor PQ adsorption, exhibited a higher degree of precursor impregnation than zeolite NaY, a high PQ adsorption. Although both as-prepared samples showed strong acetate peaks, as-prepared 8K/NaY-PQ still exhibited PQ FTIR bands stronger than as-prepared 8K/NaX-PQ, similar to those PQ-adsorbed samples. This could be implied by the fact that, in the 8% precursor loading, PQ that is adsorbed in the FAU cage could block pores and force the potassium acetate buffer solution to locate at the external surface, potentially preventing structural collapse during calcination. This result suggested that when the 8% precursor was loaded into the FAU-PQ, NaX-PQ could be impregnated in a larger amount than NaY-PQ.
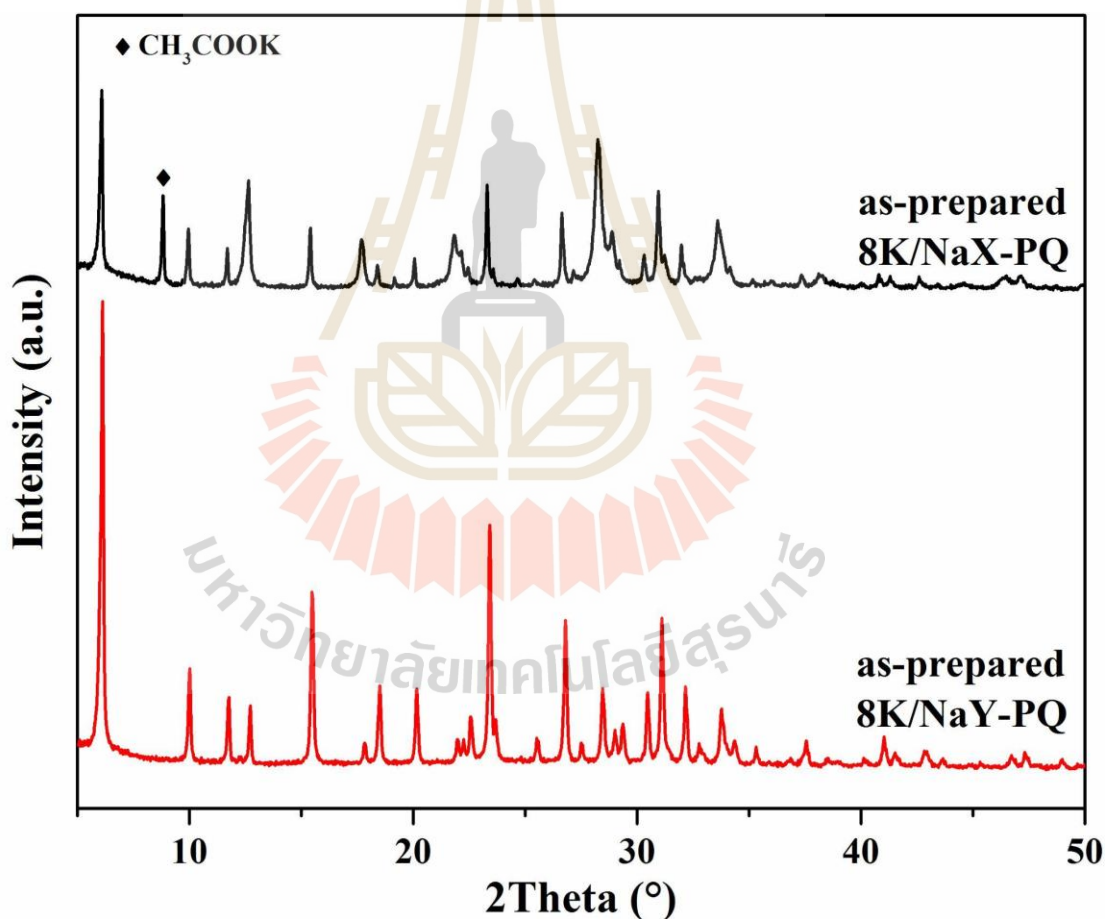

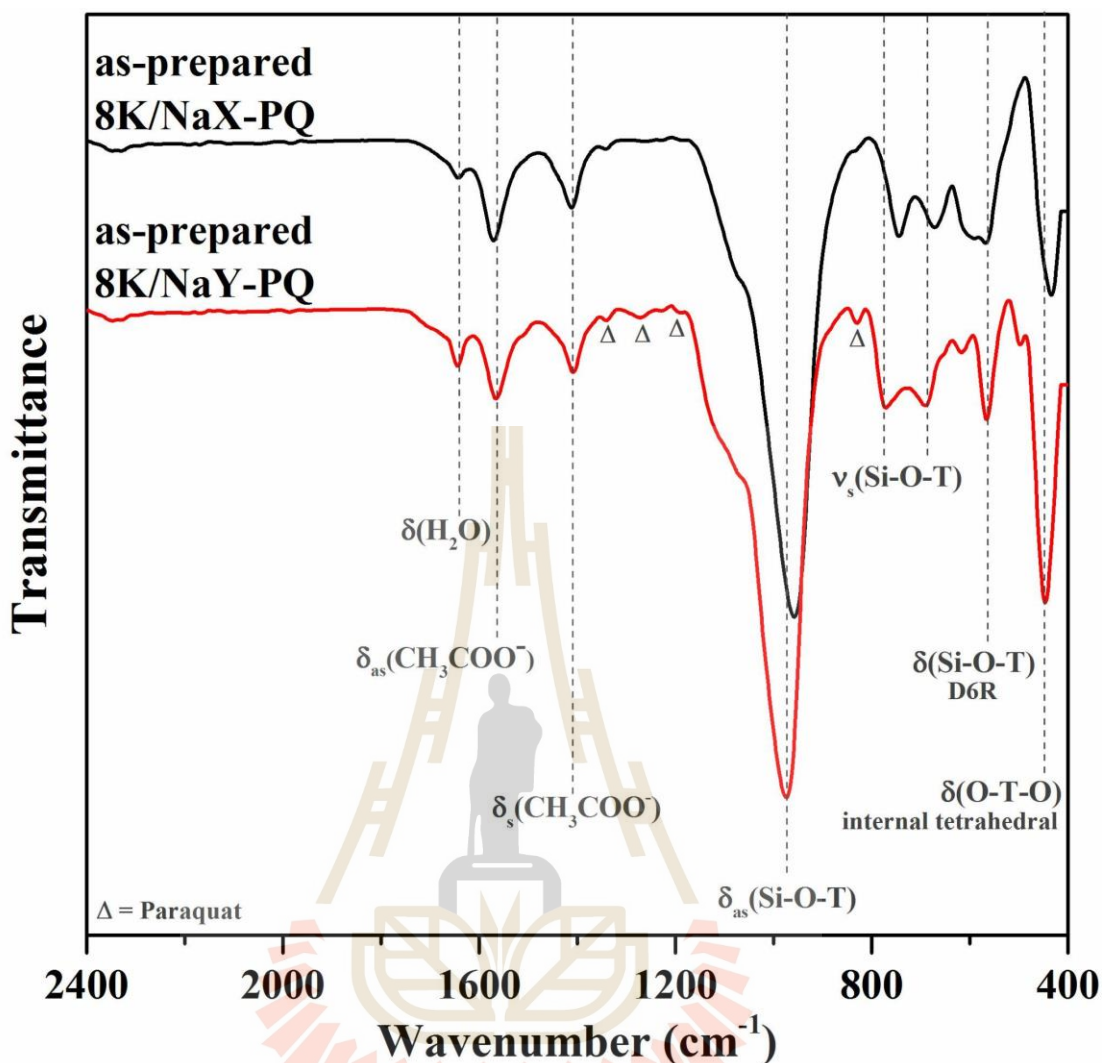**Figure 4.5** XRD patterns of the as-prepared 8K/NaX-PQ and 8K/NaY-PQ.

Figure 4.6 FTIR spectra of the as-prepared 8K/NaX-PQ and 8K/NaY-PQ.

Figures 4.7 and **4.8** display the diffractograms and FTIR curves of the 8% potassium catalysts, respectively. Firstly, the main peaks of the zeolite NaX dropped significantly with the disappearance of acetate peaks. Moreover, the zeolite NaY character resumed their former intensity without any alien peak. In FTIR analysis, the acetate peaks disappeared with broad and smaller peaks of the zeolite while two positions of carbonate were obtained in zeolite NaX sample. However, only one peak of carbonate was received in the zeolite NaY with sharp and strong peak of the zeolite. These FTIR discussions were consistent with their diffractograms. Therefore, it could confirm that the paraquats could block the pore of support, especially zeolite NaY, and prevent the structural collapse issue. Moreover, the lack of PQ adsorption capacity

in the zeolite NaX sample, which led to a higher amount of potassium acetate buffer solution inside the pore, could destroy the zeolite structure. This explains how the acetate peak was only seen in the XRD pattern of the as-prepared 8K/NaX-PQ. In the literature explanation, this collapsing framework was caused by the hydrolysis of the zeolite bonds (Si–O–Al) under the thermal condition (Kosawatthanakun et al., 2022; Peña et al., 2013), assisted by the alkali metal species, which might be the potassium ion. Thus, the findings could be summed up the general potassium heterogeneous catalysts as follows: (i) After being calcined, the acetate changed into another form (ion exchange) and (ii) the structural collapse of the catalyst was caused by the potassium acetate buffer with the calcination at 500 °C, as was often found in the earlier researches (Kosawatthanakun et al., 2022; Manadee et al., 2017; Maneechot et al., 2021; Montalbo et al., 2013; Nuttinee et al., 2012; Rakmae et al., 2016; Supamathanon et al., 2011).

In transesterification, 8K/NaX-PQ that had a collapsing structure showed ~35% yield while only 7% yield was obtained from 8K/NaY-PQ, a high XRD intensity sample. 8K/NaX-PQ could run the reaction as similar to 12K/FAU-PQ, a collapsing sample. The percentage dropped to half since the reduction of precursor concentration from 12% to 8%. On the other hand, 8K/NaY-PQ could not run the reaction. For more reason, MBOH conversion was used to explain.
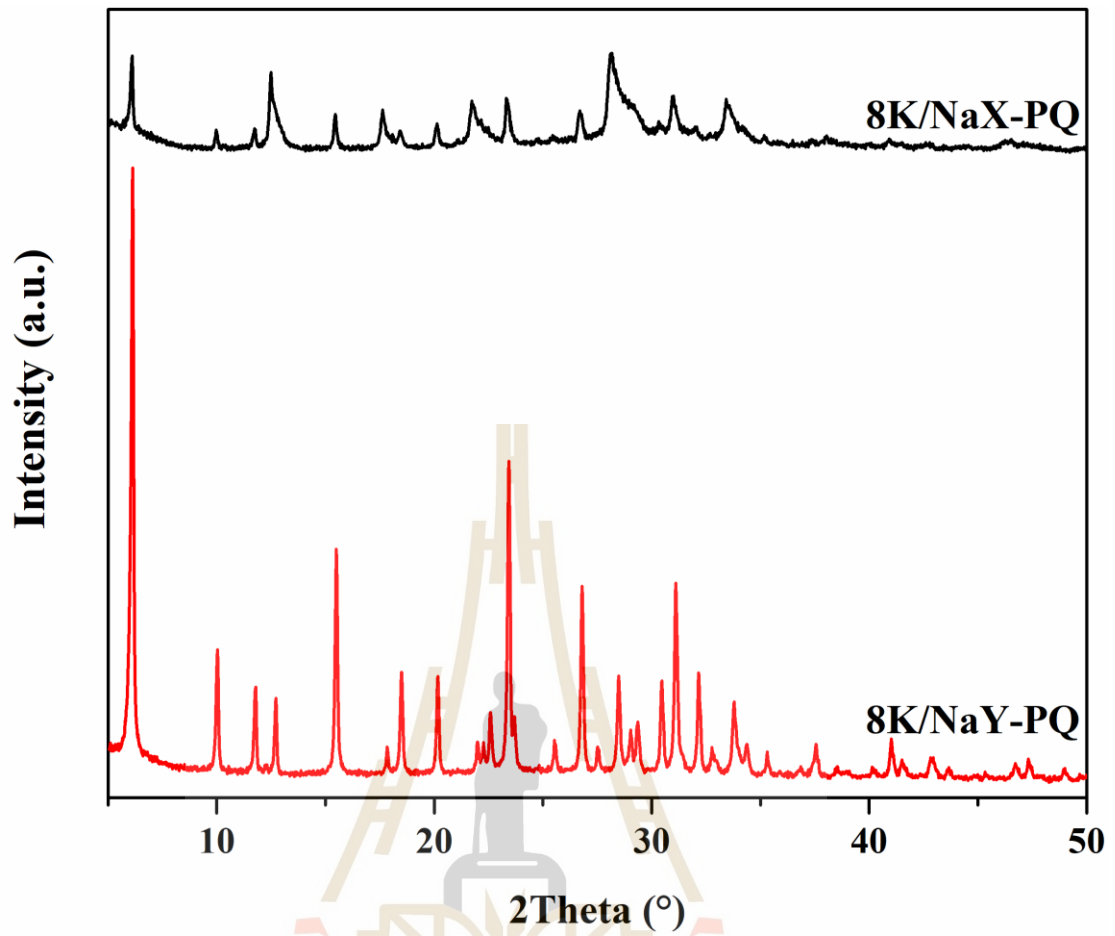
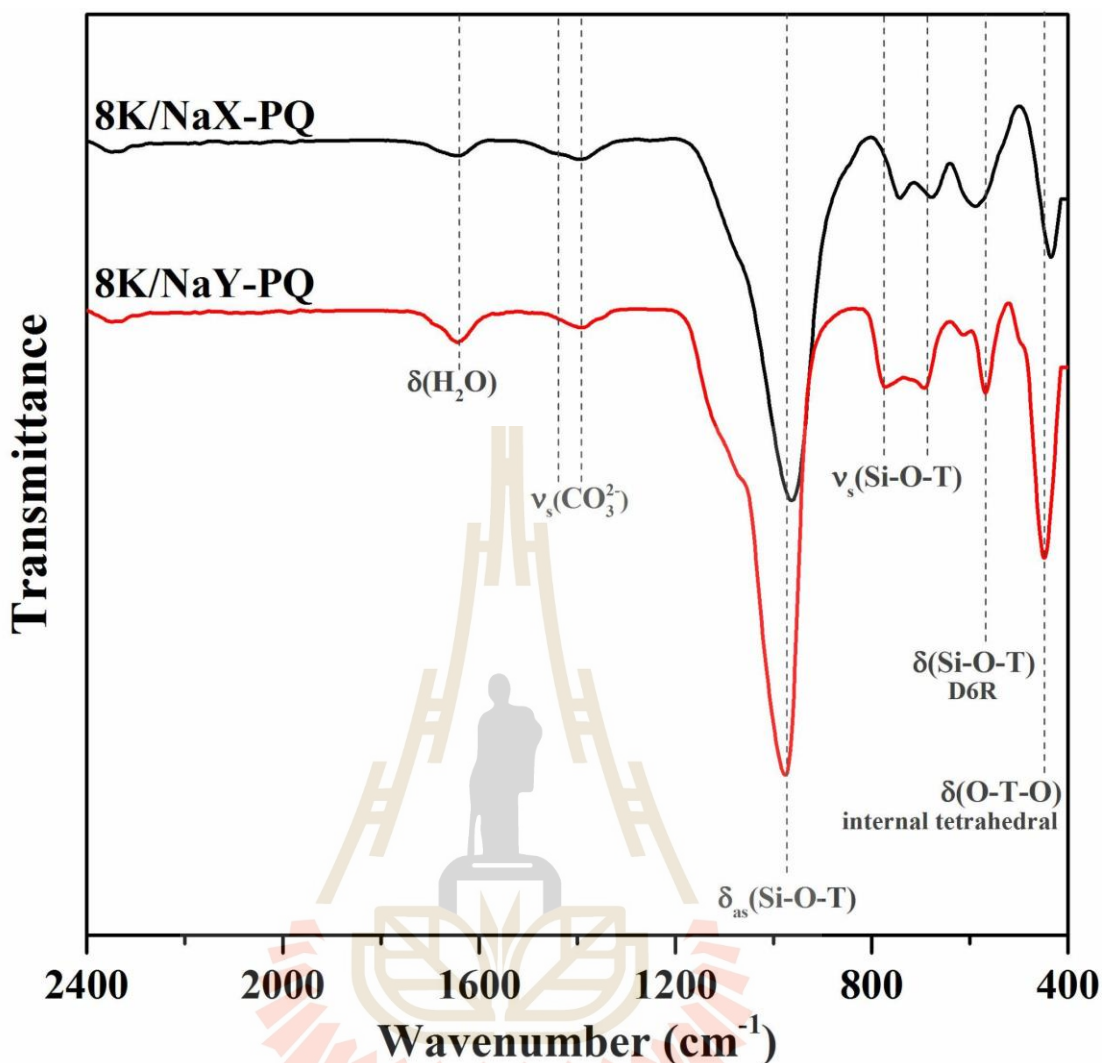**Figure 4.7** XRD patterns of 8K/NaX-PQ and 8K/NaY-PQ.

Figure 4.8 FTIR spectra of 8K/NaX-PQ and 8K/NaY-PQ.

Figure 4.9 demonstrates the MBOH (2-Methyl-3-butyn-2-ol) conversion of 8K/NaX-PQ and 8K/NaY-PQ. Most conversion was catalyzed by a basic substance, as shown in **Table 4.1**. Precisely, high conversion (>99%) of MBOH by both calcined catalysts, suggesting catalysis by alkali species (likely carbonate formed from acetate during calcination). Products were primarily acetylene (~60%) and acetone (~40%).

In those basic sites, the tendency of MBOH conversion received from the chromatogram was presented almost constant in 8K/NaX-PQ (slight drop at the beginning). The almost steady conversion was commonly seen in the structural collapsing potassium catalysts. while 8K/NaY-PQ, a higher crystallinity sample compared to the rest, showed a significant drop initially followed by a steady at the

end of the measurement. This trend of 8K/NaY-PQ sample could imply that the catalyzed substance located at the external surface of NaY-PQ. It was probably due to the zeolite NaY was clogged by paraquat, as stated above, forcing the potassium acetate buffer or active species were at the exterior. It results in high catalysis at the beginning period. Nevertheless, poor catalysis was obtained afterward. This might be due to there was no catalyzed species enough to catalyze the MBOH since it was not confined to the cage causing it to be already calcined. The highly low conversion was the catalysis of only pure support, which was similar to the MBOH conversion of bare zeolite NaY in the literature (Kosawatthanakun et al., 2022; Nuttinee et al., 2012). On the other hand, a steady and high degree of conversion was commonly seen in the literature of potassium catalysts (8K/NaX-PQ, 12K/NaX-PQ, and 12K/NaY-PQ). They discussed in the aspect of active catalyzed sites, dispersion, and MBOH accessibility. However, both published and this XRD patterns exhibited the flat line, which means it should not exist the area for dispersion and accessibility. Moreover, the BET surface area decreased dramatically, which was caused by the destroyed structure of zeolite NaX and NaY (Kosawatthanakun et al., 2022; Rakmae et al., 2016). Thus, the constant catalysis of MBOH test reaction was reported due to a high concentration of catalyzed species among the collapsing support. Moreover, because of the different ability in paraquat adsorption on zeolite NaX and NaY, as reported in the previous chapter, led to the difference between 8K/NaX-PQ and 8K/NaY-PQ.

In transesterification, 8K/NaX-PQ might have a carbonate species among the collapsing support, resulting in higher biodiesel yield. In the case of 8K/NaY-PQ, the carbonate species located at the external surface might partially decompose after calcination This decomposition led to a lower basicity than 8K/NaX-PQ, resulting in poor catalysis.
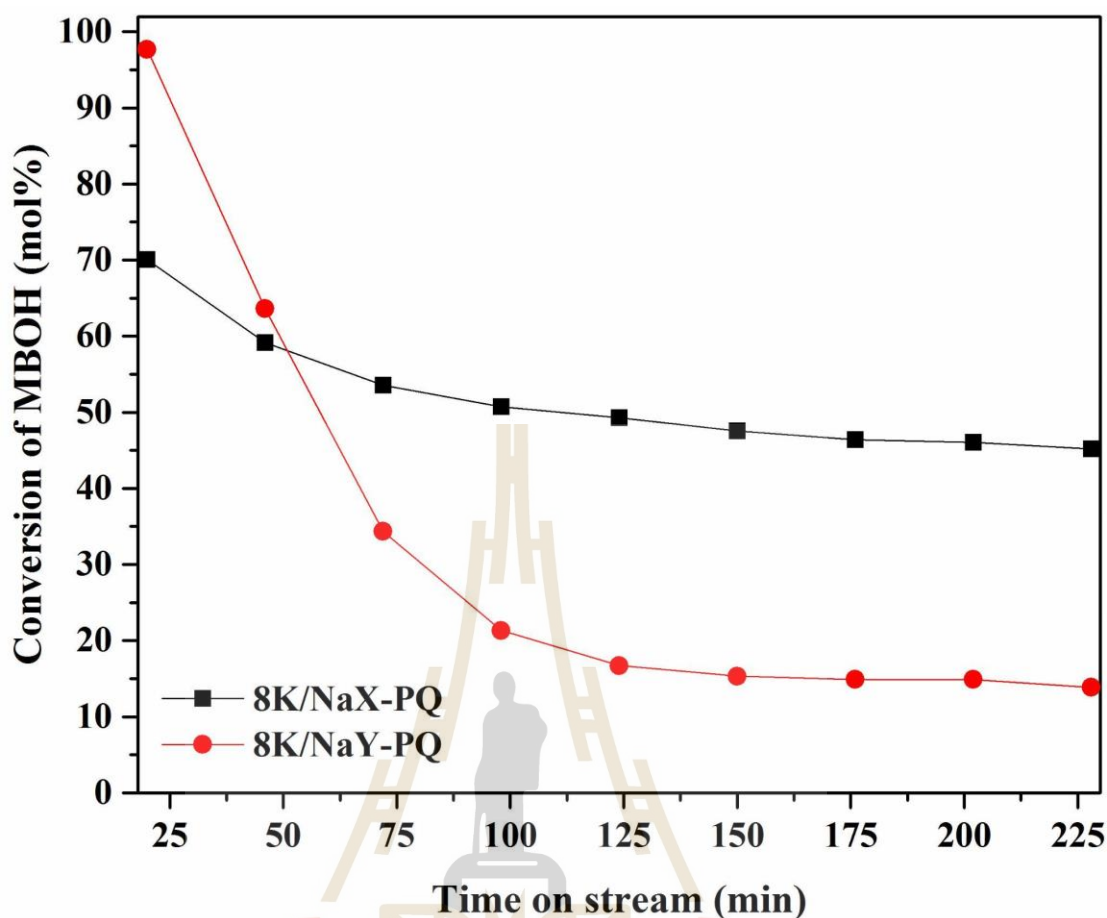
Figure 4.9 MBOH conversion of 8K/NaX-PQ and 8K/NaY-PQ; reaction temperature,

120 °C; amount of catalyst, 0.020 g.

Table 4.1 MBOH conversion and product selectivity from the MBOH decomposition of
8% catalysts analyzed by gas chromatography.

Samples	MBOH conversion (mol%)		Product selectivity (mol%)			
			Base-catalyzed site		Acid-catalyzed site	
	1st injection	Last injection	Acetylene	Acetone	MBYNE	Prenal
8K/NaX-PQ	70.0	45.2	58.2	41.6	0.2	0
8K/NaY-PQ	97.7	13.9	56.9	42.8	0.3	0

Thus, this result in this chapter might conclude the importance of zeolite that
zeolite, a porous material, traps the potassium precursor inside, and then converts to

carbonate form. The lack of zeolite cavities leads to the non-capturing of the potassium acetate buffer solution, which is eventually decomposed. However, the process of conversion from acetate to carbonate is accompanied by structural collapse. This phenomenon results in a high biodiesel yield in the first cycle, then significantly drops in the second cycle. According to the XRF results in the previous chapter, it was not only the dwindling of sodium content observed after catalysis, the disappearance of carbonate peaks in the FTIR spectra was also noticed. It is possible to infer that, contrary to what has been stated in earlier publications, the main active species for the catalysis of the transesterification of palm oil was in the carbonate form, not the potassium ion. In the upcoming chapter, this theory will be thoroughly revealed for more in-depth details.

4.5 Conclusion

This chapter studied the effect of the cavity by impregnating 8% potassium catalysts into PQ-adsorbed zeolite. The catalytic performance in transesterification revealed a significant difference. 8K/NaX-PQ achieved a much higher yield (35.6%) compared to 8K/NaY-PQ (7.1%). Analysis of the as-prepared catalysts indicated a higher peak of acetate in 8K/NaX-PQ, which encountered structural collapse. Interestingly, the absence of acetate in as-prepared 8K/NaY-PQ suggests that PQ molecules blocked the cavities, forcing the precursor to reside on the external surface. These findings point towards a critical role for zeolite cavities: they confine the precursor, facilitating its conversion to carbonate, a process essential for achieving a high biodiesel yield in the first cycle. However, this conversion leads to structural collapse in the zeolite, leading to a significant decline in reusability.
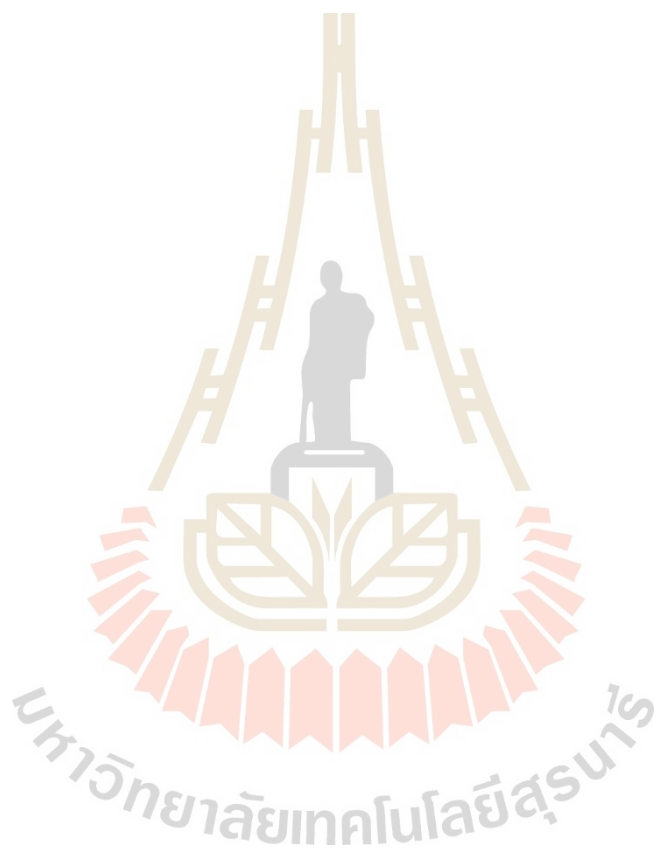
4.6 References

Intarapong, P., Luengnaruemitchai, A., and Jai-In, S. (2011). Transesterification of palm oil over KOH/NaY zeolite in a packed-bed reactor. *Int. J. Renew. Energy Res.*, *1*(4), 271–280. doi: https://doi.org/10.20508/ijrer.v1i4.81.g66

Kosawatthanakun, S., Pansakdanon, C., Sosa, N., Chanlek, N., Roessner, F., Prayoonpokarach, S., and Wittayakun, J. (2022). Comparative properties of K/NaX and K/NaY from ultrasound-assisted impregnation and performance in transesterification of palm oil. *ACS Omega, 7*(11), 9130–9141. doi: https://doi.org/ 10.1021/acsomega.1c04912

Manadee, S., Sophiphun, O., Osakoo, N., Supamathanon, N., Kidkhunthod, P., Chanlek, N., Wittayakun, J., and Prayoonpokarach, S. (2017). Identification of potassium phase in catalysts supported on zeolite NaX and performance in transesterification of Jatropha seed oil. *Fuel Process. Technol., 156*, 62–67. doi: https://doi.org/10.1016/j.fuproc.2016.09.023

Maneechot, P., Sriprapakhan, P., Manadee, S., and Artkla, R. (2021). Improvement of potassium species dispersed on hierarchical zeolite NaY by using combined methods between ultrasound and microwave-assisted impregnation as catalysts for transesterification of refined Jatropha seed oil. *Biomass & Bioenergy, 153*, 106202. doi: https://doi.org/10.1016/j.biombioe.2021.106202

Montalbo, K., de Leon, R., Sophiphun, O., Manadee, S., Prayoonpokarach, S., and Wittayakun, J. (2013). Characterization and catalytic performance of potassium loaded on rice husk silica and zeolite NaY for transesterification of Jatropha seed oil. *Quim. Nova*. *36*(8), 1116–1120. doi: https://doi.org/10.1590/S0100-4042201300 0800007

Nuttinee, S., Jatuporn, W., Sanchai, P., Wojciech, S., and Frank, R. (2012). Basic properties of potassium oxide supported on zeolite Y studied by pyrrole-TPD and catalytic conversion of methylbutynol. *Quim. Nova, 35*(9), 1719-1723. doi: https://doi.org/ 10.1590/S0100-40422012000900003

Peña, R., Romero, R., Martínez, S. L., Natividad, R., and Ramírez, A. (2013). Characterization of KNO_3/NaX catalyst for sunflower oil transesterification. *Fuel, 110*, 63–69. doi: https://doi.org/10.1016/j.fuel.2012.07.072

Rakmae, S., Keawkumay, C., Osakoo, N., Montalbo, K. D., de Leon, R. L., Kidkhunthod, P., Chanlek, N., Roessner, F., Prayoonpokarach, S., and Wittayakun, J. (2016). Realization of active species in potassium catalysts on zeolite NaY prepared by ultrasound-assisted impregnation with acetate buffer and improved performance

in transesterification of palm oil. *Fuel*, *184*, 512–517. doi: https://doi.org/10.1016/j.fuel.2016.07.035

Supamathanon, N., Wittayakun, J., and Prayoonpokarach, S. (2011). Properties of Jatropha seed oil from Northeastern Thailand and its transesterification catalyzed by potassium supported on NaY zeolite. *J. Ind. Eng. Chem.*, *17*(2), 182–185. doi: https://doi.org/10.1016/j.jiec.2011.02.004

CHAPTER V

COMPARISON OF POTASSIUM AND SODIUM CARBONATE ON
ZEOLITE SODIUM X ON PROPERTIES AND TRANSESTERIFICATION
OF PALM OIL

5.1 Abstract

Catalyst 12K/NaX prepared by impregnation with potassium acetate buffer has problems with the collapse of zeolite support and leaching of carbonate species. To prevent the zeolite collapse from calcination, this study explores the properties of 12K/NaX and 12Na/NaX catalysts prepared by direct impregnation of potassium and sodium carbonate on zeolite NaX and performance in transesterification of palm oil. In the first cycle, K_2CO_3/NaX and Na_2CO_3/NaX produced 95.9% and 70.6% of the biodiesel yields, respectively, demonstrating their activity in this reaction. However, immediate decline was found in the K_2CO_3 catalyst while Na_2CO_3 catalyst exhibited a gradual drop. This was because of the poor solubility of Na_2CO_3 in the CH_3OH/glycerol, resulting in high reusability. Moreover, since Na_2CO_3 was also active in this reaction. Therefore, carbonate should be the actual active species, supported by FTIR and TGMS techniques that report the absence of a carbonate signal, which corresponds to the decrease in biodiesel yield.

5.2 Introduction

Potassium catalysts are well known for their efficiency in the transesterification process but their reusability remains a significant challenge. This limited reusability has several drawbacks. Firstly, it necessitates the use of fresh catalysts to produce a high biodiesel yield for each reaction cycle, resulting in an increase in production costs. Secondly, the improper disposal of spent catalysts can pose environmental concerns. Furthermore, the continuous demand for fresh catalysts creates logistical challenges and disrupts the overall efficiency of the biodiesel production process. However, most

potassium catalysts reported in the literature still have poor recycling ability (Intarapong et al., 2011; Kosawatthanakun et al., 2022). Therefore, developing a reusable potassium-based catalyst system for transesterification of palm oil is crucial and challenging for achieving a more sustainable and cost-effective approach to biodiesel production.

One of the problems of zeolite-supported potassium catalysts is the structural collapse of the zeolite support. Intarapong and coworkers prepared a potassium catalyst by impregnation of 15% KOH on the zeolite NaY. A 93% biodiesel yield was received in the first cycle but dropped to 15% in the fifth cycle (Intarapong et al., 2011). It was probably due to the collapse of the zeolite structure according to the evidence from XRD pattern, FTIR spectrum, and SEM image. The cause is the use of a strong base (KOH). Later on, the potassium precursor was changed from KOH to CH_3COOK/CH_3COOH buffer solution (Kosawatthanakun et al., 2022; Manadee et al., 2017; Montalbo et al., 2013; Rakmae et al., 2016; Supamathanon et al., 2011). Unfortunately, the poor recyclability was still seen that 12K/NaX and 12K/NaY generated 97.9 and 94.4% in the first cycle, then dropped dramatically to 60% and 3% in the second run, respectively (Kosawatthanakun et al., 2022). The same cause of this problem was the structural collapse of the zeolite due to the hydrolysis of Si−O−Al bonds under thermal treatment and the assistance of alkali metal species (Kosawatthanakun et al., 2022; Montalbo et al., 2013). Besides the prevention of zeolite collapse, the potassium acetate buffer precursor is converted to carbonate after calcination (Kosawatthanakun et al., 2022; Manadee et al., 2017; Rakmae et al., 2016). However, the calcination process still resulted in the zeolite structural collapse which might correspond to poor reusability.

This chapter proposes the catalyst preparation by impregnation of potassium carbonate directly on zeolite NaX without calcination. This intention could preserve the zeolite structure and save energy from calcination. The reusability of this catalyst is investigated. Besides, sodium carbonate precursor is compared with the potassium form. Both potassium and sodium metals exhibit a similar basic nature, which was the carbonate ion. Both catalysts could run the transesterification as a homogeneous catalyst effectively (Malins, 2018). The difference between those metals was not only

their ionic radii and interaction with the reaction but the solubility was also included (Malins, 2018). The second purpose is to identify the active species between potassium ions, sodium ions, and/or carbonate ions. Moreover, this research delves specifically into the comparative analysis of potassium and sodium catalysts in the transesterification of palm oil. By investigating the performance of potassium and sodium catalysts, this work aims to gain valuable insights into the transesterification of palm oil to improve the reusability and to identify the active species for catalysis of the reaction.

5.3 Experimental

5.3.1 Chemicals and Materials

A powder of commercial zeolite NaX (Sigma-Aldrich, ~2 μm average particle size) was used in catalyst preparation. Potassium carbonate (K_2CO_3, 99%) and sodium carbonate (Na_2CO_3, 99.5% both from Carlo Erba were used to impregnate the zeolite NaX. The chemicals for the experiment of thin-layer chromatography were petroleum ether (Panreac), diethyl ether (Panreac, 99.7%), and glacial acetic acid (ACI Labscan, 99.7%). Glycerol (CARLO ERBA, 99.5%), K_2CO_3, Na_2CO_3, potassium acetate (CH_3COOK, CARLO ERBA, 99.5%), and sodium acetate (CH_3COONa, CARLO ERBA, 99.5%) were applied for leaching test.

5.3.2 Preparation of carbonate catalysts

The catalyst preparation was modified by literature (Zhang et al., 2022). Firstly, the dried commercial zeolite NaX was impregnated by a solution of potassium or sodium carbonate with a concentration of 12%w/w prepared by dissolving K_2CO_3 or Na_2CO_3 in DI water, respectively. Then, the slurry was stirred magnetically with the stirring speed of 350 rpm at ambient temperature for 3 h. Finally, the catalyst was dried at 85 °C overnight. Those catalyst samples were named K_2CO_3/NaX and Na_2CO_3/NaX, respectively.

5.3.3 Transesterification of palm oil

The transesterification reaction was done with the same procedure in Chapter III. Briefly, 0.2 g of catalyst, 2.9 g of methanol, and 5 g of palm oil were

combined in a 100-milliliter one-neck round bottom flask equipped with a Graham condenser. The experiment was carried out in a paraffin fluid with 500 rpm swirling for three hours at 60 °C. Suction filtration was applied in order to separate the final mixture, and 5 mL of methanol was employed as a rinse. By applying a rotary evaporator set to 50 °C and rotating at a speed of 60 cycles per minute, the liquid phase was vaporized in order to remove the methanol. After being moved to a vial, the vaporized liquid was allowed to separate overnight. Fatty acid methyl esters (FAMEs) were quantified using the biodiesel that was generated in the uppermost layer. Hexane and methanol were used in alternate cycles to wash the solid phase. Ultimately, the solid sample was classified as a spent catalyst after being dried at 100 °C for the whole night.

The screening biodiesel results were analyzed by thin-layer chromatography (TLC). The alumina (Al_2O_3) plate (TLC Silica gel 60 F_{254}, Merck, Germany) with a size of 8 × 4 cm was employed in this experiment as a polar stationary phase. The spotting line and solvent front were set 1 cm and 0.5 cm from the bottom and top edge, respectively. A mixture of petroleum ether: diethyl ether: glacial acetic acid (volume ratio, 85:15:1) was utilized as a mobile phase. Moreover, 7 mL of mobile phase was used in the developing chamber containing a piece of filter paper. Before developing, the TLC plate was spotted by biodiesel samples two times compared with the palm oil. After the separation, the TLC plates were irradiated by UV light to monitor the development.

The biodiesel test procedure (EN 14103) was analyzed the number of FAMEs content by using the gas chromatography technique (GC-14A, Shimadzu) and fitted with a flame ionization detector (FID/TCD, Shimadzu) using a non-polar capillary column (100% dimethylpolysiloxane, SGE, BP1) with a length of 30 m, a film thickness of 3 µm, and an internal diameter of 0.53 mm. The gas flow of nitrogen was utilized as a carrier gas. The spitless injections with a sample size of 2 µL will be performed by heating at 220 °C. The temperature program was started at 80 °C, then ramped up to 260 °C at a rate of 10 °C/min, Finally, the oven temperature was kept at 260 °C. The overall run was carried out for about 30 minutes. Moreover, the internal standard was methyl heptadecanoate, commonly known as "methyl margarate," $C17:0$

(CH₃(CH₂)₁₅COOCH₃, SIGMA-ALDRICH, 99%). The content of FAMEs (x_{FAMEs}) and the percentage of biodiesel yield in the obtained product was acquired from an equation, respectively:

$$x_{FAMEs} = \left[\frac{(\sum A_{C16:0-C18:2}) - A_{C12:0}}{A_{C12:0}}\right] \times \left[\frac{[C12:0]V_{C12:0}}{m_{sample}}\right] \quad (6)$$

where A, $[C17:0]$, $V_{C17:0}$, and m_{sample} was determined as a peak area from the chromatogram ($\sum A_{C16:0-C18:2}$ was gathered $C16:0$ (methyl hexadecanoate, known as methyl palmitate), $C18:0$ (methyl octadecanoate, known as methyl stearate), $C18:1$ n9e (methyl 9(E) octadecanoate, known as methyl elaidate), and $C18:2$ n6e (methyl *cis,cis* − 9,2 − hexadecanoate, known as methyl linoleate)), concentration, volume of $C17:0$ concentration, and mass of the analyzed biodiesel sample, respectively.

$$biodiesel\ yield\ (\%mol) = \left[\frac{m_{biodiesel}}{m_{palm\ oil}}\right] \times \left[\frac{x_{FAMEs}}{x_{triglycerides}}\right] \times \left[\frac{M_{triglycerides}}{3M_{FAMEs}}\right] \times 100 \quad (7)$$

where the terms "$m_{biodiesel}$" and "$m_{palm\ oil}$" refer to the mass of biodiesel and palm oil, respectively. Triglyceride content as a percentage was designated as $x_{triglycerides}$. The average molecular weights of triglycerides and FAMEs, respectively, was denoted as $M_{triglycerides}$ and M_{FAMEs}. The stoichiometric number (3) is multiplied at M_{FAMEs} was imposed from the balanced chemical equation for the transesterification with the proportion of one mole of triglycerides with three moles of methanol.

5.3.4 Characterization

Phases of the catalysts were analyzed by X-ray diffraction (XRD) on a Bruker D2 Phaser Diffractometer for powder XRD applications in Bragg-Brentano geometry (Bruker, Karlsruhe, Germany) with Cu Kα radiation (λ=1.5406 Å) operated at a voltage and current of 30 kV and 10 mA, respectively. The apparatus was equipped with the unique LYNXEYE XE-T detector. In addition, the scan speed and increment were used as 0.2 s/step and 0.02 s/step, respectively. The 2θ range of 5–50° was applied to gather the diffractions.

Morphology of the composites were analyzed by scanning electron microscopy with energy dispersive X-ray spectroscopy (SEM-EDS, Carl Zeiss, Auriga® series, Carl Zeiss NTS GmbH, Oberkochen, Germany) with accelerating voltage of 30 kV. The samples were spread on the carbon tape and coated with gold by sputtering.

Phase transformation study of catalysts was investigated by a Fourier transform infrared spectroscopy (FTIR, Perkin Elmer Spectrum GX) using (Bruker Tensor 27 FTIR) using ATR mode with a resolution of 2 cm^{-1}. The wavenumber range and number of scans for this experiment were used from 400 to 2400 cm^{-1} and 64, respectively.

Elemental compositions of samples were determined by energy dispersive X-ray fluorescence spectroscopy (ED-XRF, Horiba XGT-5200). The X-ray source was a Rh X-ray tube with 50 kV/mA and Mono-capillary guide tubes. The Fluorescence detector was a Peltier-cooled silicon drift detector (SDD) with an energy range of 0-40 keV and elements detected [11]Na to [92]U.

The carbonate was analyzed by thermogravimetric with mass-spectrometric (TGMS) technique (TGA-STA 449F3 NETZSCH5 analyzer). The TGA, DTG, and MS evaluations were determined from 35 °C to 500 °C with the ramp rate at 10 °C/min (46 minutes and 30 seconds). During the measurement, the sample was purged by N$_2$ with the flow rate of 50 mL/min. Besides, the sample used in the MS section (QMS 403) came from the gaseous loss in the TG. The data was also collected by point at the same range of temperature. The MS spectrum was detected at m/z 18, 28, 44, and 60, which corresponded the ion of H_2O^+, CO^+, CO_2^+, and CO_3^+, respectively.

5.4 Results and Discussion

5.4.1 Characterization of commercial zeolite NaX

Figure 5.1 presents the characterization data of bare commercial zeolite NaX including the appearance, XRD pattern, SEM image, and FTIR spectrum. NaX is a white powder (**Figure 5.1a**). The XRD pattern displays characteristic peaks of the FAU zeolite (**Figure 5.1b**). The main FAU peaks are at 6°, 10°, 11.6°, 15.4°, 20°, 23.2°, 26.5°, and 30.8° (x symbol) (Pobson & Lillerud, 2001)). However, numerous alien peaks (A

symbol) at 7°, 12.5°, 16°, 21.6°, 24°, 27°, and 29.9° are observed. Those peaks are characteristics of zeolite NaA. **Figures 5.1c** and **5.1d** display the SEM images with different magnifications showing a cluster of polyhedral morphology of the zeolite NaX particles along with some the edge-cut cubic morphologies of the zeolite NaA as an impurity phase.

The Fourier transform infrared spectrum of the commercial zeolite NaX is displayed in **Figure 5.1e**. Generally, the peak around 1650 cm^{-1} was the bending vibration (δ) of the adsorbed moisture on the surface of the zeolite. The strong peak at 979 cm^{-1} with a little hump on the left side is contributed to asymmetric stretching vibration (ν_{as}) in the interior tetrahedra of the Si–O–T bond (whether T was shortened Si or Al). A pair of peaks at 777 cm^{-1} and 698 cm^{-1}, 567 cm^{-1}, and the sharp last-right peak at 450 cm^{-1} are linked to symmetric stretching vibration (ν_s) of the Si–O–T bond, the T–O bending vibration (δ) at exterior links, and the internal tetrahedral bending of the O–T–O bond, respectively (Karge, 2001; Keawkumay et al., 2019).
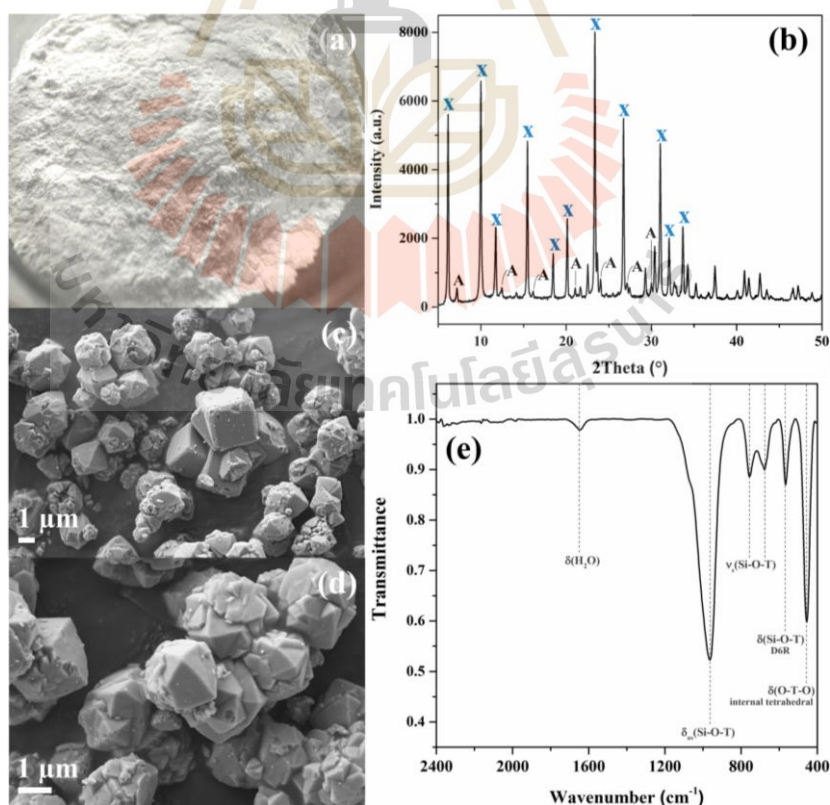

Figure 5.1 Characterization data of bare commercial zeolite NaX including the appearance (a), XRD pattern (b), SEM image (c) and (d), and FTIR spectrum (e).

5.4.2 Characterization of carbonate-based catalysts

The photographs of K_2CO_3/NaX and Na_2CO_3/NaX in **Figures 5.2a** and **5.2b** show that they are white powder similar to the bare support. Their XRD patterns are compared with K_2CO_3 and Na_2CO_3 in **Figure 5.3** and **5.4**. When zeolite NaX was covered by the carbonate salts, their XRD peak intensities decreased. Moreover, after the impregnation, the intensity at 10° in the XRD patterns of both catalysts decreased when compared to the third peak at 12°. This characteristic was the behavior of the adsorbate's inclusion at the (220) plane (Keawkumay et al., 2019). However, peaks of carbonate salts between 25° to 35° were not observed, which could indicate that both precursors were well dispersed on the support. Furthermore, the distinctive peaks of zeolite NaX still remained, indicating that the characteristics of the zeolite NaX were retained after the impregnation of the carbonate salts. This might improve the catalyst's reusability in terms of salt recovery, the functional groups on its surface, and the area of the zeolite to allow the salt to re-precipitate after the transesterification reaction is carried out.

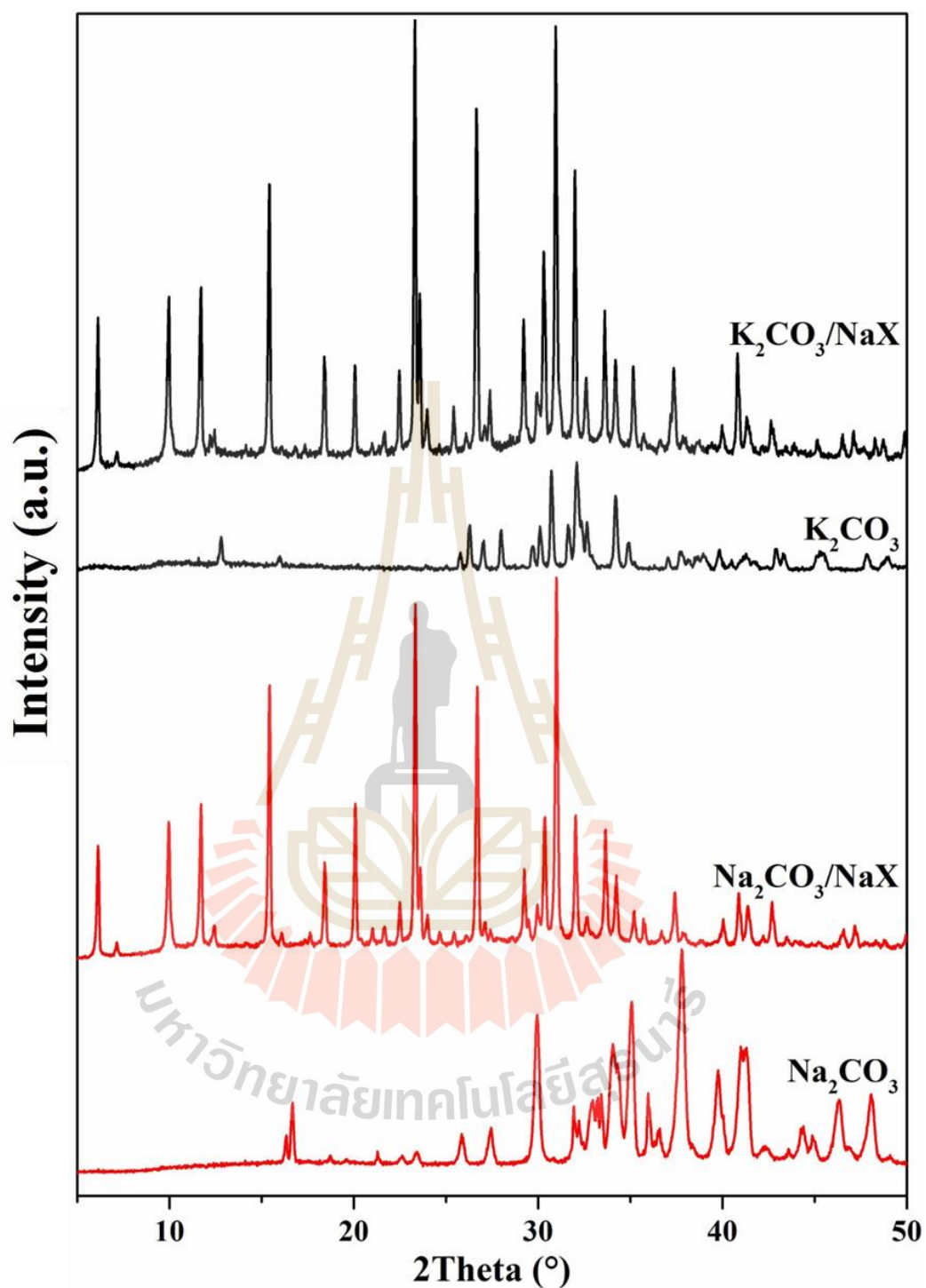**Figure 5.2** Photographs of K_2CO_3/NaX (a) and Na_2CO_3/NaX (b).

Figure 5.3 XRD patterns of K_2CO_3/NaX and Na_2CO_3/NaX compared with K_2CO_3 and Na_2CO_3, respectively.

Figure 5.4 illustrates FTIR spectra of K_2CO_3/NaX and Na_2CO_3/NaX. Note that the measurement was run in ATR mode, implying that the carbonate intensity

should not be utilized to estimate the quantity. After both potassium carbonate and sodium carbonate impregnation on the commercial zeolite NaX, there was no broad peak of zeolite. This observation means the structure of zeolite was preserved, which was in line with the XRD patterns. Furthermore, the vibrational band at 1452 cm^{-1} was shown, which was characteristic of monodentate carbonates (Polisi et al., 2019). The slight shoulder at 1340 cm^{-1} was the chemisorbed CO_2 or the signals of bicarbonates (Polisi et al., 2019).
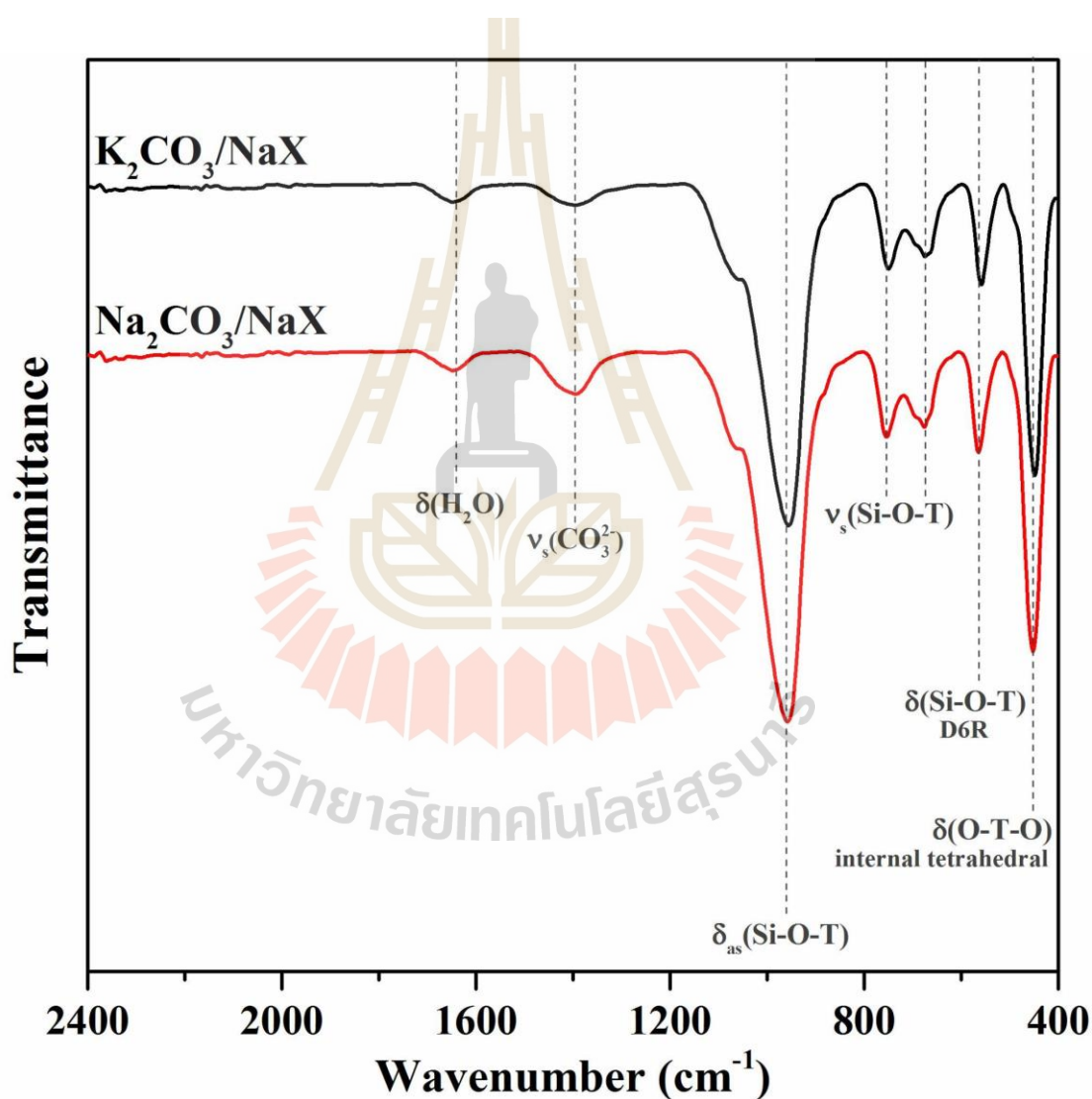
Figure 5.4 FTIR spectra of K_2CO_3/NaX and Na_2CO_3/NaX.

The elemental compositions of both fresh and spent catalysts were measured by X-ray fluorescence analysis (XRF) including Si, Al, Na, and K, as displayed

in **Table 5.1**. The Si/Al of the commercial zeolite NaX was 1.6 and this ratio did not change after the zeolite was added with carbonate salts. According to the XRD patterns and FTIR spectra, the similarity of the ratio could imply the retention of their zeolite structure. After the support was impregnated by K_2CO_3 solution, 5.7% atomic of potassium was reported while the percentage of sodium decreased slightly from 8.7% to 6.5%, indicating the proportion of potassium inside the zeolite. Moreover, since the Na_2CO_3/NaX catalyst was prepared in percent weight by weight (12 %w/w), the 10.6% mass percentage of potassium (not shown) was detected in this sample. In the case of Na_2CO_3/NaX catalyst, sodium content increased from 8.7% to 11.2% from the impregnation of the Na_2CO_3 solution. However, it was difficult to report mass percentage of sodium because it was already in the bare zeolite.

Table 5.1 Elemental compositions from XRF in the %atomic unit of fresh carbonate catalysts including Si, Al, Na, and K.

Samples	%atomic				Si/Al
	Si	Al	Na	K	
Commercial NaX	19.1	11.9	8.7	N/A	1.6
K_2CO_3/NaX	17.8	11.2	6.5	5.7	1.6
Na_2CO_3/NaX	18.3	11.3	11.2	N/A	1.6

N/A: not available

5.4.3 Catalytic performance of carbonate-based catalysts

Figure 5.5 illustrates the TLC chromatograms of the product from the reaction of transesterification of palm oil catalyzed by K_2CO_3/NaX and Na_2CO_3/NaX with various cycles compared with original palm oil. The number on the circle was the retardation factor or rate of flow (R_f). In brief, palm oil was developed slowly with an R_f of approximately 0.50–0.52. In the case of the potassium catalyst, the highest spot with the R_f value of 0.74 was displayed on the TLC plate. Then, the distance traveled decreased, and the R_f was calculated as 0.57 and 0.51 in the second and third cycles, respectively. It could be concluded that a very high biodiesel yield was earned in the

first cycle, then half-dropped in the next cycle; eventually, there was no discernible biodiesel production in the last cycle. Thus, this could imply that the leaching of potassium carbonate still occurred.

In the case of the sodium catalyst, the first spot with the R_f value of 0.66 was shown on the TLC plate. Interestingly, the R_f value was still maintained the distance traveled in the second cycle. However, this distance slightly dwindled, and the R_f was 0.57, 0.52, and 0.51 in the further cycles, respectively. It could be implied that the Na_2CO_3/NaX catalyst could drive the transesterification reaction of palm oil; however, biodiesel production gradually decreased as well. It could reach the conclusion that when the Na_2CO_3/NaX catalyst was carried out through this reaction, the reusability was not excellent. Nevertheless, in a comparison of K_2CO_3/NaX catalyst that the dramatic decline was observed, Na_2CO_3/NaX catalyst still showed greater an R_f value than K_2CO_3/NaX catalyst at the second and third cycles. It means that Na_2CO_3/NaX catalyst exhibited better reusability than K_2CO_3/NaX catalyst. K_2CO_3/NaX catalyst could be utilized for only one run, while Na_2CO_3/NaX catalyst could be applied for the transesterification of palm oil for three cycles. Note that this experiment was just a screening investigation of the catalytic performance. The products were analyzed by GC-FID to determine the percentage of the biodiesel yield.
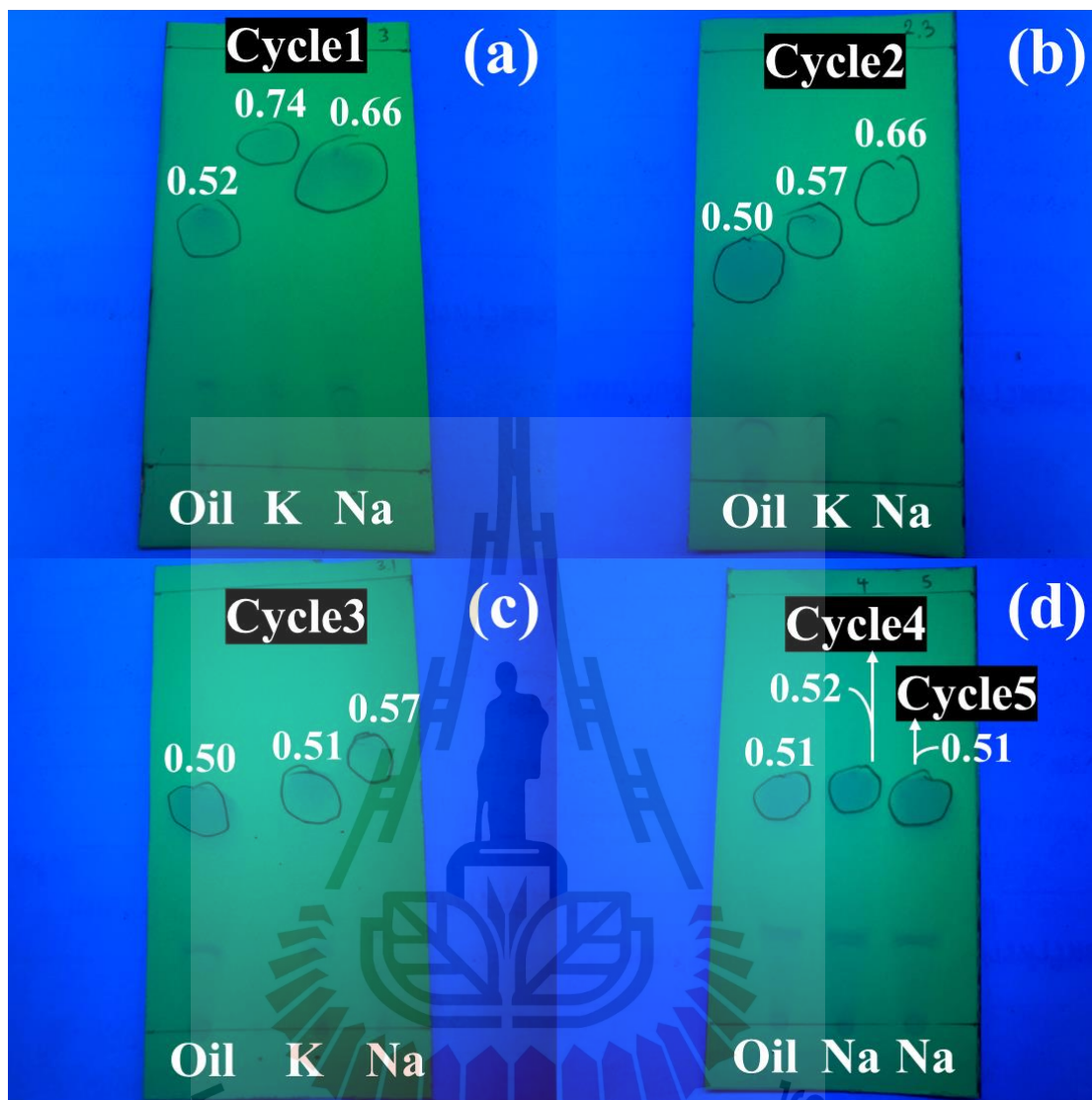
Figure 5.5 TLC plates of product from transesterification of palm oil catalyzed by K_2CO_3/NaX and Na_2CO_3/NaX with various cycles.

Figure 5.6 displays the biodiesel yield from transesterification of palm oil over the potassium carbonate supported on the commercial zeolite NaX catalyst for three cycles. Their chromatograms were shown in **Figure 5.7**. It was not surprising that the first cycle produced an extremely high biodiesel yield of 95.9%, which then declined steeply to 7.7% and 2.0% in the second and third cycles, respectively. This pattern of behavior was consistent with the TLC investigation, the results in the previous chapter, as well as in the literature (Kosawatthanakun et al., 2022). So,

potassium carbonate was the effective active species for the catalysis in the transesterification in the first cycle, but inactive in the further cycle.
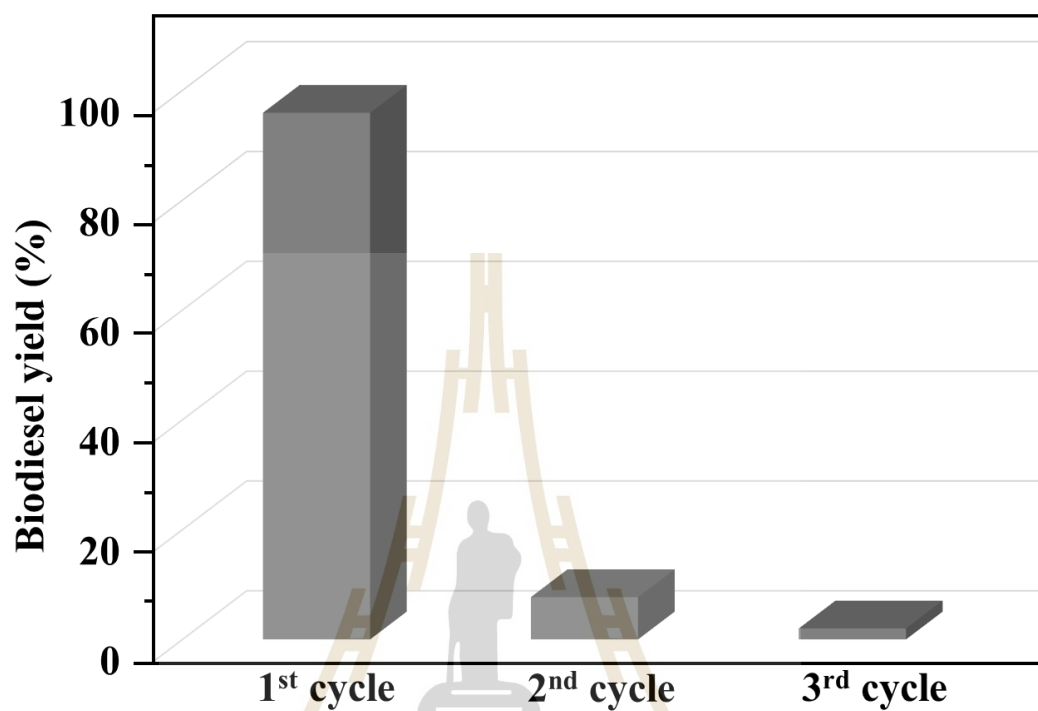
Figure 5.6 Biodiesel yield from transesterification reaction of palm oil catalyzed at 60 °C for 3 h by 0.2 g of K_2CO_3/NaX for three cycles.
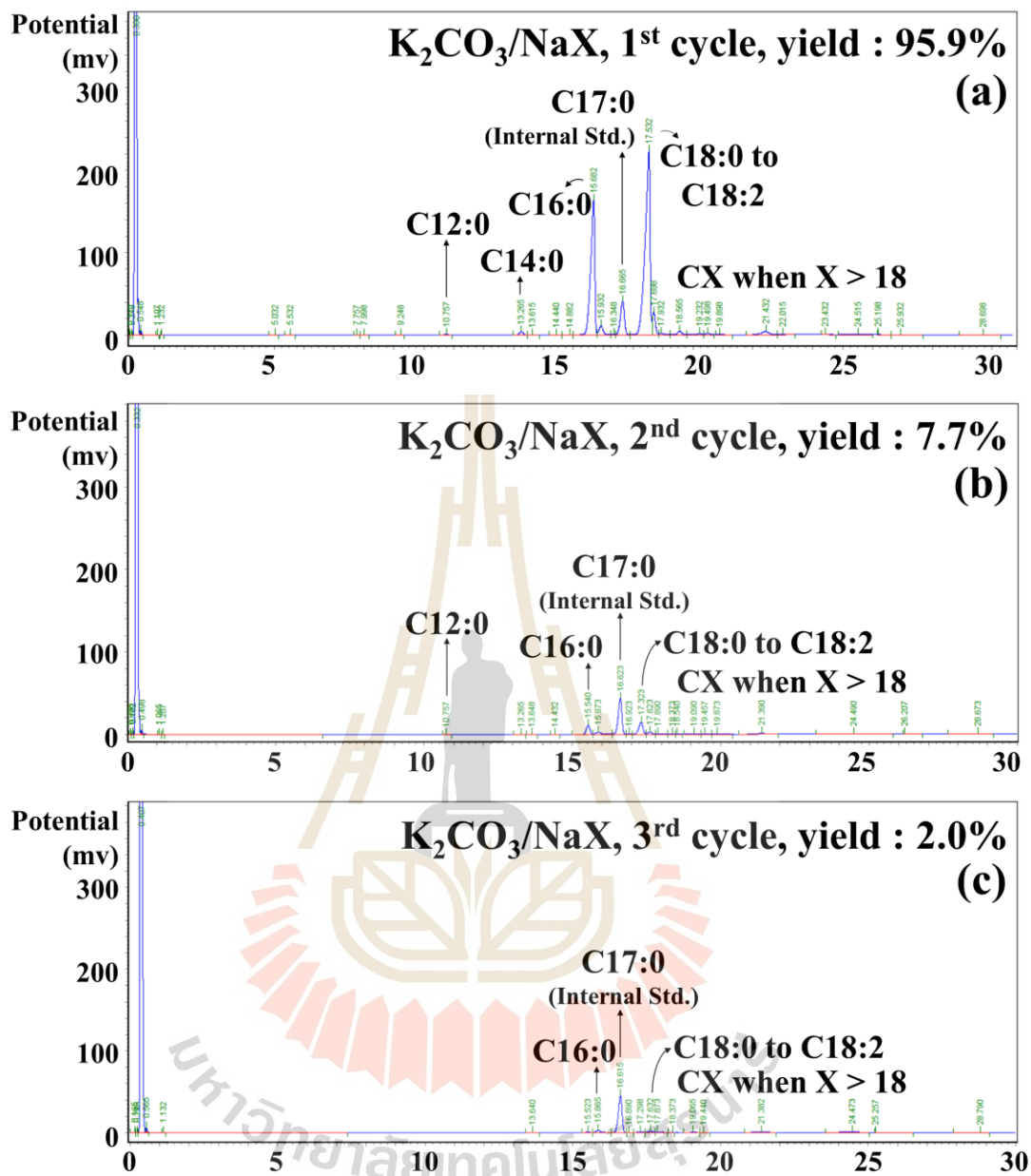
Figure 5.7 Chromatograms of biodiesel from the 1st (a), 2nd (b), and 3rd (c) cycles catalyzed by K_2CO_3/NaX.

Figure 5.8 demonstrates the biodiesel yield from transesterification of palm oil over the sodium carbonate catalyst supported on the commercial zeolite NaX for five cycles. Their chromatograms were shown in **Figure 5.9**. The gradual dwindle of biodiesel yield was received including 70.6%, 32.1%, 16.5%, 1.5%, and not detected yield from the first to fifth cycles, respectively. This observation was

consistent with the TLC results. So, Na_2CO_3/NaX catalyst could run the transesterification reaction with moderate catalysis, compared with the potassium. Moreover, Na_2CO_3/NaX exhibited better reusability than K_2CO_3/NaX. The reason for this difference might be the solubility of each precursor, which was explained in the literature (Malins, 2018).

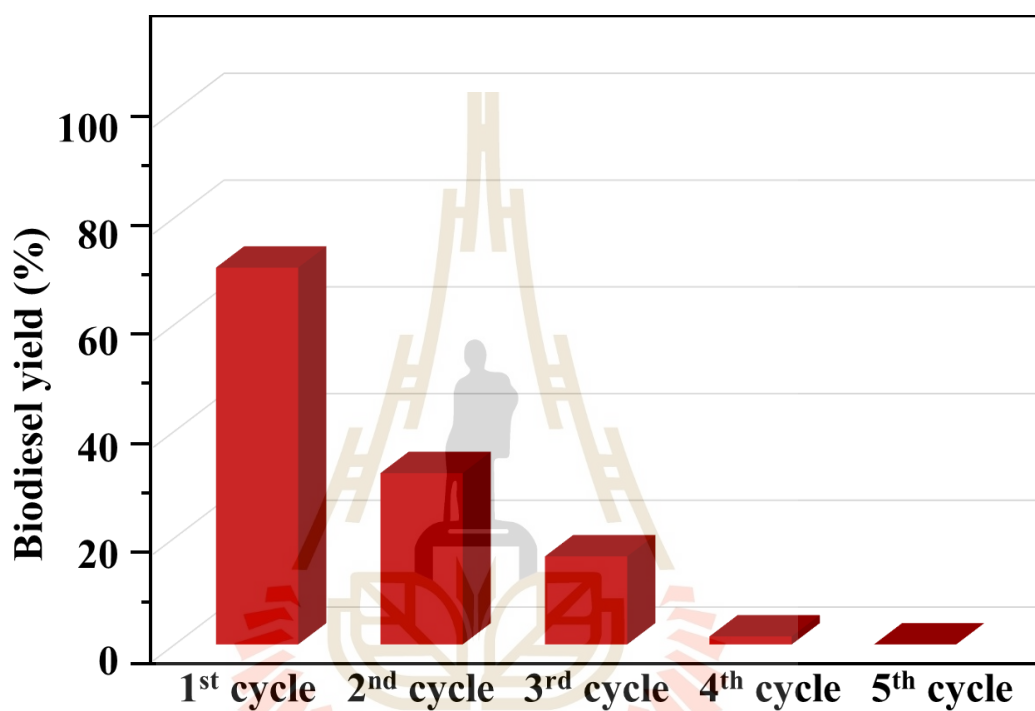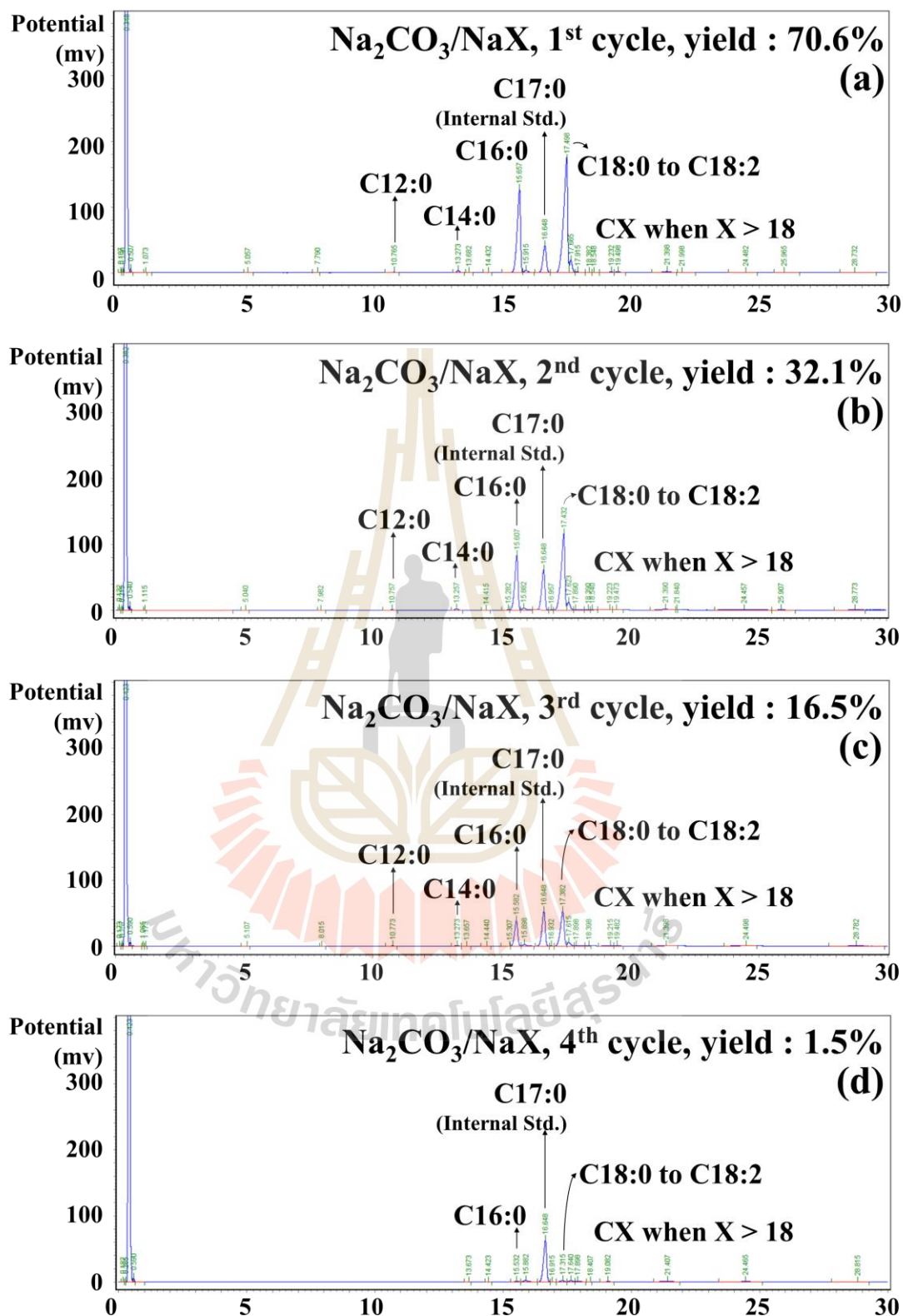**Figure 5.8** Biodiesel yield from transesterification reaction of palm oil catalyzed at 60 °C for 3 h by 0.2 g of Na_2CO_3/NaX for five cycles.

Figure 5.9 Chromatograms of biodiesel from the 1st (a), 2nd (b), 3rd (c), and 4th (d)

cycles catalyzed by Na$_2$CO$_3$/NaX.

5.4.4 Study of spent carbonate-based catalysts

The diffractograms of the fresh and spent catalysts, K_2CO_3/NaX and Na_2CO_3/NaX are compared in **Figures 5.10** and **5.11**, respectively. Firstly, after the zeolite NaX was impregnated by carbonate salts (both K_2CO_3 and Na_2CO_3), the intensity of the zeolite peak significantly decreased, as mentioned previously. However, the trait of the XRD patterns of the spent catalysts between potassium and sodium was different. For potassium catalyst, the intensity reverted to being high after the catalyst was used for the first time (**Figure 5.8**). Then, intensity was maintained even though the catalyst was utilized for two cycles. This could imply that K_2CO_3/NaX could not only catalyze the palm oil transesterification, but the structural collapsing problem was also solved. The reusability, nevertheless, proved unsuccessful. This trait of instant peak reversion was caused by the high solubility of K_2CO_3 in the transesterification system, resulting in a high degree of leaching after the first catalysis.

In the case of sodium catalyst, after the catalyst was employed in the first cycle, the intensity of zeolite peak was still maintained being low (**Figure 5.10**). Moreover, the intensity at 10° stayed lower than 12°. This indicated that the Na_2CO_3 was still covered on the zeolite surface. However, the alternation of the intensity between 10° and 12° was not only gradually reverted but the main peaks of zeolite were also slowly returned being high. This character of gradual peak reversion was caused by the poor solubility of Na_2CO_3 in the transesterification system, leading to slight leaching after the first catalysis.

These results, both potassium and sodium catalysts, were consistent with the previous findings about solubility. Compared with K_2CO_3, Na_2CO_3 had less solubility in the glycerol and methanol mixture, but it had a better recovery property and was more reusable, which led to a higher yield in the second and third runs. While K_2CO_3 had higher solubility in such a mixture or lack of recovery characteristic, producing a very high yield in the first run (>90%), then dramatically dropped in the further run. Although Na_2CO_3 was less soluble than K_2CO_3 in this experiment, the better reusability was granted. As a result, solubility was also vital to the design of the catalyst.
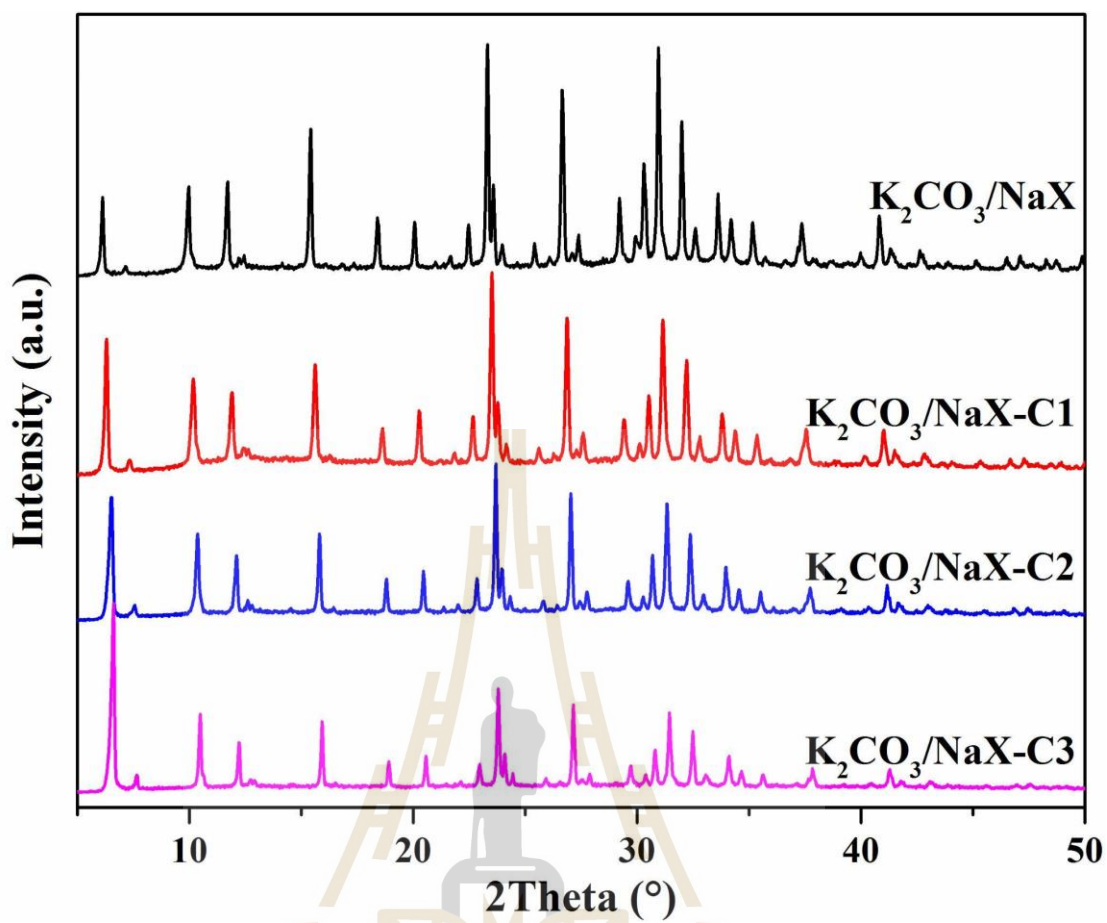
Figure 5.10 XRD patterns of fresh K_2CO_3/NaX (black line) and spent K_2CO_3/NaX-C1 to C3 (red, blue, and magenta lines, respectively).
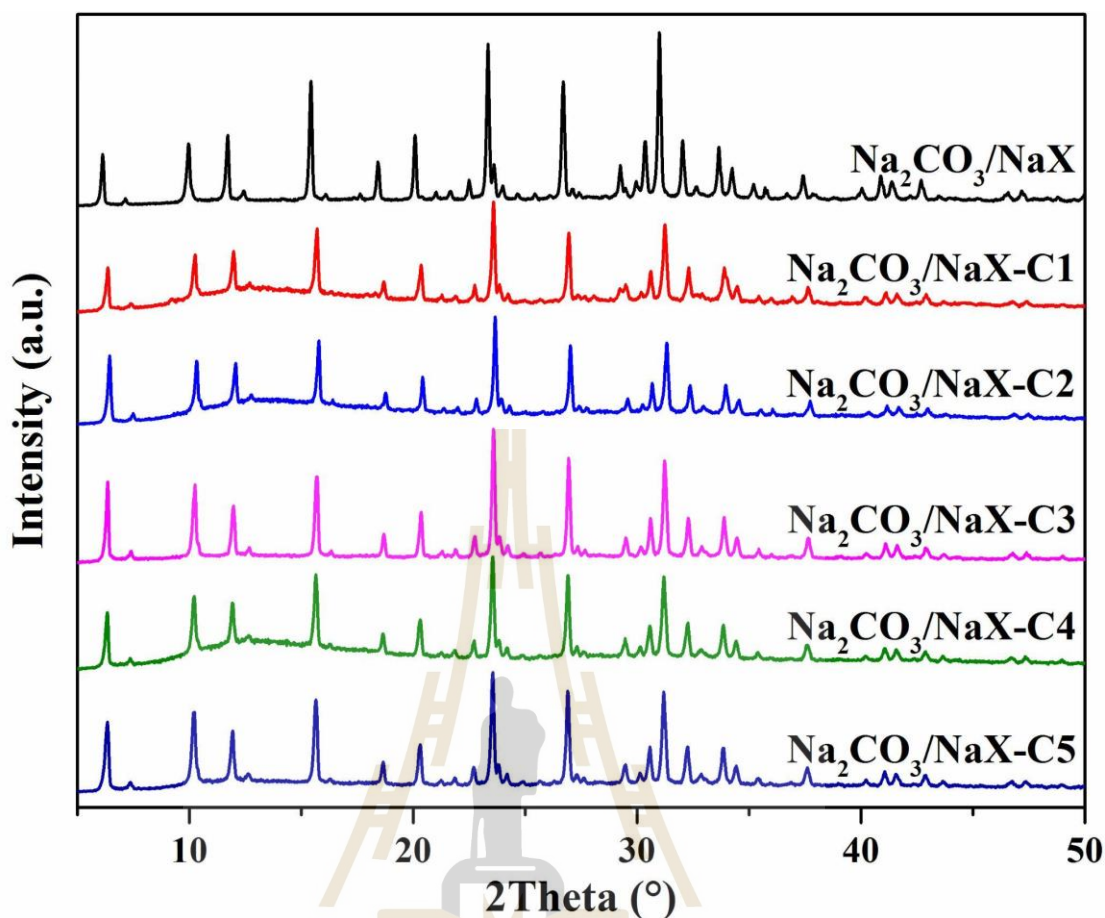
Figure 5.11 XRD patterns of fresh Na$_2$CO$_3$/NaX (black line) and spent Na$_2$CO$_3$/NaX-C1 to C5 (red, blue, magenta, green, and dark blue lines, respectively).

The former interpretation noted that the potassium ion, an active species, leached into the glycerol layer and biodiesel products. However, the observation in this investigation noticed the absence of the vibrational band of carbonate in the FTIR curve, as shown in **Figure 5.12**. After the catalyst was utilized in the first cycle, the peak of carbonate half-decreased, then completely disappeared in the second and third cycles. Moreover, the atomic percent of potassium also gradually dropped from 5.7% to 4.5%, then declined further to mid-3% in the 2nd and 3rd cycles while the sodium composition was first decreased from 6.5% to 4.7%, afterward increased to 6.1% and 7.7%, respectively, as shown in **Table 5.2**. It indicated that the carbonate species in the potassium form could effectively run the transesterification of palm oil, especially in the first cycle. However, there was no heterogeneity property in this catalyst due to not only the poor reusability results, but the shortage of carbonate,

potassium, and sodium species was also noticed. This observation was consistent with the high solubility of the potassium carbonate in the mixture of glycerol/methanol, a substance received from the transesterification reaction (Malins, 2018). This property could easily drive the precursor (K_2CO_3) from the framework of zeolite NaX to the liquid phase of the reaction mixture, resulting in direct catalysis. Nevertheless, the absence of both carbonate peak from FTIR and potassium content from XRF suggested that K_2CO_3 was easily dissolved in the mixture of glycerol/methanol, as reported in such publication, leading to a very high biodiesel yield in the first cycle, then dropped in the second and third cycles, as described previously. However, 7.7% of biodiesel was still received in the second run, accompanied by the existence of a partial carbonate peak in the FTIR spectrum and potassium composition (4.5%). This finding implies that some potassium carbonate residue was still present inside the zeolite structure. However, the sodium component also dwindled from 6.5% to 4.7%, hinting that the ion exchange between Na^+ and K^+ occurred, and then Na_2CO_3 was produced as another active species to catalyze the transesterification reaction. This discussion could confirm and summarize the hypothesis proposed in the previous chapter that the ion exchange between sodium ions (Na^+) from the charge-balancing cation on the surface of zeolite NaX and potassium ions (K^+) from the precursor happened. Subsequently, Na_2CO_3 was created as an additional reactive compound to accelerate the transesterification. This exchange was confirmed by the catalysis in the 3rd cycle. In this cycle, only 2.0% of biodiesel yield was obtained. Yet, the vibrational band of carbonate disappeared. Moreover, the potassium percent dropped to 3.5% with the proportional rise of sodium content to 6.1%. There was no carbonate material for charge compensation of potassium. Therefore, sodium has to be replaced with the potassium found in the XRF analysis. This notice could confirm the ion exchange phenomenon between K^+ and Na^+.
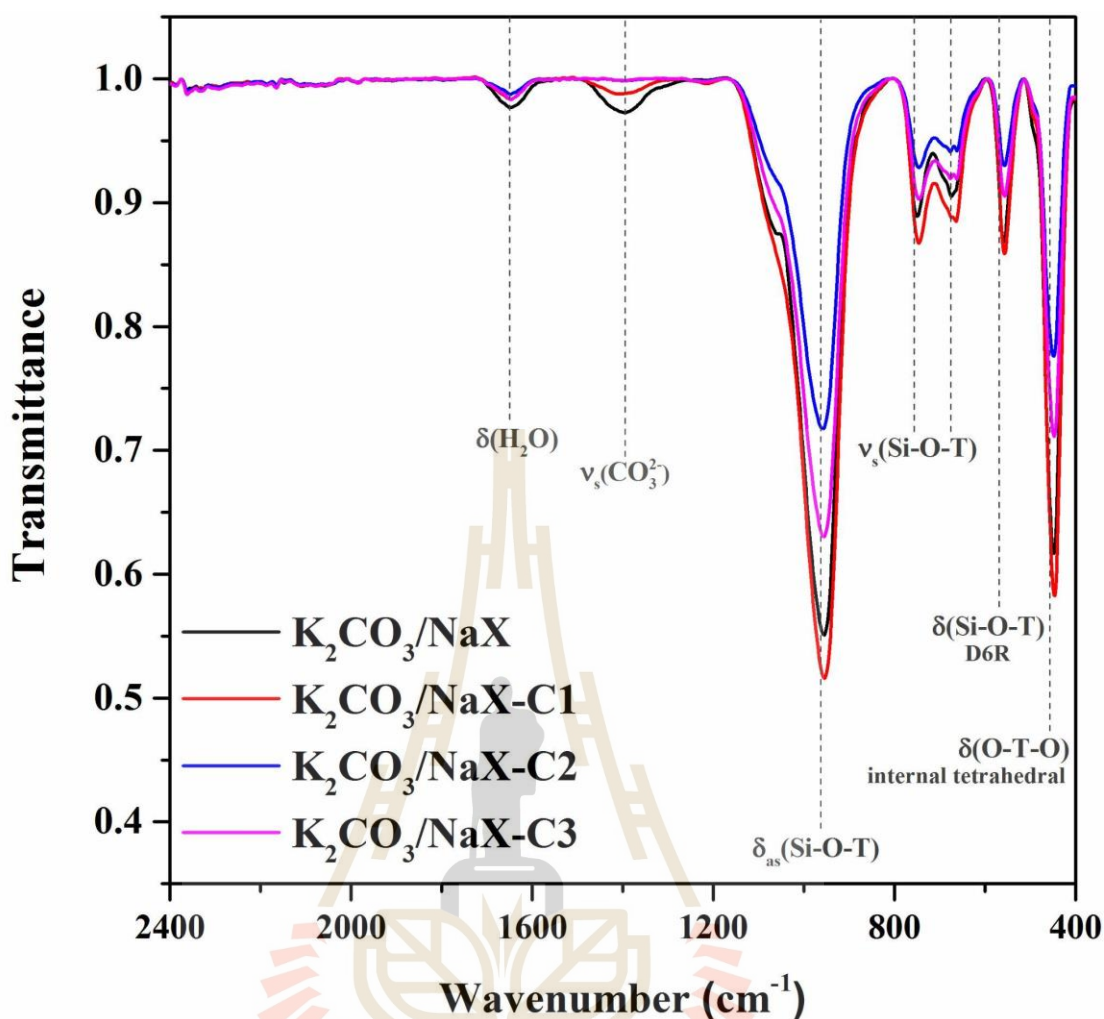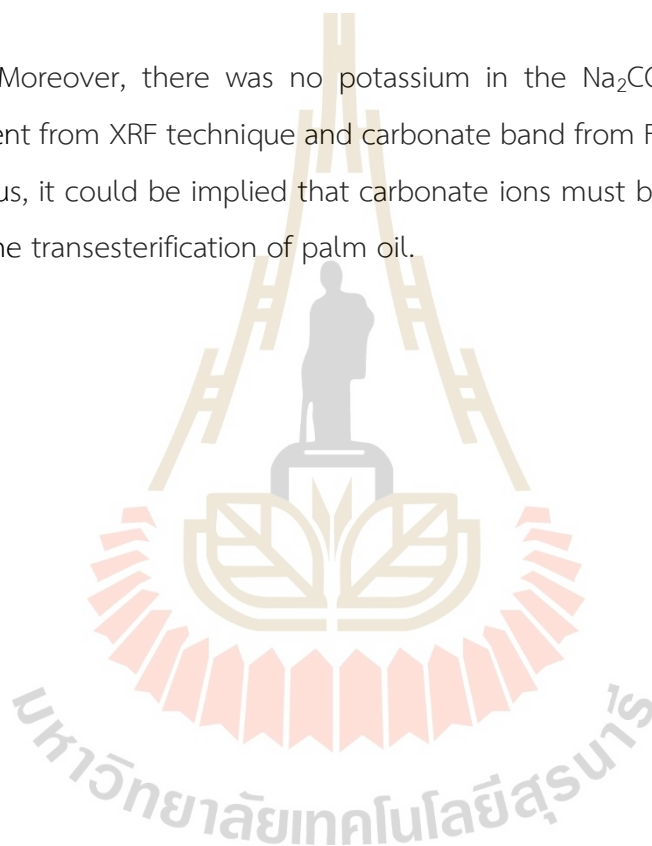
Figure 5.12 FTIR spectra of fresh K_2CO_3/NaX (black line) and spent K_2CO_3/NaX-C1 to C3 (red, blue, and magenta lines, respectively).

In the case of sodium catalyst, the gradual decrease in the carbonate FTIR peak was also seen, as shown in **Figure 5.13**. So, it could be concluded that sodium carbonate still had a lack of reusability. However, the sodium content from the XRF technique increased from 11.2% to 14.5%, implying that the sodium carbonate that stuck inside the framework of zeolite NaX might slightly dissolve in the mixture of products and then leach into the external surface, resulting in the higher sodium content measured by the screening method. After the catalyst was employed in the second and third cycles, the amount of sodium significantly decreased from 14.5% to 9.2% and 5.2%, respectively, indicating that Na_2CO_3 gradually leached out. However, only 1.5% and no detection of biodiesel yield were obtained in the fourth and fifth

cycles, respectively, accompanied by the disappearance of the carbonate band in the FTIR spectra and the return of the sodium content to about 8–9%, suggesting no Na_2CO_3 remained inside the zeolite structure. Na_2CO_3, which supplied less solubility in the glycerol and methanol mixture than K_2CO_3, had a greater reusability or in the aspect of higher recovery property, resulting in a higher yield in the second and third runs. Therefore, the solubility was also crucial for the design of the catalyst and in this experiment, Na_2CO_3 showed lower solubility than K_2CO_3, thus the higher reusability was given.

Moreover, there was no potassium in the Na_2CO_3/NaX catalyst. Only sodium content from XRF technique and carbonate band from FTIR examination were detected. Thus, it could be implied that carbonate ions must be an active substance to catalyze the transesterification of palm oil.
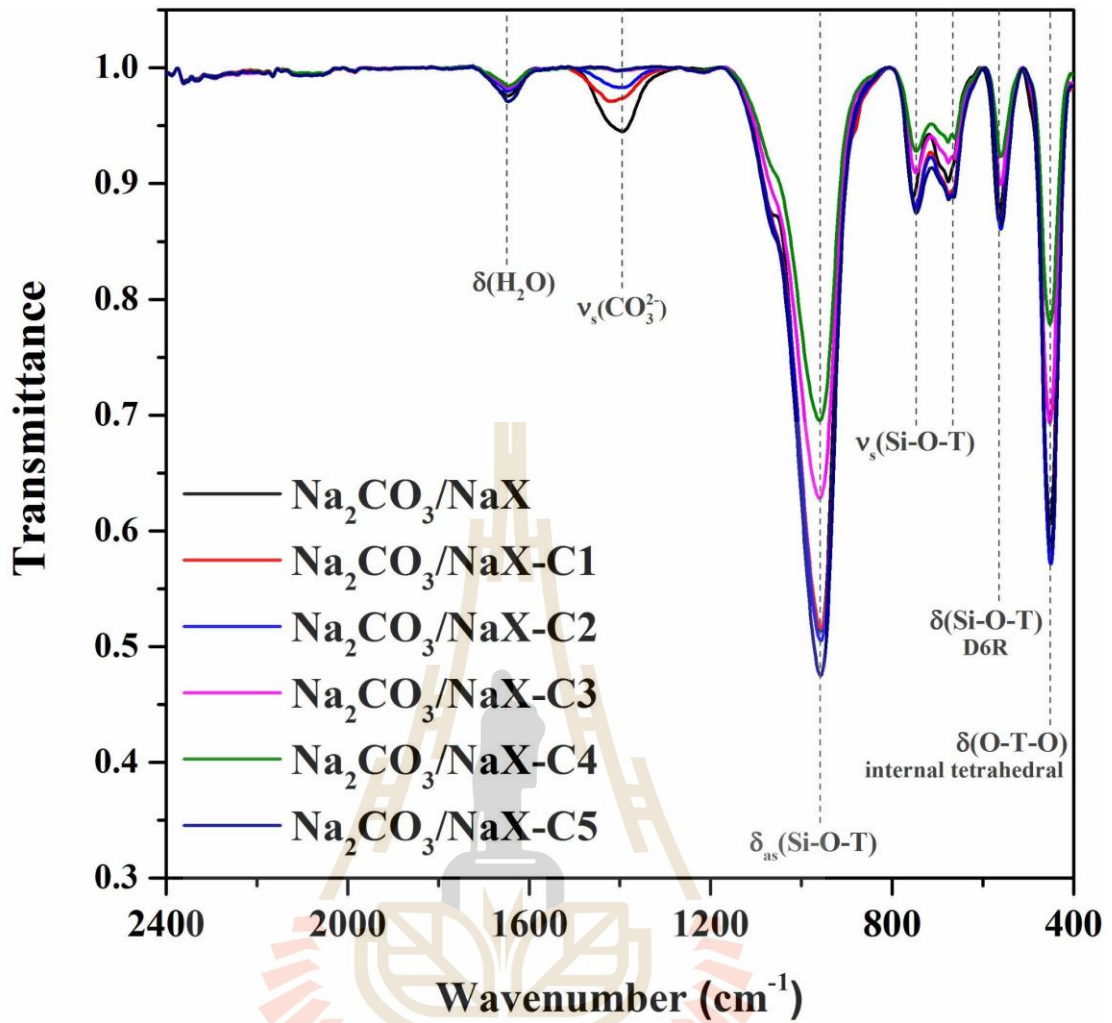
Figure 5.13 FTIR spectra of fresh K_2CO_3/NaX (black line) and spent K_2CO_3/NaX-C1 to C3 (red, blue, magenta, green, and dark blue lines, respectively).

Table 5.2 Elemental compositions from XRF in the %atomic unit of spent carbonate catalysts including Si, Al, Na, and K.

Samples	%atomic				Si/Al
	Si	Al	Na	K	
Spent K_2CO_3/NaX-C1	18.9	11.7	4.7	4.5	1.6
Spent K_2CO_3/NaX-C2	18.8	11.7	6.1	3.5	1.6
Spent K_2CO_3/NaX-C3	18.1	11.4	7.7	3.7	1.6
Spent Na_2CO_3/NaX-C1	17.1	10.8	14.5	N/A	1.6
Spent Na_2CO_3/NaX-C2	18.9	11.8	9.2	N/A	1.6
Spent Na_2CO_3/NaX-C3	20.5	12.2	5.2	N/A	1.7
Spent Na_2CO_3/NaX-C4	19.3	14.2	8.3	N/A	1.4
Spent Na_2CO_3/NaX-C5	19.1	11.8	8.8	N/A	1.6

N/A: not available

The thermogravimetric analysis - mass spectroscopy (TGA - MS) was employed to confirm the carbonate species of the catalysts. **Figure 5.14** displays the thermograms of bare zeolite NaX, fresh catalyst, and spent catalysts from 1st and 3rd cycles of K_2CO_3 and Na_2CO_3 catalysts. Unfortunately, a little error occurred during the initial TGA investigation of the bare commercial zeolite NaX sample (black line) as a result of the detector malfunctioning. However, it was accessible subsequently and this data was available. Typically, zeolite NaX, K_2CO_3/NaX, and Na_2CO_3/NaX showed only one weight loss from 50 to 250 °C, which belongs to the moisture decomposition. Approximately, 22% of water was evaporated from bare zeolite NaX while both fresh catalysts provided only 17%. It was caused by the existence of carbonate at the zeolite surface, according to FTIR.

In the spent K_2CO_3/NaX samples, two ranges of weight loss were observed in both 1st and 3rd cycles, including 50–250 °C and minimally 300–350 °C, which corresponded to the evaporation of the adsorbed water and the loss of the organic compounds, respectively as shown in **Figure 5.14a**. This pattern was also noticed in the 3rd cycle of the used sodium carbonate catalyst (Na_2CO_3/NaX-C3). However, three

periods of weight decomposition were exhibited in the 1st cycle of the spent Na_2CO_3 catalyst (Na_2CO_3/NaX-C1), comprising 75–125 °C, 125–250 °C and 300–350 °C, as shown in **Figure 5.14b**. For further clarifications of the lost species, the information will be reported, discussed, and interpreted by MS.
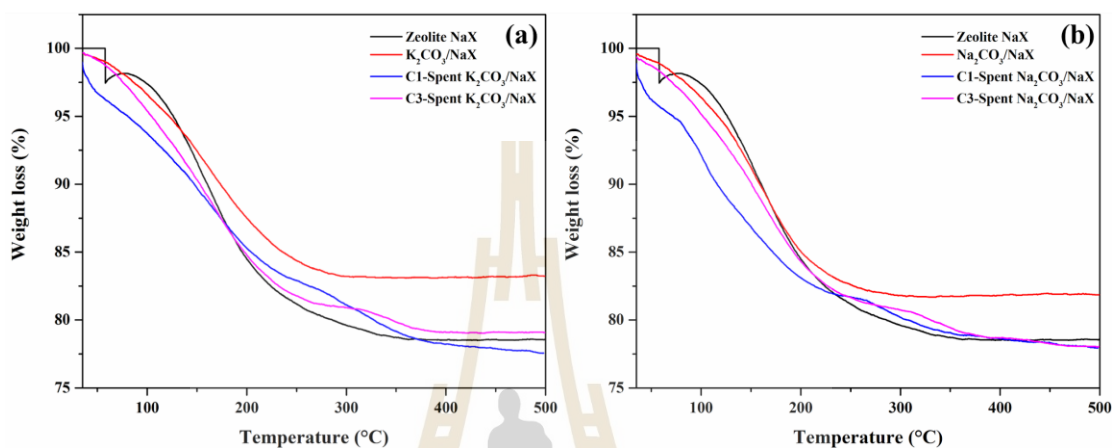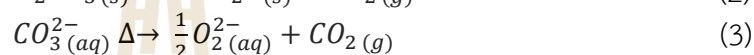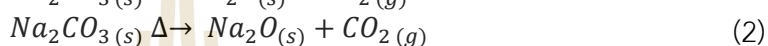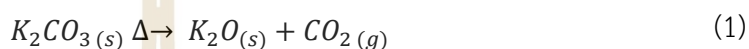

Figure 5.14 Thermograms of bare zeolite NaX (black line), fresh catalysts (red line), spent catalysts from 1st (blue line) and 3rd (pink line) cycles of K_2CO_3 (a) and Na_2CO_3 (b) catalysts.

Figure 5.15 demonstrates mass spectra profiles of bare zeolite NaX, fresh catalyst, and spent catalysts from 1st and 3rd cycles, which were detected at m/z 18 (**5.15a**, H_2O^+), 28 (**5.15b**, CO^+), 44 (**5.15c**, CO_2^+), and 60 (**5.15d**, CO_3^+). To more clear and comprehensible observations, the isolated graphs were reported in **appendix S1** and **S2** (zeolite NaX), **S3** and **S4** (K_2CO_3/NaX), **S5** and **S6**, and **S7** and **S8** (spent catalysts from 1st and 3rd cycles, respectively).

At m/z 18 (H_2O^+), zeolite NaX exhibited a highly strong current around 150–200 °C followed by fresh catalyst and spent catalysts from the 1st and 3rd cycles, respectively. Besides, a right shift was also observed when the catalyst was used. The reduction of the water peak might be due to the presence of chemical substances at the zeolite surface, such as carbonate in the fresh catalyst or others in the spent catalysts since a tiny peak of m/z 18 was found in the range of 300–400 °C. For more details, it will be further interpreted at another m/z.

At m/z 28 (CO^+), there is no peak in both bare zeolite NaX and K_2CO_3/NaX. However, a small peak was shown around 100 and 200 °C in the spent catalysts. Furthermore, one broad peak appeared between 300 to 400 °C in the K_2CO_3/NaX-C3. It could be implied that there is another chemical substance left inside the catalyst powder from the transesterification reaction.

At m/z 44 (CO_2^+), this number was considered the most important mass per charge number due to the carbonate compound being decomposed in the form of CO_2 gas, as shown in equations 1, 2, and 3 (Kim and Lee, 2001; Lehman et al., 1998).

$$K_2CO_{3\,(s)} \xrightarrow{\Delta} K_2O_{(s)} + CO_{2\,(g)} \tag{1}$$
$$Na_2CO_{3\,(s)} \xrightarrow{\Delta} Na_2O_{(s)} + CO_{2\,(g)} \tag{2}$$
$$CO_{3\,(aq)}^{2-} \xrightarrow{\Delta} \frac{1}{2}O_{2\,(aq)}^{2-} + CO_{2\,(g)} \tag{3}$$

Firstly, no any peak was detected in bare support even though zeolite NaX had a strong capacity to adsorb the carbon dioxide (CO_2) gas (Polisi et al., 2019). After the zeolite NaX was impregnated by K_2CO_3, the MS spectrum of this sample showed three regions, consisting of 50–125 °C, 200–350 °C and 350–400 °C. There are no findings that report the loss CO_2^+ in the first region. However, since the lost temperature was pretty low, thus it might be the loss of the loosely physical interaction of carbonate species and zeolite NaX surface. This kind of CO_2^+ loss is projected to be the decomposition of physically adsorbed carbonate on the zeolite since there are only carbonate bands in FTIR spectra without CO_2 peak. In the second region, fresh K_2CO_3/NaX showed a strong current, followed by the spent catalysts from 1st cycle. In addition, there were no peaks found in K_2CO_3/NaX-C3 at this location. This result was suitably consistent with the disappearance of the carbonate peak in the spent catalysts from FTIR results. At 350–400 °C, fresh K_2CO_3/NaX displayed a shortly broad peak, which might be a strong interaction between carbonate and zeolite NaX surface such as monodentate and bidentate carbonate (only observed on zeolite NaX (Polisi et al., 2019)). Nonetheless, after the catalyst was applied to the reaction of transesterification of palm oil in the 1st cycle, in addition to the second period decreasing, new peaks at the higher temperature range including 300, 300–400 °C, and 450–500 °C were presented. At these ranges, it usually is the thermal decomposition of organic compounds. Combining this data with the previous results from TG, MS, and catalytic performance suggested that

the substance that decomposed from the support framework might have been palm oil, biodiesel, and/or glycerol, etc. Moreover, after the TGMS was carried out by all spent catalysts, the white powder turned to black, as depicted in **Figure S9**, which might be the color of carbon. Moreover, after the catalyst was run in the 3rd cycle, only a broad peak at 300–400 °C was appeared. According to catalytic performance, which was only 2.0% biodiesel yield was produced, implying that a significant amount of palm oil was left behind. Thus, it should be the thermal decomposition of palm oil that has a high proportion of organic compounds at the end of the reaction and is stuck in the zeolite cage.

Lastly, at m/z 60 (CO_3^+), only noise was observed in all of the samples. It probably due to the decomposition of carbonate was broken down in the form of CO_2 gas, as based on the proposed reactions in the **equation (1)–(3)**.
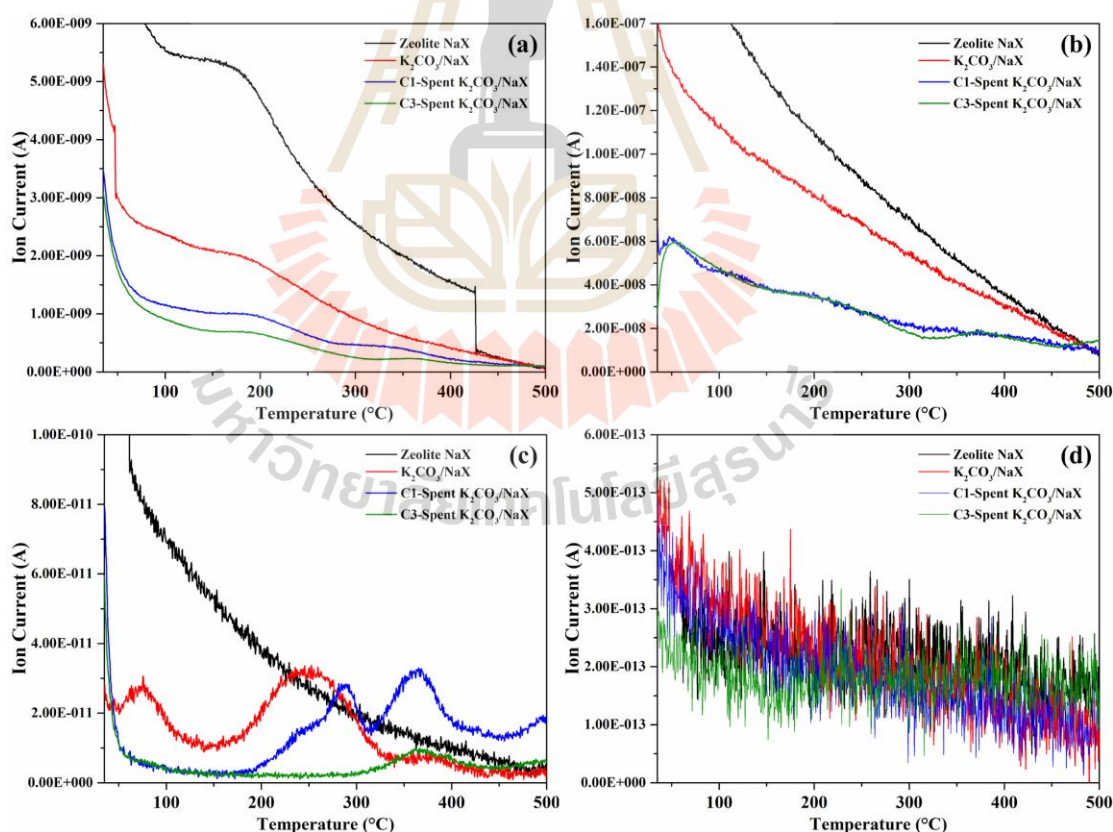
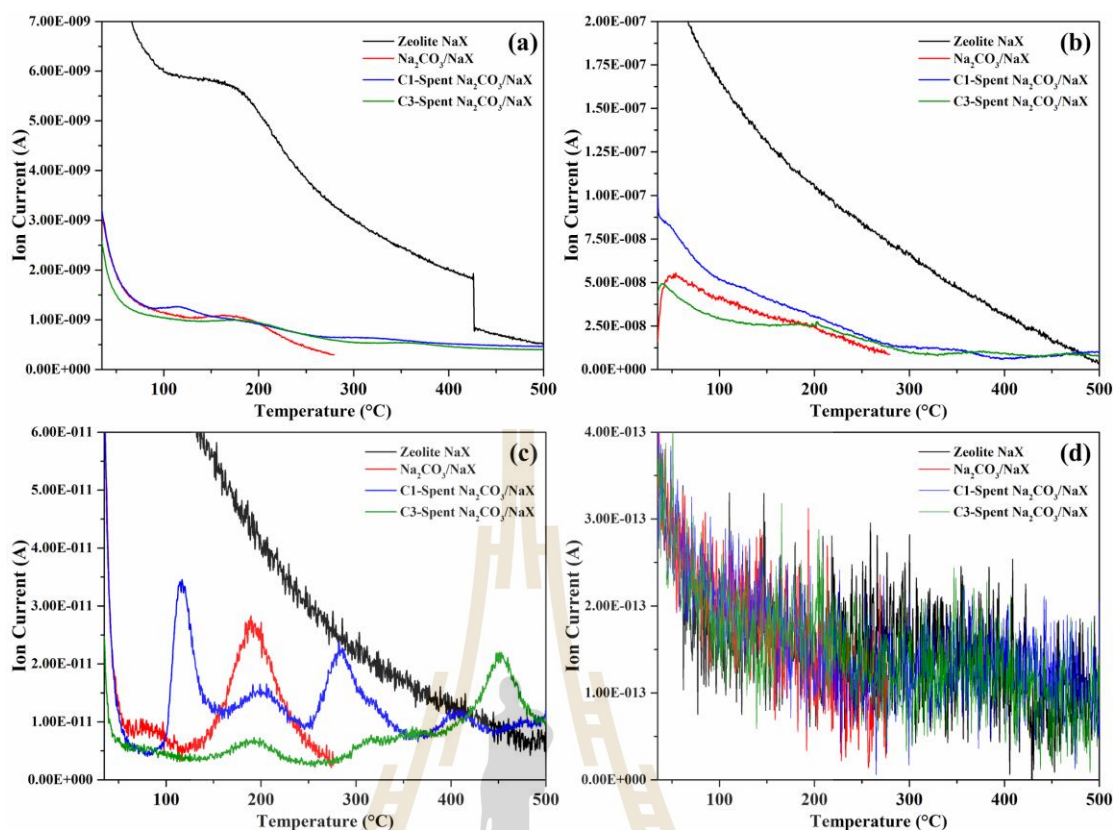**Figure 5.15** Mass spectra of bare zeolite NaX (black line), fresh potassium catalyst (red line), spent catalysts from 1st (blue line) and 3rd (green line) cycles, detected at m/z of 18 (a, H_2O^+), 28 (b, CO^+), 44 (c, CO_2^+), and 60 (d, CO_3^+).

Figure 5.16 illustrates mass spectra of bare zeolite NaX, fresh Na_2CO_3/NaX catalyst, spent catalysts from 1st and 3rd cycles, which detected at 18 (**5.16a**, H_2O^+), 28 (**5.16b**, CO^+), 44 (**5.16c**, CO_2^+), and 60 (**5.16d**, CO_3^+). To more details, the single curves were reported in the **appendix S1** and **S2** (zeolite NaX), **S10** and **S11** (Na_2CO_3/NaX), **S12** and **S13**, and **S14** and **S15** (spent catalysts from 1st and 3rd cycles, respectively). A slightly unclear technical issue in the Na_2CO_3/NaX led to the inability to collect results over 280 °C for unknown reasons.

At m/z 18 (H_2O^+), all samples showed low ion current around 150–200 °C compared with the bare zeolite NaX. The water peak in the Na_2CO_3/NaX sample also displayed a slightly right shift, which was similar to the K_2CO_3/NaX sample. However, the broad peak between 100 to 150 °C was presented in Na_2CO_3/NaX-C1. It might be the thermal decomposition of weak-interacted water with a zeolite surface or residue from the transesterification. In addition, a tiny peak of m/z 18 was also found in the spent sodium catalyst at the range of 300–400 °C. Therefore, it was possible to interpret with the same discussion of potassium sample that there was palm oil, biodiesel, and/or glycerol left after the cleaning process even if there was no FTIR (ATR mode) peaks of carbon, hydrogen, and oxygen. Noticeably, poor reusability was usually found in the general cleaning process, which was the rinsing with methanol and hexane, alternately, as the same as this work. On the other hand, a very high recyclability up to 5 cycles was received in the calcined-spent catalyst, which was executed at 600 °C for 2 h (Maneechot et al., 2021; Wu et al., 2014).

At m/z 28 (CO^+), the results showed a similar pattern to the potassium catalyst samples, including no peak in fresh catalyst, a small peak around 100–200 °C, and 300–400 °C in the spent catalysts. Thus, it was feasible to express with the previous interpretation that the cleaning process was not effective enough, resulting in the spent catalyst powder from the transesterification still containing glycerol, biodiesel, and/or palm oil inside the zeolite.

At m/z 44 (CO_2^+), no peak was basically found in the bare zeolite NaX. After impregnation with Na_2CO_3, the MS spectrum showed two regions, including 50–125 °C and 200–350 °C, which was the same period in potassium carbonate catalyst. So, it might belong the loss of CO_2 gas from the weakly physical interaction of

carbonate on the surface of zeolite support and from the impregnated carbonate, respectively. Moreover, Na$_2$CO$_3$/NaX-C1 exhibited a highly strong peak at 250–350 °C, 350–450 °C, and 450–500 °C and Na$_2$CO$_3$/NaX-C3 provided a weak ion current around 300–400 °C and a high peak at 400–500 °C. It might be the organic compounds that is left after cleaning, as stated previously. Interestingly, the gradual reduction between 250–350 °C range was noticed after the utilizing of catalyst. Besides, a small peak could be still observed in Na$_2$CO$_3$/NaX-C3. This might refer to that even after three catalyst runs, carbonate was still detectable. Hence, accompanied by the slight drop of the carbonate peak from FTIR, this m/z 44 spectrum is compelling evidence reporting the low solubility of Na$_2$CO$_3$ in the transesterification system whilst there is no signal here in the K$_2$CO$_3$/NaX-C3 sample. Thus, it could be concluded that Na$_2$CO$_3$ has a poor solubility in the mixture of methanol and glycerol, leading to the effective recovery ability and also the moderate maintenance of reusability in the transesterification of palm oil.

At m/z 60 (CO_3^+), only noise was also observed in every sample. This might be due to the decomposition that occurred in such equations.

Figure 5.16   Mass spectra of bare zeolite NaX (black line), fresh sodium catalyst (red line), spent catalysts from 1st (blue line) and 3rd (green line) cycles, detected at m/z of 18 (a, H_2O^+), 28 (b, CO^+), 44 (c, CO_2^+), and 60 (d, CO_3^+).

5.5 Conclusion

This chapter studied the carbonate catalyst (K_2CO_3/NaX and Na_2CO_3/NaX) for transesterification of palm oil. Those catalysts were successfully synthesized with the direct impregnation and without calcination process. K_2CO_3/NaX showed a very high catalytic performance in the first cycle (95.9%), then dramatically dropped in the second cycle (7.1%). This result was consistent with a high solubility of K_2CO_3 in the CH_3OH/glycerol mixture, resulting in highly active catalysis and also leaching. While Na_2CO_3/NaX showed 70.6% biodiesel yield, then gradually dropped. This was due to the poor solubility of Na_2CO_3 in such mixture, leading to the lower catalysis, high recovery property of Na_2CO_3, and moderate reusability. Thus, the information in this

chapter about the precursor solubility was useful for the further design of catalysts in the transesterification reaction.

5.6 References

Intarapong, P., Luengnaruemitchai, A., and Jai-In, S. (2011). Transesterification of palm oil over KOH/NaY zeolite in a packed-bed reactor. *Int. J. Renew. Energy Res.*, *1*(4), 271–280. doi: https://doi.org/10.20508/ijrer.v1i4.81.g66

Karge, H. G. (2001). Chapter 15 - Characterization by IR spectroscopy. In H. Robson & K. P. Lillerud (Eds.), *Verified Syntheses of Zeolitic Materials* (pp. 69–71). Elsevier Science. doi: https://doi.org/10.1016/B978-044450703-7/50113-7

Keawkumay, C., Rongchapo, W., Sosa, N., Suthirakun, S., Koleva, I. Z., Aleksandrov, H. A., Vayssilov, G. N., and Wittayakun, J. (2019). Paraquat adsorption on NaY zeolite at various Si/Al ratios: A combined experimental and computational study. *Mater. Chem. Phys.*, *238*, 121824. doi: https://doi.org/10.1016/j.matchemphys.2019.121824

Kim, J.-W. and Lee, H.-G. (2001). Thermal and carbothermic decomposition of Na_2CO_3 and Li_2CO_3. *Metall. Mater. Trans. B*, *32*(1), 17–24. doi: https://doi.org/10.1007/s11663-001-0003-0

Kosawatthanakun, S., Pansakdanon, C., Sosa, N., Chanlek, N., Roessner, F., Prayoonpokarach, S., and Wittayakun, J. (2022). Comparative properties of K/NaX and K/NaY from ultrasound-assisted impregnation and performance in transesterification of palm oil. *ACS Omega, 7*(11), 9130–9141. doi: https://doi.org/10.1021/acsomega.1c04912

Lehman, R. L., Gentry, J. S., and Glumac, N. G. (1998). Thermal stability of potassium carbonate near its melting point. *Thermochimica Acta*, *316*(1), 1–9. doi: https://doi.org/10.1016/S0040-6031(98)00289-5

Malins, K. (2018). The potential of K_3PO_4, K_2CO_3, Na_3PO_4 and Na_2CO_3 as reusable alkaline catalysts for practical application in biodiesel production. *Fuel Process. Technol.*, *179*, 302–312. doi: https://doi.org/10.1016/j.fuproc.2018.07.017

Manadee, S., Sophiphun, O., Osakoo, N., Supamathanon, N., Kidkhunthod, P., Chanlek, N., Wittayakun, J., and Prayoonpokarach, S. (2017). Identification of potassium phase in catalysts supported on zeolite NaX and performance in transesterification of Jatropha seed oil. *Fuel Process. Technol.*, *156*, 62–67. doi: https://doi.org/10.1016/j.fuproc.2016.09.023

Maneechot, P., Sriprapakhan, P., Manadee, S., and Artkla, R. (2021). Improvement of potassium species dispersed on hierarchical zeolite NaY by using combined methods between ultrasound and microwave-assisted impregnation as catalysts for transesterification of refined Jatropha seed oil. *Biomass & Bioenergy*, *153*, 106202. doi: https://doi.org/10.1016/j.biombioe.2021.106202

Montalbo, K., de Leon, R., Sophiphun, O., Manadee, S., Prayoonpokarach, S., and Wittayakun, J. (2013). Characterization and catalytic performance of potassium loaded on rice husk silica and zeolite NaY for transesterification of Jatropha seed oil. *Quim. Nova*. *36*(8), 1116–1120. doi: https://doi.org/10.1590/S0100-40422013000800007

Pobson, H. and Lillerud, K. P. (2001). *Verified syntheses of zeolitic materials*. https://api.semanticscholar.org/CorpusID:92665995

Polisi, M., Grand, J., Arletti, R., Barrier, N., Komaty, S., Zaarour, M., Mintova, S., and Vezzalini, G. (2019). CO_2 adsorption/desorption in FAU zeolite nanocrystals: *In Situ* Synchrotron X-ray Powder Diffraction and *In Situ* Fourier Transform Infrared Spectroscopic study. *J. Phys. Chem. C*, *123*(4), 2361–2369. doi: https://doi.org/10.1021/acs.jpcc.8b11811

Rakmae, S., Keawkumay, C., Osakoo, N., Montalbo, K. D., de Leon, R. L., Kidkhunthod, P., Chanlek, N., Roessner, F., Prayoonpokarach, S., and Wittayakun, J. (2016). Realization of active species in potassium catalysts on zeolite NaY prepared by ultrasound-assisted impregnation with acetate buffer and improved performance in transesterification of palm oil. *Fuel*, *184*, 512–517. doi: https://doi.org/10.1016/j.fuel.2016.07.035

Supamathanon, N., Wittayakun, J., and Prayoonpokarach, S. (2011). Properties of Jatropha seed oil from Northeastern Thailand and its transesterification catalyzed

by potassium supported on NaY zeolite. *J. Ind. Eng. Chem.*, *17*(2), 182–185. doi: https://doi.org/10.1016/j.jiec.2011.02.004

Wu, H., Zhang, J., Liu, Y., Zheng, J., and Wei, Q. (2014). Biodiesel production from Jatropha oil using mesoporous molecular sieves supporting K_2SiO_3 as catalysts for transesterification. *Fuel Process. Technol.*, *119*, 114–120. doi: https://doi.org/10.10 16/j.fuproc.2013.10.021

Zhang, T., Li, B., Li, H., Liu, Y., Li, J., Zhao, B., Zhang, X., and Wang, J. (2022). The efficient and green synthesis of biodiesel from crude oil without degumming catalyzed by sodium carbonate supported MoS_2. *RSC Advances, 12*(38), 24456–24464. doi: https://doi.org/10.1039/D2RA04198G

CHAPTER VI

CONCLUSIONS

This thesis presents a novel knowledge about the heterogeneous catalyst for transesterification of palm oil. Two main approaches were summarized as following: the influence of FAU cavity on the potassium catalyst and the new strategic synthesis of the carbonate catalyst for this reaction. The initial investigation focused on the paraquat-adsorbed potassium catalysts on zeolites NaX and NaY. Both 12K/NaX-PQ and 12K/NaY-PQ samples exhibited structural collapse. About 60% biodiesel yield was obtained in the first cycle, which was opposed the literature. It was due to the partial decomposition of precursor, which was located at the external surface. Then, the yield significantly dropped to about 3% in the second cycle, suggesting the similar results with the previous research. However, such drop was accompanied by the decrease of sodium and carbonate. This finding indicates that ion exchange occurs, resulting in a loss of structure. Also, 12% potassium was considered too high to study the effect of the FAU cavity on catalyst preparation.

For more clarity, the precursor concentration was reduced to 8%. Firstly, PQ could block the zeolite pore, especially NaY, resulting in precursor was located at the external surface. Conversely, zeolite NaX had lower adsorption capacity, leading to a larger degree of impregnation. 8K/NaY-PQ could maintain its structure while 8K/NaX-PQ displayed collapsing structure similar to those 12% samples. Moreover, only 7.1% was obtained by the catalysis of 8K/NaY-PQ while 8K/NaX-PQ showed 35.6%. This finding suggests that the importance of the FAU cavity is to assist the acetate converted to carbonate on support. If the support had no cavity, the precursor was decomposed. However, the potassium precursor under the thermal treatment was still the cause of the collapsing issue. It is probably due to the hydrolysis of the zeolitic bond (Si–O–Al) assisted by alkali metal (potassium from ion exchange), resulting in poor reusability.

To improve the heterogeneous catalyst for transesterification of palm oil, the carbonate salt (K_2CO_3 and Na_2CO_3) was directly impregnated into the zeolite NaX without calcination. Both salts were also studied in the aspect of solubility in the CH_3OH/glycerol mixture. Since K_2CO_3 had highly better solubility than Na_2CO_3, it thus exhibited in the first cycle with an extremely high yield up to 95.9% while 70.6% was obtained in the sodium catalyst. Interestingly, poor solubility, attributed to the high recovery, resulted in the catalysis in the further cycle, while the potassium catalyst showed similar results as in the literature. Moreover, Na_2CO_3/NaX could also exhibit catalytic activity in the reaction, even in the absence of potassium, indicating that the carbonate should be the actual active species. Thus, this thesis could be concluded that the structure of support in the heterogeneous catalyst was not only crucial for reusability, but the solubility of the carbonate precursor also resulted in the catalysis of the transesterification.
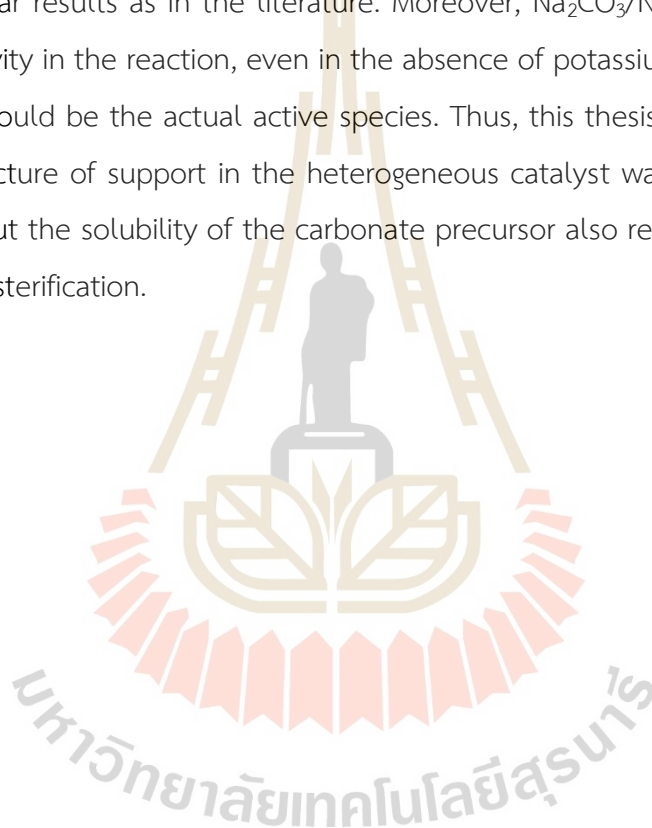
APPENDICES
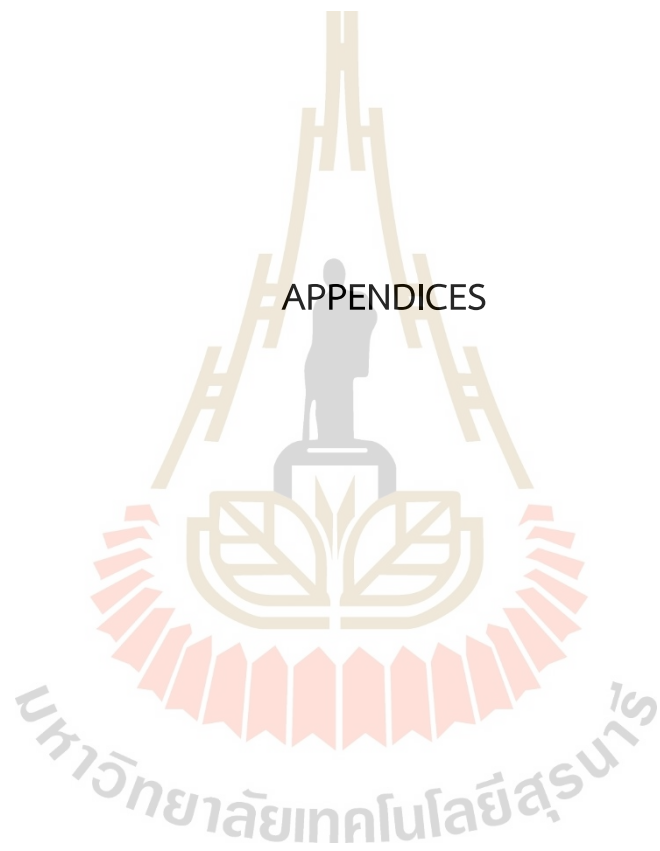
APPENDIX A

FIGURES IN CHAPTER III, IV, AND V
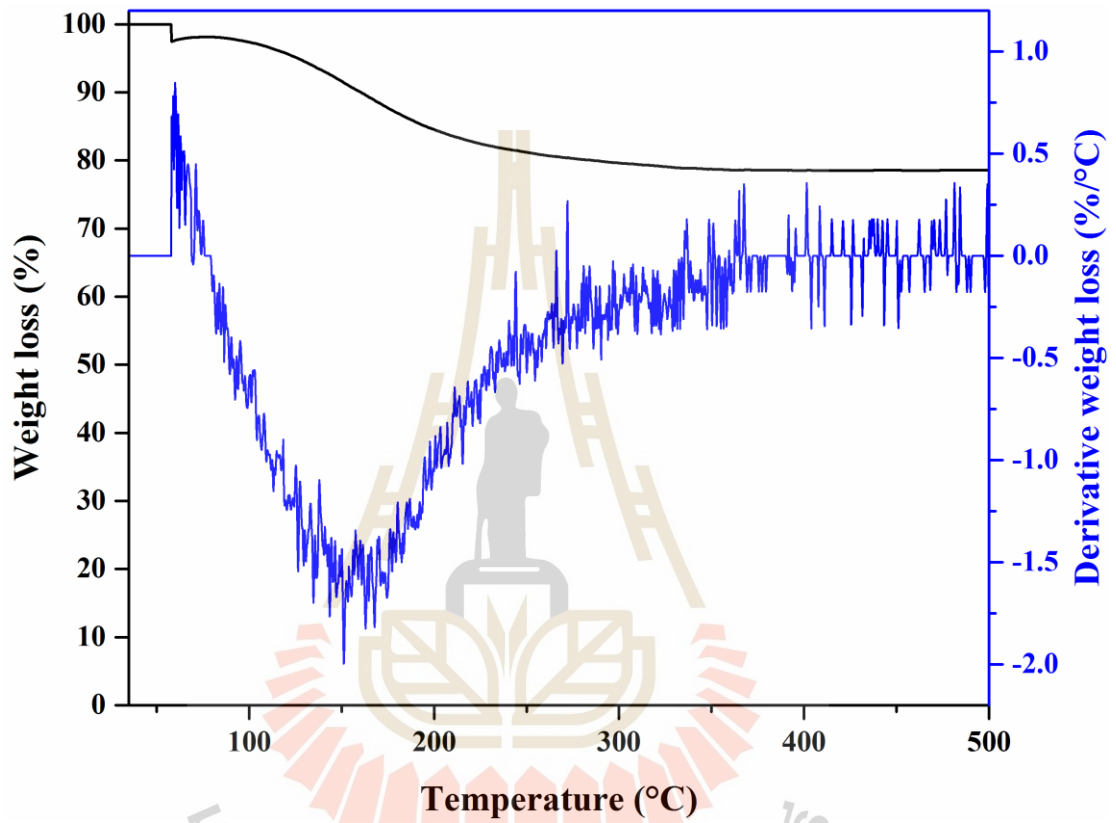
Figure S1 Thermogram with DTG of zeolite NaX.
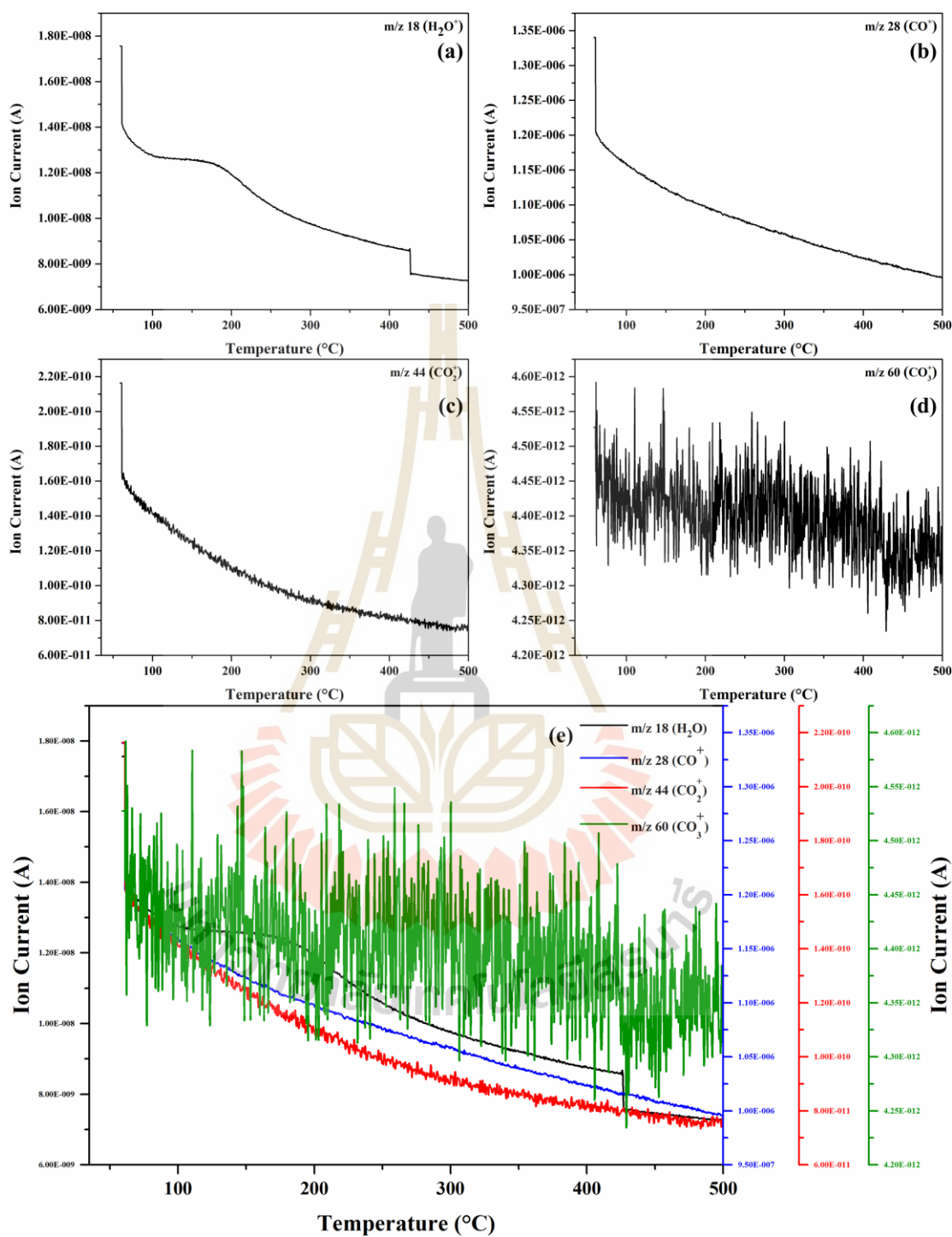
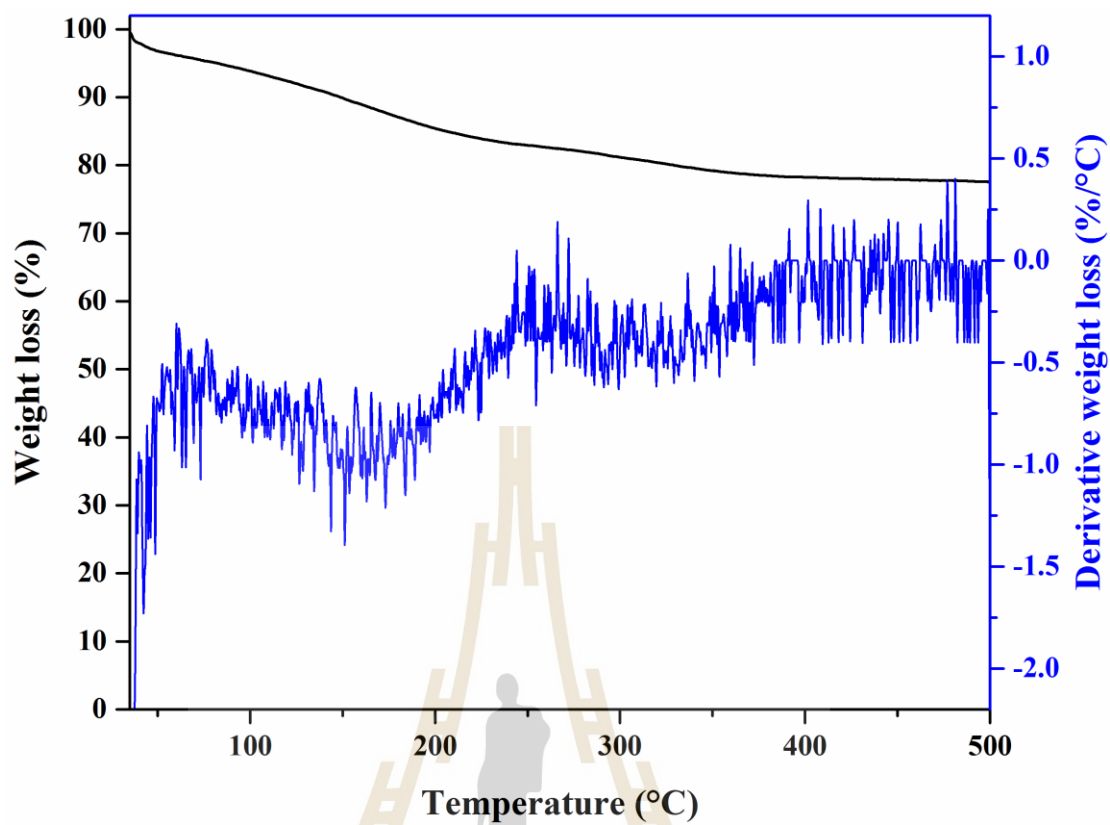**Figure S2** TGMS spectrum at m/z 18 (a), 28 (b), 44 (c), 60 (d), and compilation (e) of zeolite NaX.
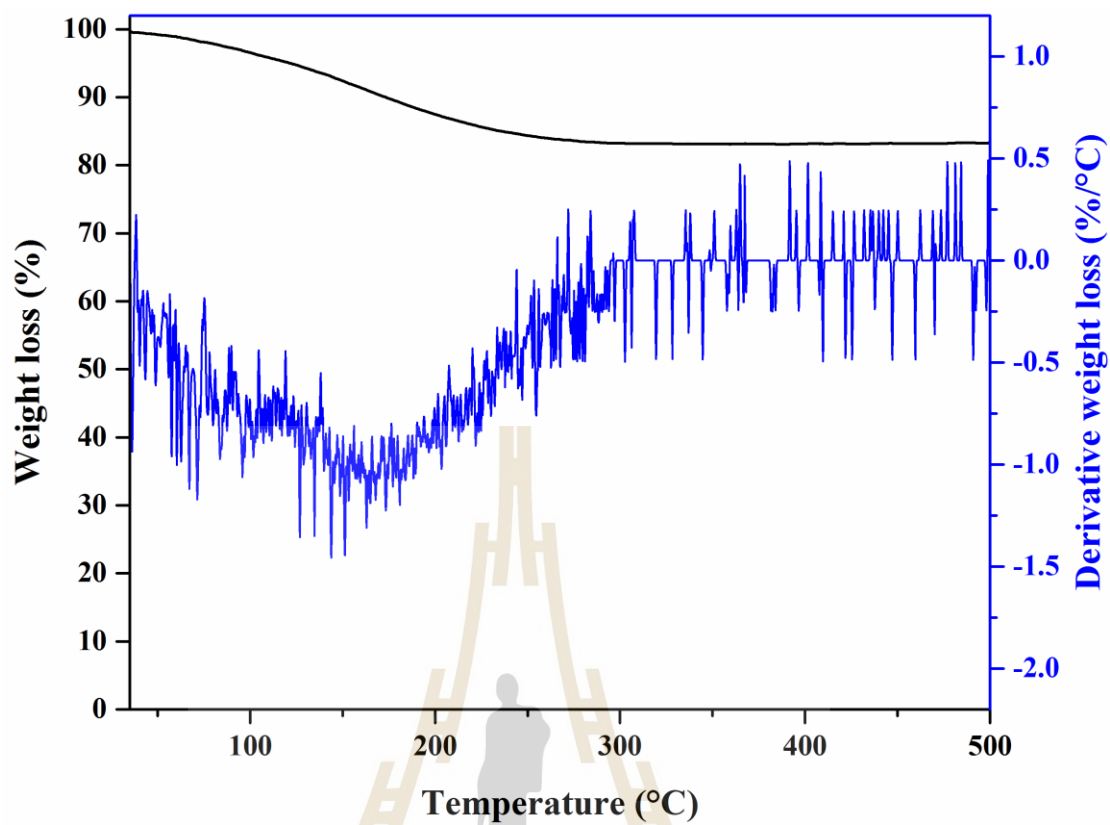
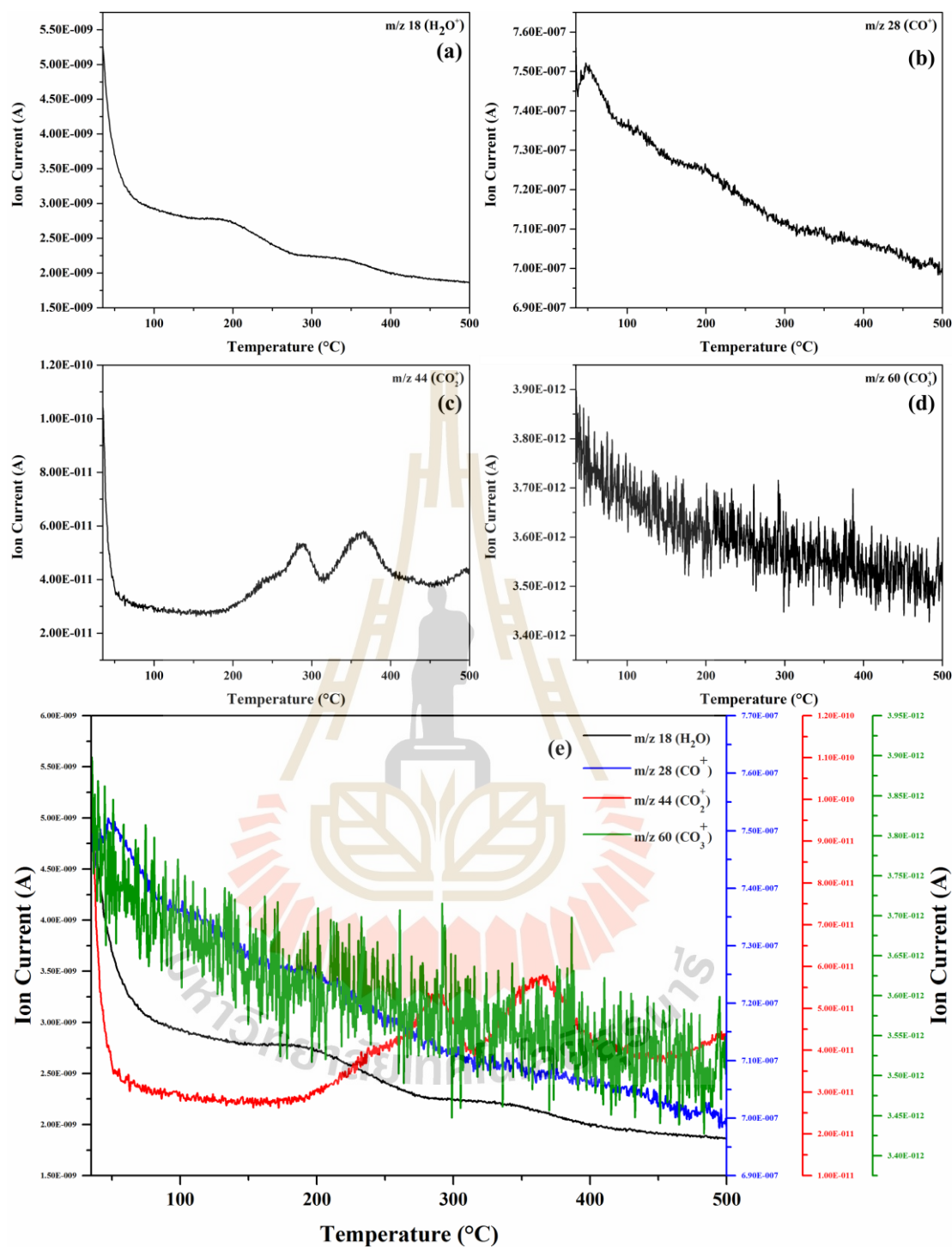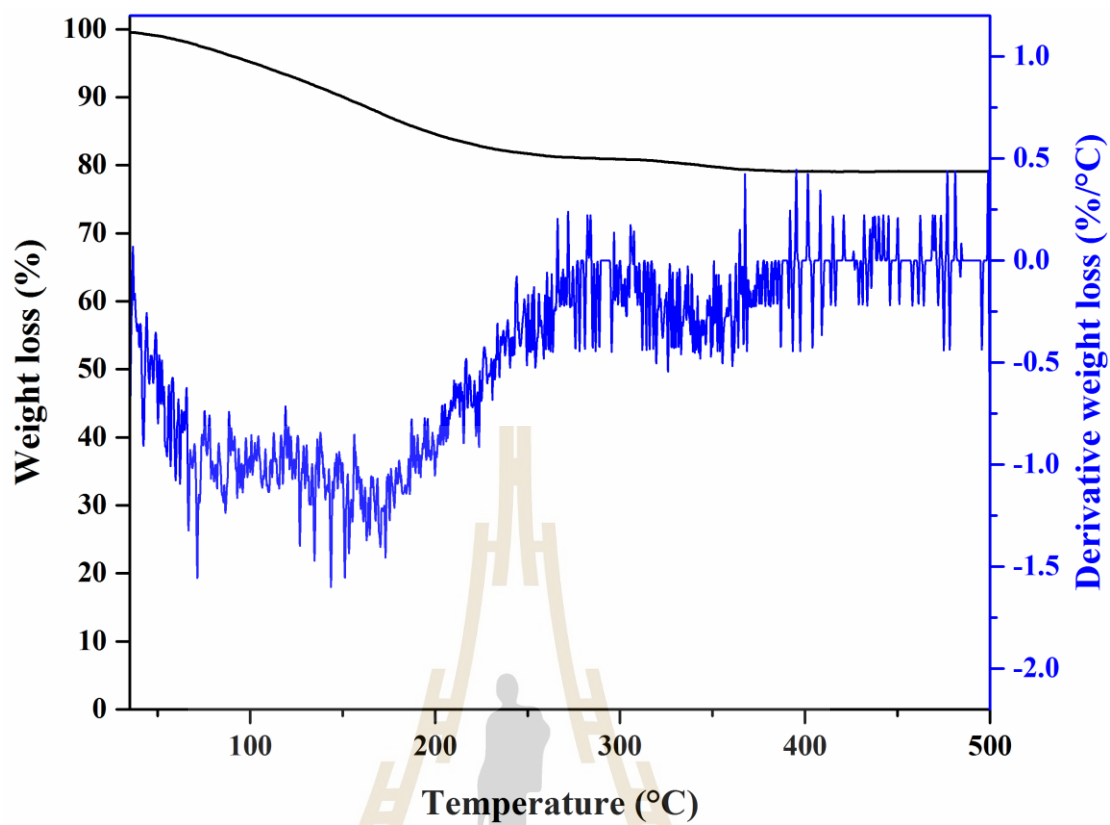**Figure S3** Thermogram with DTG of K$_2$CO$_3$/NaX.
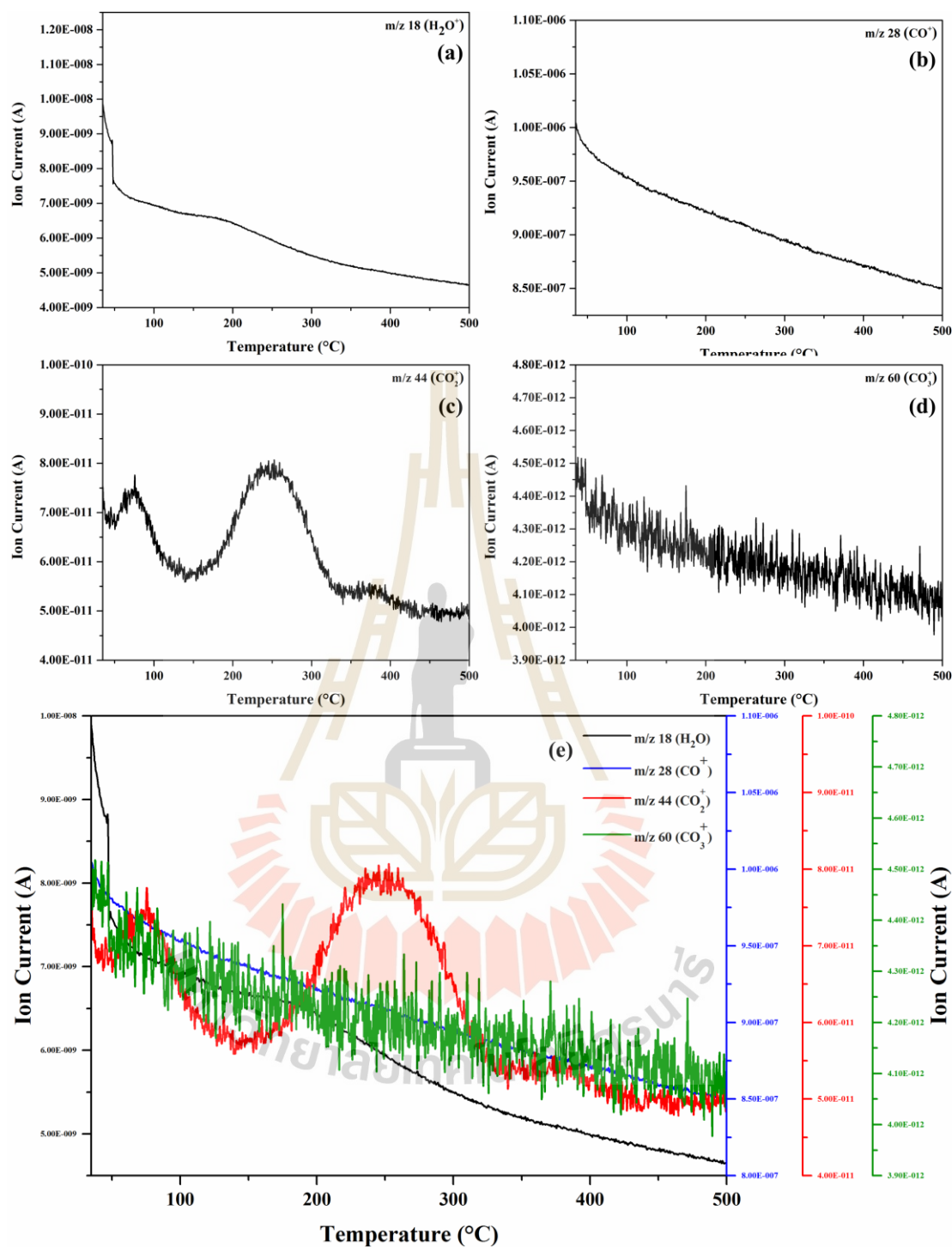
Figure S4 TGMS spectrum at m/z 18 (a), 28 (b), 44 (c), 60 (d), and compilation (e) of K$_2$CO$_3$/NaX.
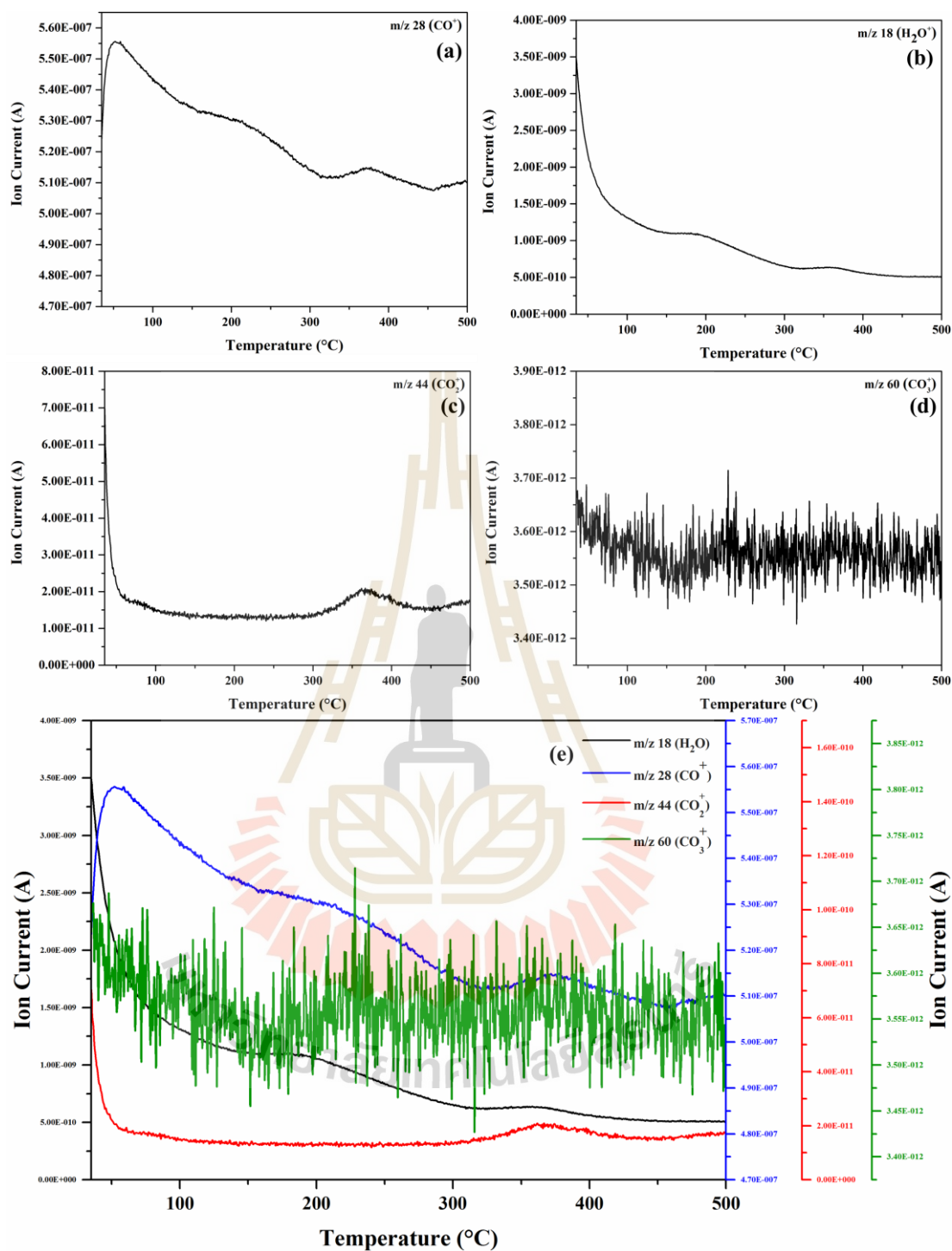
Figure S5 Thermogram with DTG of K_2CO_3/NaX-C1.

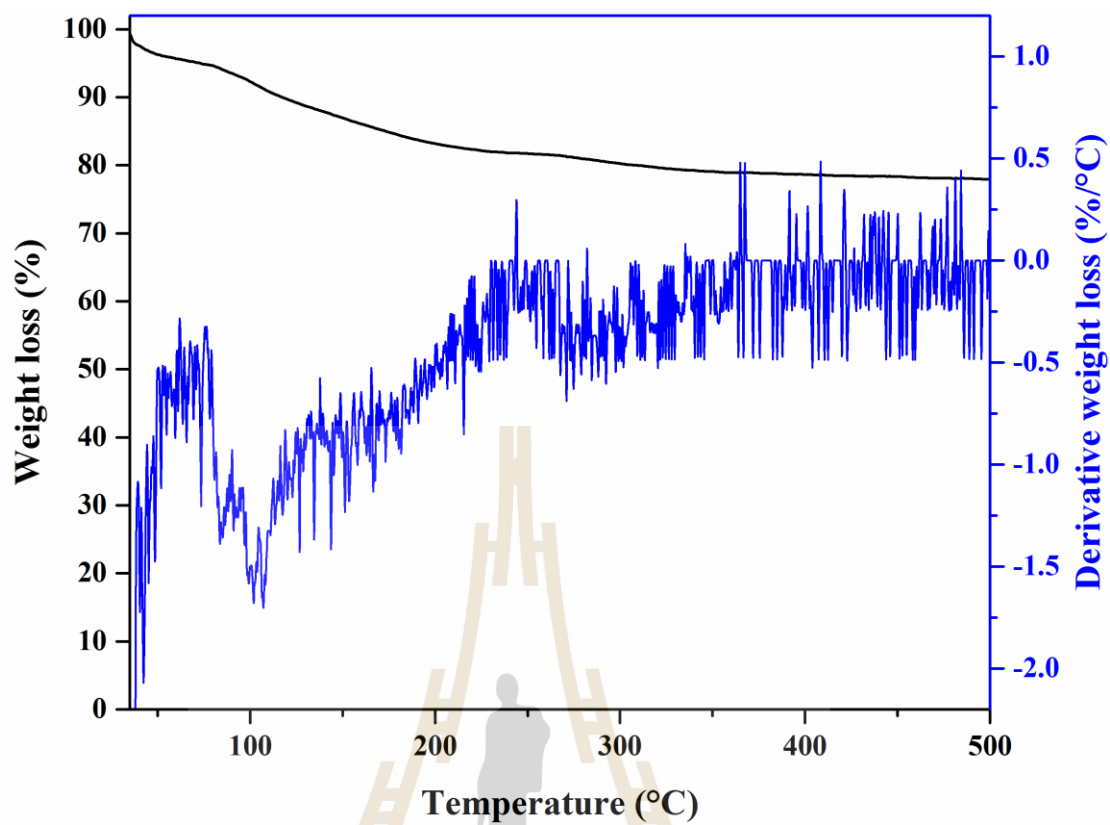**Figure S6** TGMS spectrum at m/z 18 (a), 28 (b), 44 (c), 60 (d), and compilation (e) of K₂CO₃/NaX-C1.

Figure S7 Thermogram with DTG of K$_2$CO$_3$/NaX-C3.

Figure S8 TGMS spectrum at m/z 18 (a), 28 (b), 44 (c), 60 (d), and compilation (e) of K$_2$CO$_3$/NaX-C3.

Figure S1 The appearance of treated-spent catalyst at 500 °C from TGA.
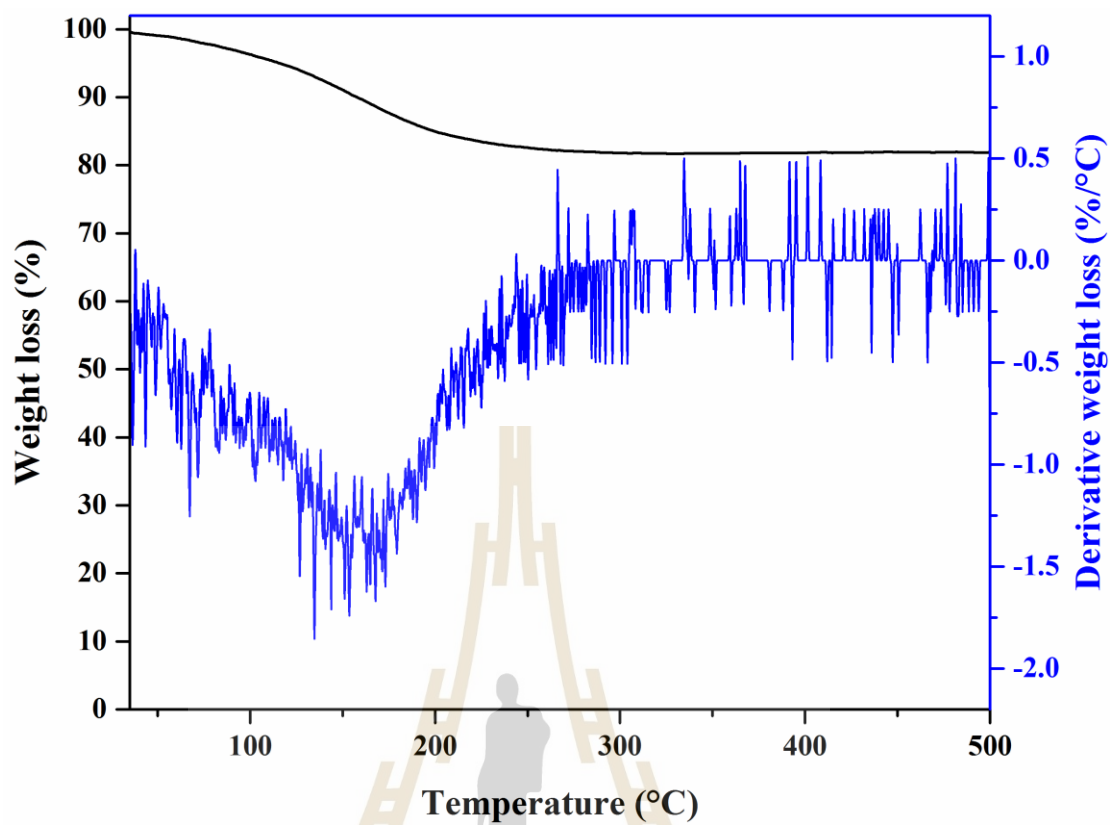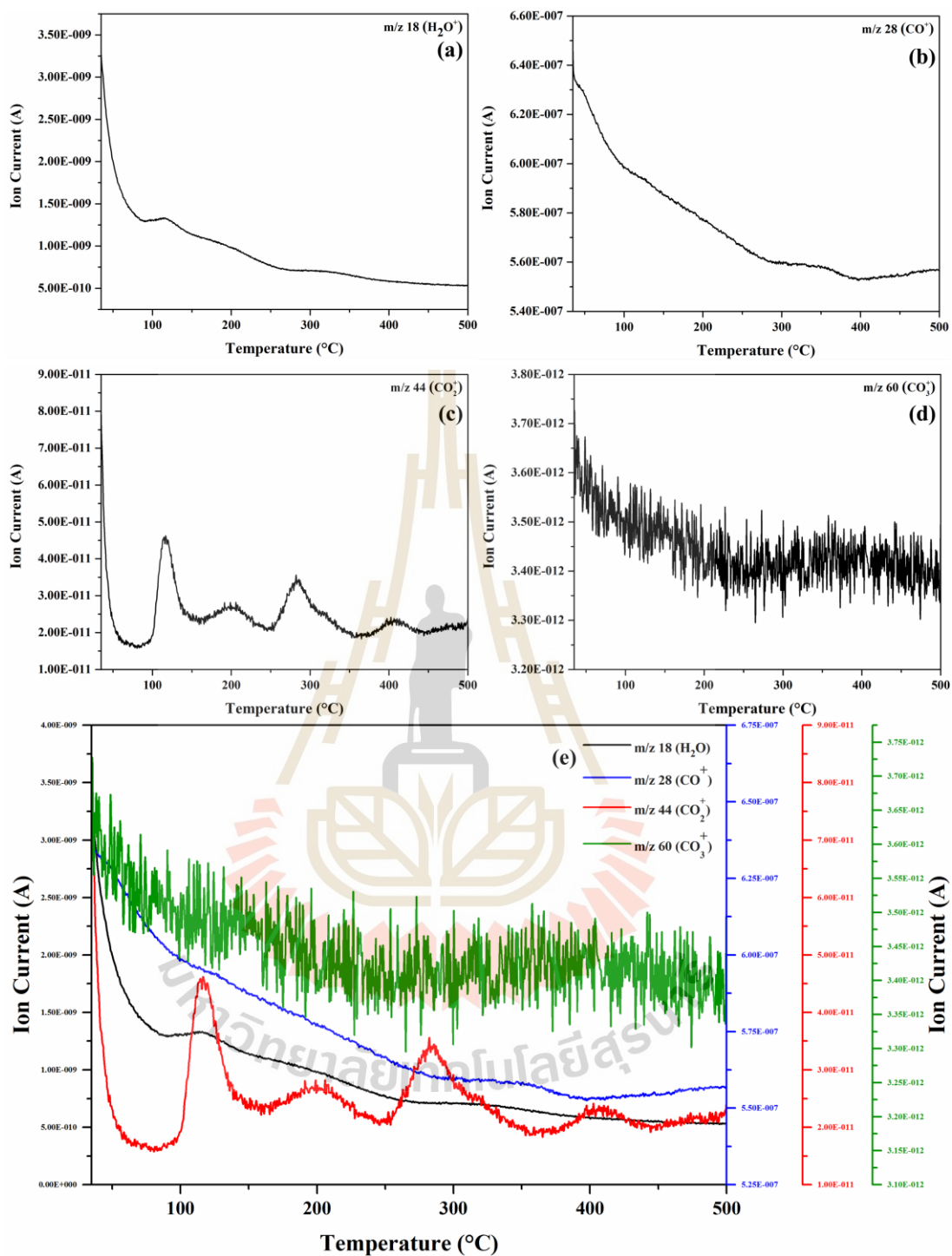
Figure S10 Thermogram with DTG of Na$_2$CO$_3$/NaX.
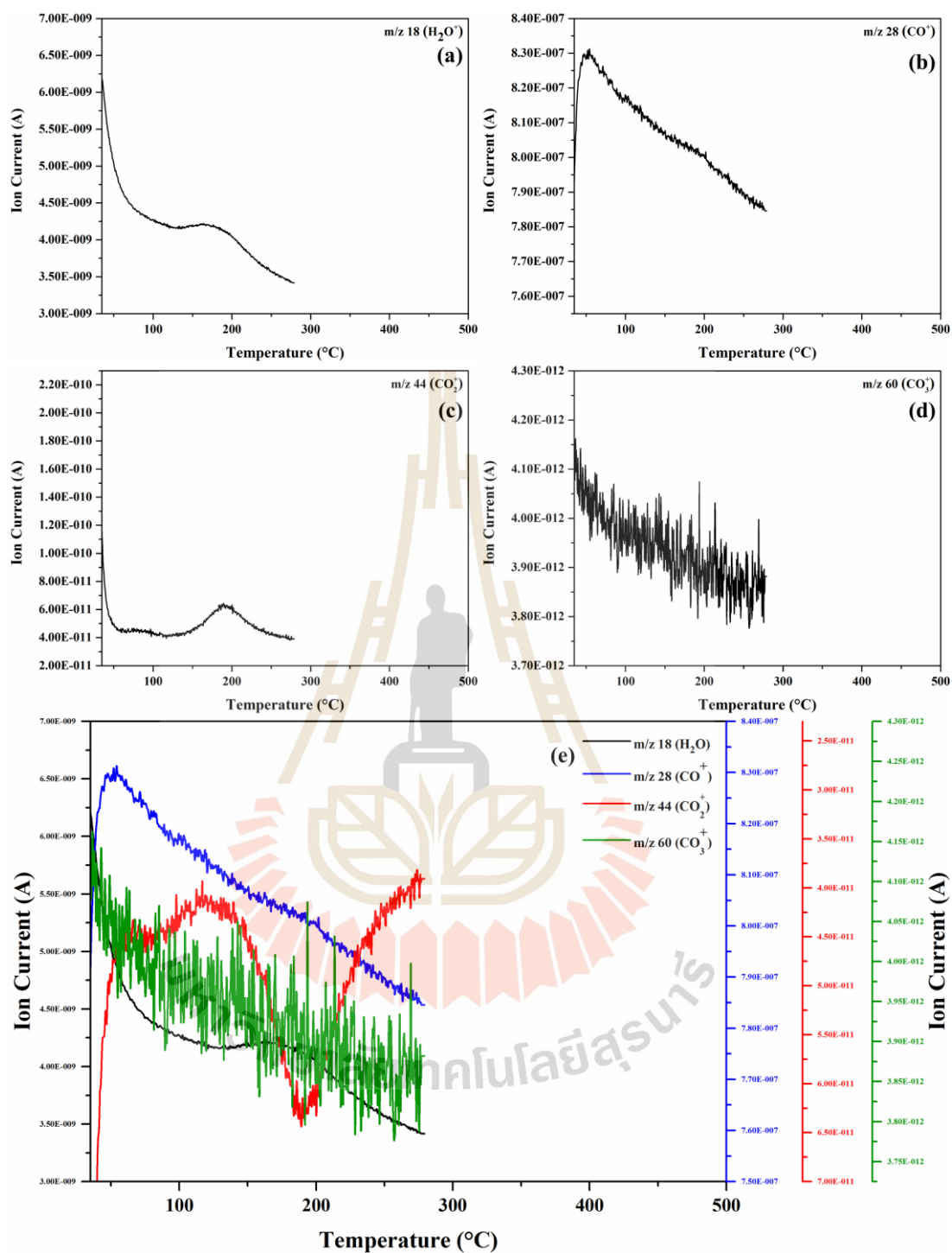
Figure S11 TGMS spectrum at m/z 18 (a), 28 (b), 44 (c), 60 (d), and compilation (e) of Na_2CO_3/NaX.

Figure S12 Thermogram with DTG of Na_2CO_3/NaX-C1.

Figure S13 TGMS spectrum at m/z 18 (a), 28 (b), 44 (c), 60 (d), and compilation (e) of Na₂CO₃/NaX-C1.

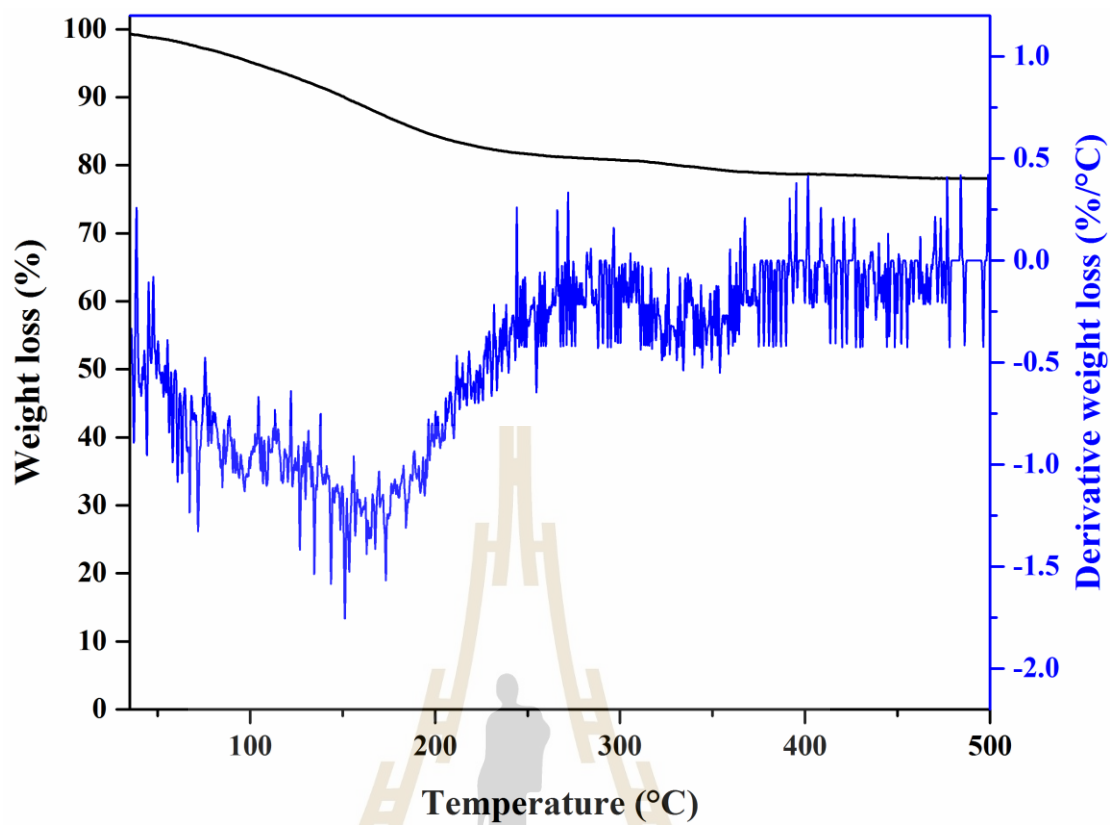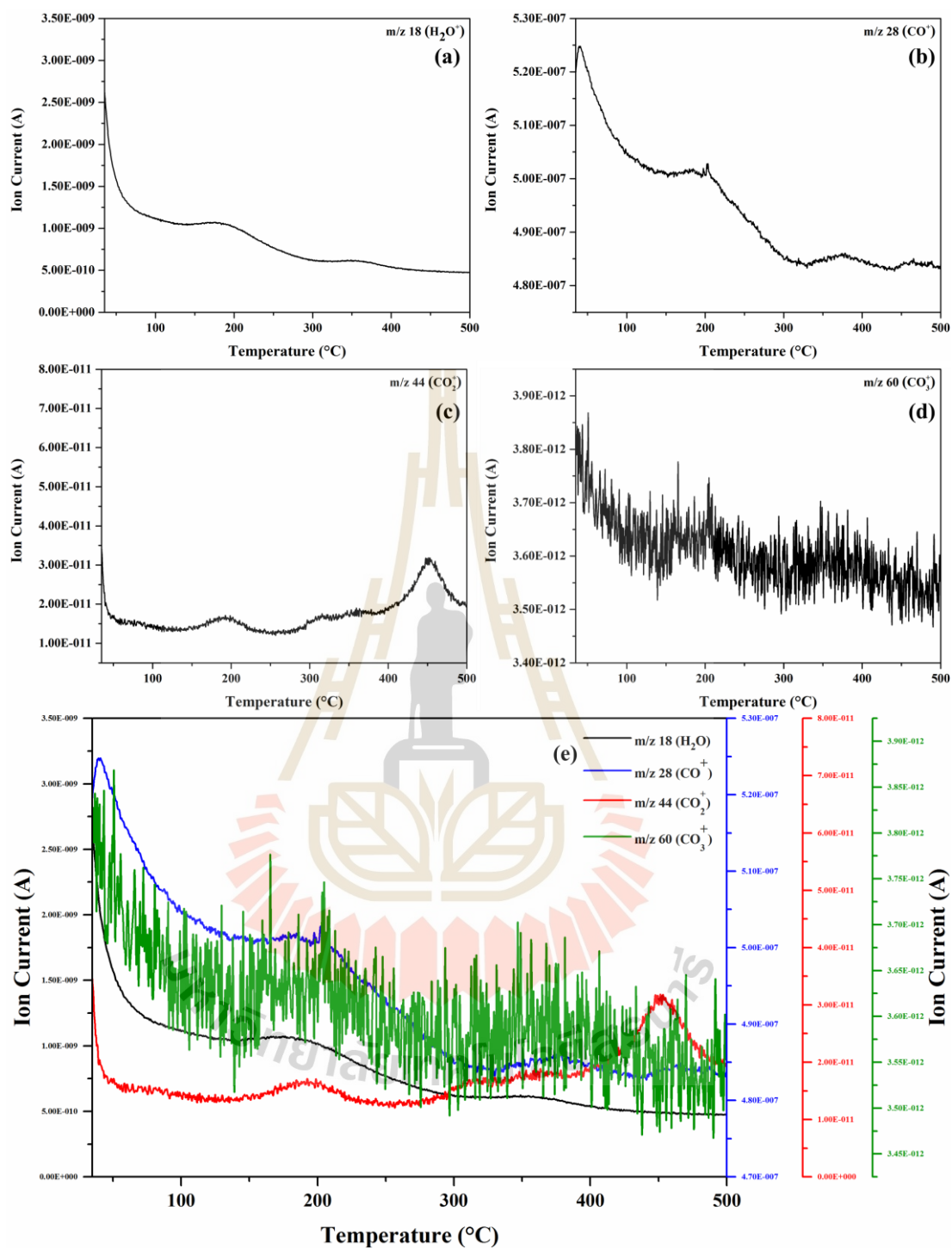**Figure S14** Thermogram with DTG of Na_2CO_3/NaX-C3.

Figure S15 TGMS spectrum at m/z 18 (a), 28 (b), 44 (c), 60 (d), and compilation (e) of Na$_2$CO$_3$/NaX-C3.

APPENDIX B

PUBLICATIONS

B.1   List of publications

Krukkratoke, K., Keawkumay, C., Tayraukham, P., Prompiputtanapon, K., Khemthong, P., Prayoonpokarach, S., and Wittayakun, J. (2022). Strategic synthesis to disperse zeolite NaY in Lead tree wood. *Crystals*. *12*(4), 504. doi: https://doi.org/10.3390/cryst12040504

Sereerattanakorn, P., Tayraukham, P., Osakoo, N., Krukkratoke, P., Keawkumay, K., Wittayakun, J., Pornnongsan, N., Deekamwong, K., and Prayoonpokarach, S. (2023). The synthesis of well-dispersed and uniform-sized zeolite NaY by adding non-refluxed and acid-refluxed cogon grass. *Materials*. *16*(23), 7330. doi: https://doi.org/10.3390/ma16237330

Keawkumay, C., Krukkratoke, P., Youngjan, S., Osakoo, N., Deekamwong, K., Khemthong, P., Phanthasri, J., Prayoonpokarach, S., and Wittayakun, J. (2024). Extraction of silica from sugarcane bagasse ash and its utilization in zeolite 4A synthesis for CO_2 adsorption. *RSC Advances*. *14*, 19472–19482. doi: https://doi.org/10.1039/d4ra02207f

CURRICULUM VITAE

Panot Krukkratoke was born on December 1st, 1996, in Nakhon Ratchasima, Thailand. He received his B.Sc. in Chemistry (First-class honors) in 2019 from the School of Chemistry, Institute of Science, Suranaree University of Technology (SUT), Nakhon Ratchasima, Thailand. He had an opportunity to be intern student for 6 months at National Nanotechnology Center (NANOTEC), National Science and Technology Development Agency (NSTDA), Thailand, in the topic of synthesis of amine-doped activated carbon for iron adsorption, which was under supervision of Dr. Sirapassorn Kiatphuengporn. During his senior year in bachelor's degree, he also studied research in the synthesis of zeolite NaY with various water contents for paraquat adsorption under the supervision of Prof. Dr. Jatuporn Wittayakun. In 2019, he continued to hunt the master's degree at the School of Chemistry, SUT under the supervision of Prof. Dr. Jatuporn Wittayakun and Dr. Pongtanawat Khemthong from the NANOTEC with Thailand Graduate Institute of Science and Technology (TGIST) scholarship along 2 years. The thesis of the strategic synthesis to disperse zeolite NaY in Lead tree wood was published in 2022. Then, He kept to pursue in Doctoral degree during 2021 – 2023 at the same program under the supervision of Prof. Dr. Jatuporn Wittayakun and Assoc. Prof. Dr. Sanchai Prayoonpokarach (co-advisor). He received the Kitti Bundit scholarship supported by SUT. In 2022, he was at Carl von Ossietzky Universität Oldenburg, Germany, for 3 months to carry out the MBOH conversion experiment, which was under the supervision of Prof. Dr. Frank Rößner. Now, he has published the articles in the international journals (listed in APPENDIX B) during the course of his doctor's degree.